ANNÉE 2016

THÈSE / UNIVERSITÉ DE RENNES 1
sous le sceau de l'Université Bretagne Loire

pour le grade de

DOCTEUR DE L'UNIVERSITÉ DE RENNES 1

Mention : Traitement de Signal et Télécommunications

Ecole doctorale MATISSE

présentée par

Oumar Alassane BARRO

préparée à l'unité de recherche IETR (UMR 6164)
(Institut d'Electronique et de Télécommunications de Rennes
UFR Informatique et Electronique

Design and manufacturing reconfigurable antennas using plasma

Thèse soutenue à Rennes le 14 Octobre 2016

devant le jury composé de :

Paola RUSSO
Professeur, Università Politecnica delle Marche Ancona, Italy / rapporteur

Smail TEDJINI
Professeur, Université de Grenoble-Alpes, France / rapporteur

Jérôme SOKOLOFF
Maitre de conférence HDR, LAPLACE, Université de Toulouse, France / examinateur

Mohamed HIMDI
Professeur, Université de Rennes 1, Rennes, France / directeur de thèse

Olivier LAFOND
Maitre de conférence HDR, Université de Rennes 1, Rennes, France / co-directeur de thèse

En mémoire de mon grand-père (Mame Tidia),

A mes parents,

A ma femme,

A ma famille,

A tous ceux qui me sont chers…

Acknowledgments

Bismillahirahmanirahim,

First and foremost, I am grateful to **Allah**, the Gracious and the Merciful, for all that I am and all that I have and I pray on his messenger **Muhammad** (SA).

I would like to express my sincere gratitude to my respected supervisors, Prof. **Mohamed Himdi**, Assc. Prof. **Olivier Lafond** for their guidance, help and insight motivation throughout two years working with them at IETR. Their guidance helped me in all the time of research and writing of this thesis. I could not have imagined having a better supervisors and mentors for my Ph.D study.

It is pleasure to acknowledge my gratitude to the reviewers, Prof. **Paola Russo** and Prof. **Smail Tedjini** for accepting my thesis work and without forgetting the others juries, Assc. Prof. **Jérôme Sokoloff** and Eng. **Sylvain Bolioli**. Their comments and suggestions before and during my defense are very useful to improve my work in the future endeavors.

I would like to thank Assc. Prof. **Franck Colombel** for believing in me, for his help and advice.

I also would like to mention my thousand thank to Mr. **Laurent Cronier**, Mr. **Christophe Guiton** and Mr. **Jean Christophe Lacun** for helping me to come out with excellent antenna prototypes. The sweet memories when we were working together to complete my prototype will always remain in my heart. Thanks Mr. **Jerome Sol** for his excellent works in antenna measurements.

To my collegues, **Evgueni**, **Yaakoub**, **Cheikh Diallo**, **Jonathan**, **Carole**, **Gilles**, **Antoine**, **Aziz**, **Alexis** , **Kevin**, **Mamadou**, **Daouda**, **Pape Fam**, **Roza**, **Abdullah Haskou**, **Abdou khadir**, thank you for your friendship, supports and help throughout my days at IETR. The sweet memories that we had shared are safely embedded in my heart and it will not be erased over time.

I dedicate this thesis to my father **Alassane Racine**, my mother **Fatoumata Talla**, my uncle **Malick Talla** who spared no effort to put me in the best conditions of study. This is a gift that I make them for all the sacrifices and efforts for the success of their children. I also dedicate this thesis to all my family, my brothers and sisters, I also encourage perseverance in telling them, that success is at the end of the effort.

Words unable to describe how thankful I am to my wife **Racky Mamadou Wane** for her unconditional support during this thesis. Thank you again.

I address my grateful feeling to my parents in-law (**Mamadou Sada Wane** and **Racky Wane**) for their belief in me and their prayers.

My thanks also go to all members of the "Dahira Baye of RENNES", in particular **Cheikh Amadou Fall**, **Cheikh Moussa Ndiaye**, **Cheikh Ousmane Diène** for their hepls prayers.

To my friends in Rennes **Cheikh Mbaye**, **Lama**, **Dame**, **Thierno Barro**, **Palaye**, **Tapha Diagne**, **Zaff**, **Makha**, **Keita**, **Borso**, **Ass Ba**, **Baye Baba**, **Baba Ndao**, **Ousmane Magassa**, **Saliou**, **Iba Diouf**, **Alioune Leye**, **Koro**, **Babacar Ndiaye**, **Dieuf Dieul**, **Coumba Sow**, **Aby Faye Diagne**, **Amina Ndiaye**, **Wemsy Diagne**, **Saly Ba**, **Rouguy**, **Khadija**, **Fanta Ba**, thank you for bringing in moments of immense joy and laughter.

I want to thank my childhood friends, I did not want to venture to give names, just for can not forget someone. However, I can not but mention a few among of them: **Papis**, **Laye Madass**, **Abdou Gandiaye**, **Elage Ibra**...

To my friends and all those names I missed to mention. I would like to thank you all for your moral support and motivation.

Dieureudieufee Baye Niass

Table of contents

Résumé en Français

0.1 Introduction

Le plasma est le quatrième état de la matière avec une permittivité complexe qui peut être exploitée pour donner des avantages aux systèmes de communication. Cette permittivité négative lui permet d'avoir des caractéristiques similaires aux matériaux métalliques en termes de conductivité électrique. Depuis de nombreuses années, les antennes plasma ont été étudiées en raison de leur capacité à être conductrices ou transparentes vis à vis des ondes électromagnétiques (furtivité). L'utilisation d'antennes à base de plasma peut donc permettre un contrôle électronique du rayonnement et non plus mécanique. Par conséquent, cette thèse vise à utiliser le plasma comme une alternative au métal dans la construction des antennes reconfigurables.

0.2 État de l'art

Le premier objectif de cette thèse concerne l'étude de l'état de l'art sur l'utilisation du plasma en électromagnétisme. La théorie de l'interaction des ondes électromagnétiques avec le plasma permet d'avoir les équations liant les caractéristiques du plasma. Les deux paramètres fondamentaux que sont la fréquence angulaire et la fréquence de collision définissent le plasma et aussi les zones de fonctionnement des antennes plasma. Lorsque la pulsation de l'onde éléctromagnétique est supérieure à la pulsation plasma, la constante de propagation est réelle, la permittivité est positive et l'onde se propage dans le plasma. Dans ce cas, le milieu plasma a des propriétés diélectriques. Lorsque la pulsation de l'onde électromagnétique est inférieure à la pulsation plasma, la constante de propagation est imaginaire, la permittivité est négative et le milieu plasma peut avoir des propriétés conductrices. Il peut réfléchir ou absorber l'onde incidente en fonction de la fréquence de collision.

Une caractérisation est donc nécessaire pour avoir les paramètres du plasma. Deux types de caractérisation sont trouvés dans la littérature. Le premier utilise un seul tube fluorescent (voir Figure 1) et le second utilise plusieurs tubes fluorescents formant un mur plasma (voir Figure 2).

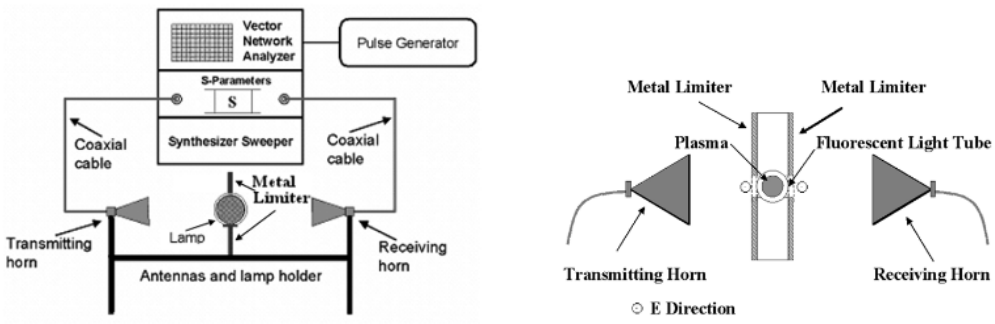

(a) (b)

Figure 1: Montage expérimental. (a) Schéma synoptique du système de mesure. (b) Vue détaillée accentuée sur le limiteur pour bloquer et contrôler le signal à travers le tube fluorescent.

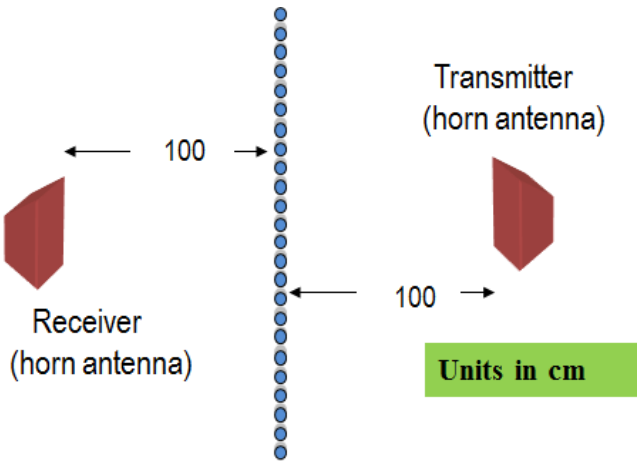

Figure 2: Dispositif de caractérisation.

Ensuite, une association de tubes à plasma peut être utilisée comme un équivalent de réflecteur métallique. On peut voir dans la littérature que plusieurs types de réflecteurs de plasma faits avec des tubes fluorescents ont été réalisés et peuvent être de forme parabolique, triangulaire, circulaire et même carrée.

Mais le plasma peut également être utilisé pour réaliser des antennes plasmas où l'élément rayonnement est un tube fluorescent. N'ayant pas accès directement au plasma contenu dans le tube, des techniques de couplage sont nécessaires pour que l'onde électromagnétique issue d'un émetteur soit rayonnée par l'antenne plasma formée par un tube. Dans la littérature, on trouve deux techniques de couplage : inductif ou capacitif. Le couplage capacitif est le plus utilisé en raison de sa simplicité de mise en œuvre.

0.3 Effets de blindage d'une cage de Faraday à plasma

Deux types d'antennes placées à l'intérieur d'une lampe fluorescente de forme spirale ont été étudiées :

- Une antenne patch circulaire
- Une antenne monopole

L'étude de ces deux configurations a pour objectif d'évaluer l'impact de la polarisation de l'antenne avec la lampe spirale. Ces antennes fonctionnant à 2.45 GHz sont simulées, réalisées et mesurées.

0.3.1 Antenne patch à l'intérieur de la lampe

Sur la figure 3, nous présentons la lampe de forme spirale utilisée comme cage de Faraday. Le système antennaire est constitué d'une antenne patch résonant à 2.45 GHz placée à l'intérieur de la lampe (voir Figure 3(a)).

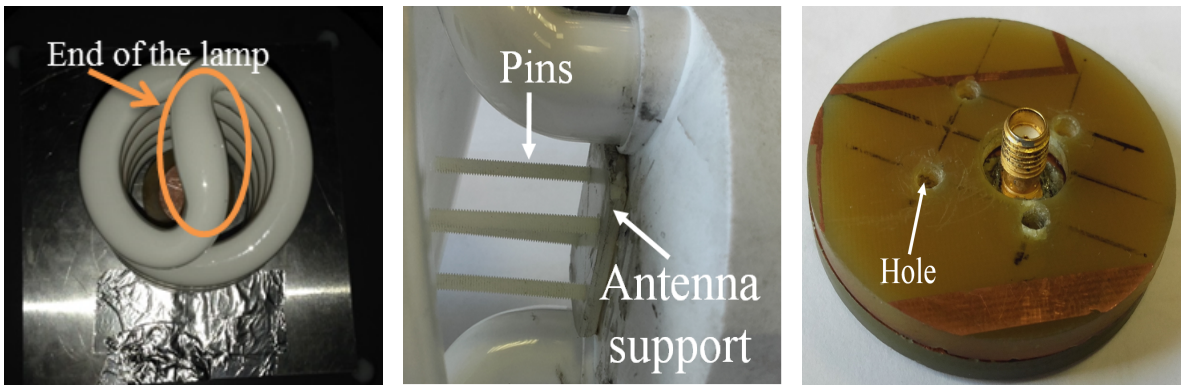

(a) (b) (c)

Figure 3: Prototypes fabriqués. (a) La cage de Faraday avec l'antenne à l'intérieur. (b) Support de l'antenne. (c) Substrat troué pour supporter l'antenne.

En fonction de la forme de la lampe, deux cas sont étudiés :

- Premier cas : si la polarisation de l'antenne est parallèle à la partie supérieure de la lampe
- Deuxième cas : si la polarisation de lampe est orthogonale à la partie supérieure de la lampe.

Les performances du système antennaire dans les deux cas ont été mesurées et démontrent que la lampe présente des effets de blindage d'une cage de Faraday sur un secteur angulaire ±20° autour de l'axe dans le premier cas. De plus, cette elle permet de reconfigurer le diagramme de rayonnement du patch.

Si la lampe est éteinte, le diagramme de rayonnement correspond à celui de l'antenne patch. Ce résultat prouve que le verre constituant le tube contenant le plasma est transparent aux ondes électromagnétiques. Lorsque la lampe est allumée, le gain sur le secteur angulaire ($\theta = \pm 20°$) chute de 12 dB dans le premier cas et de 5 dB dans le deuxième cas. Les résultats de mesures sont en bon accord avec la simulation. Ces résultats montrent clairement l'impact de la polarisation.

0.3.2 Antenne monopole à l'intérieur de la lampe

Un autre système antennaire est étudié. Il s'agit d'un monopole placé à l'intérieur de la lampe (voir Figure 4). Le monopole fonctionnant à 2.45 GHz est polarisé suivant l'axe z.

Figure 4: Monopole à l'intérieur de la lampe.

Les performances du système antennaire ont été mesurées et montrent que la différence de gain entre l'état allumé et l'état éteint est de 5 dB. Ce résultat prouve que la lampe ne fonctionne pas comme une cage de Faraday car la polarisation du monopole est orthogonale à la partie spirale de la lampe. De plus le diagramme de rayonnement de l'antenne n'est pas reconfigurable.

0.4 Réseaux d'antennes reconfigurables

Deux types de réseaux d'antennes utilisant des tubes fluorescents pour reconfigurer la largeur du faisceau à mi-puissance ont été étudiés :

- Réseau de patchs
- Réseau d'antennes à fentes

Ces antennes fonctionnant à 2.45 GHz sont simulées, réalisées et mesurées.

0.4.1 Réseau de patchs

Les figures 5 et 6 présentent un réseau de patchs avec un mur de plasma utilisant des tubes fluorescents pour reconfigurer la largeur du faisceau à mi-puissance. A chaque élément rayonnant est superposé un tube fluorescent. Les performances de cette antenne ont été mesurées et montrent qu'il est possible de reconfigurer la largeur du faisceau à mi-puissance du diagramme de rayonnement en ionisant ou non un ou plusieurs tubes fluorescents. On note également que l'accord entre la théorie et la mesure est satisfaisant.

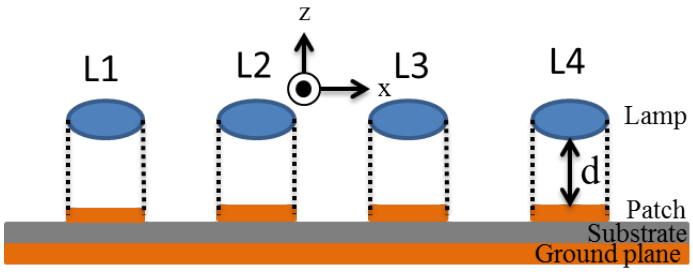

Figure 5: Géometrie du système.

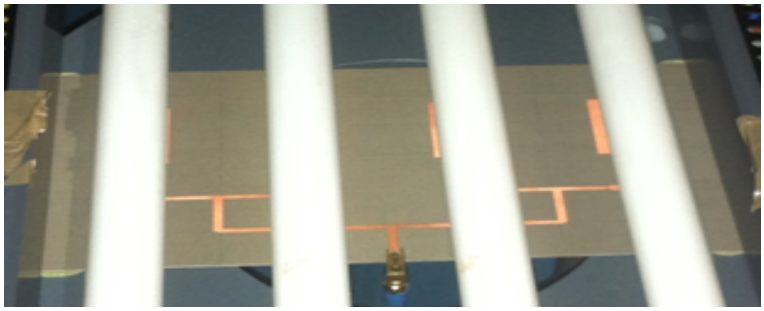

Figure 6: Prototype réalisé.

L'antenne permet d'avoir une multitude de configurations. Cependant cinq configurations ont été étudiées en allumant une, deux, trois, quatre lampes et quand tous lampes sont éteintes. L'ouverture mesurée du diagramme de rayonnement dans le plan H varie de 23° à 38° et le gain mesuré varie de 9.2 à -0.8 dBi.

0.4.2 Réseau d'antennes à fentes

Un réseau d'antennes à fentes avec des volets permettant de reconfigurer l'ouverture du diagramme de rayonnement en fermant l'ouverture des fentes est présenté sur la figure 7.

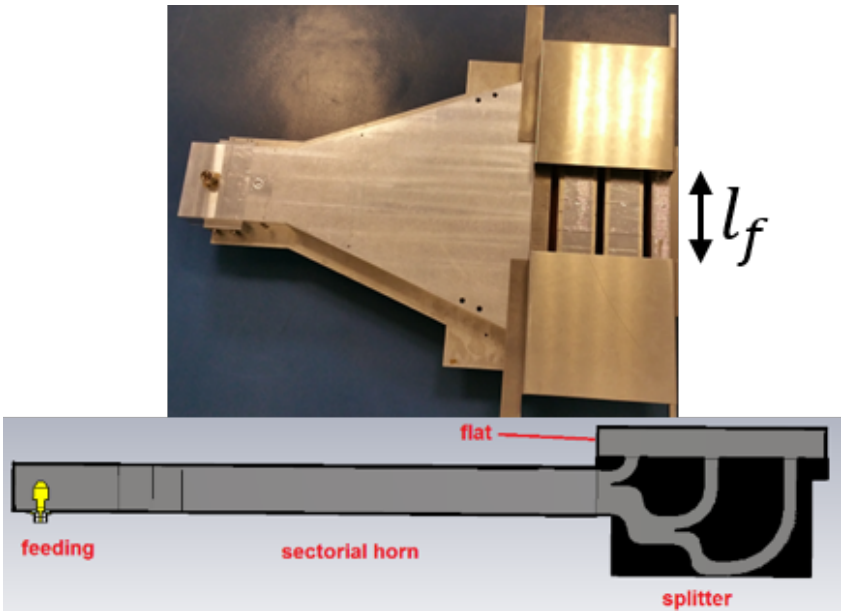

Figure 7: Prototype de l'antenne réalisé.

Deux types de volets ont été utilisés :

- Volets métalliques
- Volets faits avec des tubes fluorescents

Les performances de l'antenne avec les deux types de volets ont été mesurées et donnent des résultats similaires. La mesure est en bon accord avec la simulation.

Dans le cas des volets métalliques, l'ouverture du diagramme de rayonnement mesurée dans le plan H varie de 17.8° (ouverture des volets de 400 mm) à 63.1° (ouverture des volets de 100 mm) et le gain réalisé varie de 17 à 9.9 dBi.

Lorsque des tubes fluorescents sont utilisés comme volets, l'ouverture mesurée dans le plan H varie de 18° (ouverture des volets de 400 mm) à 66.7° (ouverture des volets de 100 mm) et le gain réalisé varie de 17.1 à 10 dBi.

Ces résultats confirment que l'antenne constituée de volets plasma est aussi performante que l'antenne à volets métalliques mais présente en outre l'avantage d'être contrôlée électroniquement. De plus elle reste bien adapté quelque soit la configuration ce qui n'était pas toujours le cas avec l'antenne munie de volets métalliques.

0.5 Antennes plasma

Cette partie s'intéresse à la réalisation d'antennes plasma utilisant un tube fluorescent comme élément rayonnant. Deux types d'antennes (monopole et dipôle) ont été réalisés (voir Figure 8) et leur performances ont été évaluées à plusieurs fréquences.

Figure 8: Antenne plasma fabriquée.

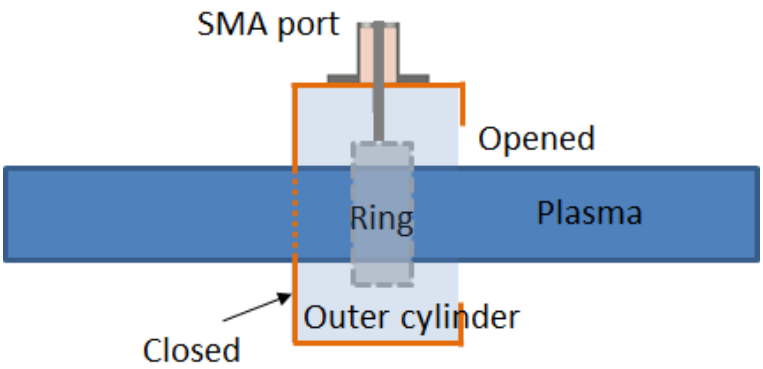

(a)

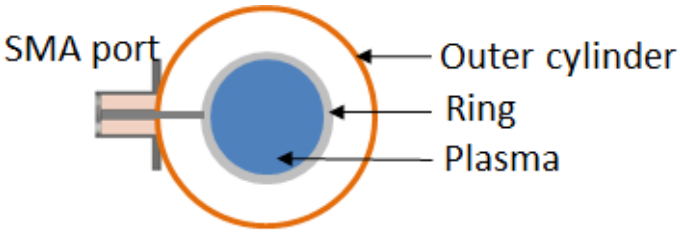

(b)

Figure 9: Système de couplage. (a) Vue de coupe. (b) Vue de dessous.

Les antennes sont fabriqués avec un tube fluorescent couplé électromagnétiquement avec un système d'excitation dédié. Ce dernier est constitué d'un anneau entourant le tube et d'un cylindre venant entourer l'anneau. Le cylindre est fermé en bas et ouvert vers le haut cela permettant d'avoir un champ électrique dans le sens de la longueur de la lampe. Le système de couplage est présenté sur la figure 9.

Les résultats simulés et mesurés sont tout à fait en bon accord, excepté un décalage en fréquence du fonctionnementt de l'antenne. Cet écart en fréquence pourrait être réduit par une meilleure connaissance de la fréquence de plasma. A notre connaissance, ces systèmes antennaires réalisés à base de lampe plasma sont parmi les premiers à avoir été étudiés complètement c'est à dire en obtenant les diagrammes de rayonnement et un gain satisfaisant.

0.6 Conclusion

L'utilisation du plasma dans les systèmes de communication est très intéressante car le plasma peut apparaître et disparaître en quelques microsecondes. Au début de cette thèse un état de l'art sur le plasma est présenté. La théorie de l'interaction des ondes électromagnétiques avec le plasma est introduite. Le principal paramètre qui régit l'interaction est le rapport entre la fréquence de l'onde électromagnétique et la fréquence angulaire du plasma, qui est à son tour liée à la densité d'électrons du plasma. Les procédés de caractérisation du plasma dans la littérature ont été présentés. L'état de l'art sur le plasma utilisé pour la conception d'antennes à réflecteur et d'éléments rayonnants proprement dit a également été fait.

Une lampe fluorescente spirale utilisée comme une cage de Faraday est présentée. Deux types d'antennes (patch et monopole) fonctionnant à 2,45 GHz ont été placés à l'intérieur de la lampe permettant de voir l'impact de la polarisation. Les systèmes d'antenne ont été simulés, fabriqués et mesurés. Les performances des systèmes d'antenne (patch + lampe) et (monopole + lampe) ont été validées expérimentalement. Il est intéressant de noter que le rayonnement du patch (premier cas) peut être fortement réduit lorsque la lampe est allumée. Cela signifie que la lampe présente des effets de blindage telle une cage de Faraday en particulier dans le secteur angulaire $\theta = \pm 20°$ et permet aussi de reconfigurer le digramme de rayonnement du patch.

Des réseaux d'antennes associés à des tubes à plasma pour reconfigurer l'ouverture du diagramme de rayonnement dans le plan H ont par la suite été étudiés. Deux systèmes d'antennes ont été simulés, fabriqués et mesurés. Le premier est un réseau de patch où chaque patch est superposé à un tube fluorescent et le second est un réseau à fentes où des tubes fluorescents sont utilisés comme volets pour modifier l'ouverture rayonnante des fentes. Les performances du réseau de patchs avec mur de plasma ont été validées et il a été prouvé que l'ouverture du diagramme est reconfigurable. Les diagrammes de rayonnement mesurés sont en bon accord avec ceux de la simulation. Les performances du réseau d'antennes à fentes ont également été validées et il a été prouvé que les performances de l'antenne avec des volets faits de tubes fluorescents sont semblables à celles des volets métalliques mais avec l'avantage d'être électroniquement reconfigurable.

En utilisant un tube fluorescent excité par une sonde coaxiale via un système de cou-

plage optimisé, deux antennes (monopole et dipôle) ont été simulées, fabriquées et mesurées à plusieurs fréquences. Sur la base des résultats de mesure, on peut conclure que la lampe fluorescente alimentée en courant alternatif peut être utilisée pour émettre ou recevoir des signaux radiofréquences. Les diagrammes de rayonnement mesurés sont en bon accord avec ceux de la simulation, mais un décalage en fréquence du fonctionnement de l'antenne est observé.

Chapter 1

General Introduction

1.1 Context and motivation of the study

The development of the communication systems grows rapidly. Therefore the necessity of the communication systems to become flexible in terms of performance is crucial. This development pushes the antenna designers to realize antennas which have: ability to be reconfigured mechanically or electrically, capability to control beam patterns and to remain low cost.

In this manuscript we are interested in plasma as reconfigurable media. This ionized gas has interesting electromagnetic properties. In particular, cold plasmas have a complex permittivity whose the real part may be negative or between zero and one. This magnitude depends on the pressure of the gas, the electron density and the frequency of the electromagnetic wave with which it interacts. In general, plasma can act like a conductor and can disappear if it is de-energized. The reconfigurable behaviors offered by plasma are the factor why plasma antenna concepts are studied here.

In particular, for military applications, this reconfigurabity is very important because the possibility of having conducting elements only when the useful signal needs to be transmitted makes antenna detection by hostile radars difficult.

Since many years, plasma antennas have been studied due to their ability to be conductor or transparent [1, 2]. Plasma is the fourth state of the matter. When the plasma inside a tube is energized (state ON), the media performs like a conductive element capable to reflect radio signal like a metal. But, when the tube is de-energized (state OFF), the plasma is non-conductor and acts like a dielectric media. Plasma can be controlled electrically to act like a radiator, reflector or even as an absorber and because of these factors, the research activities in plasma field are kept active and vibrant. Since then, there is a considerable amount of inventions made by many research institutions and groups to exploit plasma as antenna [3–8].

1.2 Objectives and research contributions

The realized works in this thesis are based on four main objectives:

The first objective is to retake the parameters of the plasma fluorescent lamps characterized by a previous Phd student in our laboratory as starting point. Theses parameters are used in order to realize plasma antennas but we remark that these parameters change from one type of lamp to another one.

The second objective is to design and realize Faraday shield effect system using plasma fluorescent lamp in order to protect an antenna from external high power aggression. A spiral plasma fluorescent lamp is used as Faraday shield effect. Two antennas such as patch and monopole antennas operating at 2.45 GHz are designed and surrounded. This objective can only be realized once the defined plasma characterization is finalized. The performances such as reflection coefficient, gain and radiation patterns in simulation and measurement are compared.

The third objective is to design and realize plasma antennas based on plasma medium in order to reconfigure the half-power-beam-width. Two types of antennas operating at 2.45 GHz have been considered. For each antenna, an adaptive wall of plasma is realized by using plasma fluorescent lamps and this wall is placed above the antenna. The performances in terms of reflection coefficient, gain and radiation patterns in simulation and measurement are compared.

The fourth objective is to analyze the performances of plasma as radiating element. The available fluorescent lamp is used as radiator and this lamp is excited using domestic AC supply. A system of coupling is realized and allows to have monopole or dipole plasma antenna. Since the plasma can be used to radiate radio signal, it is also can be called as plasma antenna. For further investigations, the plasma antennas were measured using our laboratory facilities and their performances between ON and OFF states are used to validate the ability of plasma antenna to effectively radiate radio signal.

1.3 Thesis structure

This thesis is divided in four main chapters.

The second chapter is a bibliographic part which allows to do a state of art on plasma in communication systems. The fundamental of the plasma is investigated in this chapter by deriving the equations governing the interaction of plasma and electromagnetic waves. Measurements setup and results which lead to selection of plasma parameters are explained in this chapter. The use of plasma as reflector and radiating element found in the literature are also presented.

The third chapter discusses about the use of plasma as shielding effect. A spiral compact fluorescent lamp is used to realize the Faraday shielding effect. Two kind of antennas which are patch and monopole are placed inside the plasma Faraday cage. The performance of the reconfigurable system is observed in terms of input reflection coefficient, gain and radiation pattern via simulations and measurement.

The fourth chapter presents the realization of reconfigurable antennas using plasma tubes allowing to obtain reconfigurable Half-Power-Beam-Width (HPBW) of the radiation patterns. Two original structures have been studied in this chapter which are a printed patches array and a slot antennas array. In each antenna, an appropriate wall of plasma is put above in order to reconfigure the half power beam width. The design and optimization are thoroughly explained within the chapter. The theoretical and experimental results for several configurations that have been realized in this research work are also compared.

The fifth chapter deals with plasma as radiator element. A coupling technique is also explained in this chapter. This is followed by the fabrication of two plasma antennas using commercially available fluorescent lamp which are monopole and dipole. The antennas performances are discussed based on plasma ON and OFF states.

This thesis ends with a general conclusion containing the main points of the work and point out on what remain to be done.

Bibliography

[1] U. S. Inan and M. Gokowski, *Principles of Plasma Physics for Engineers and Scientists*. Cambridge University Press, Dec. 2010.

[2] M. Laroussi and J. R. Roth, "Numerical calculation of the reflection, absorption, and transmission of microwaves by a nonuniform plasma slab," *IEEE Transactions on Plasma Science*, vol. 21, no. 4, pp. 366–372, Aug. 1993.

[3] G. G. Borg, J. H. Harris, D. G. Miljak, and N. M. Martin, "Application of plasma columns to radiofrequency antennas," *Applied Physics Letters*, vol. 74, no. 22, p. 3272, 1999. [Online]. Available: http://scitation.aip.org/content/aip/journal/apl/74/22/10.1063/1.123317

[4] J. P. Rayner, A. P. Whichello, and A. D. Cheetham, "Physical characteristics of plasma antennas," *IEEE Transactions on Plasma Science*, vol. 32, no. 1, pp. 269–281, Feb. 2004.

[5] G. Cerri, R. D. Leo, V. M. Primiani, and P. Russo, "Measurement of the Properties of a Plasma Column Used as a Radiating Element," *IEEE Transactions on Instrumentation and Measurement*, vol. 57, no. 2, pp. 242–247, Feb. 2008.

[6] I. Alexeff, T. Anderson, S. Parameswaran, E. P. Pradeep, J. Hulloli, and P. Hulloli, "Experimental and theoretical results with plasma antennas," *IEEE Transactions on Plasma Science*, vol. 34, no. 2, pp. 166–172, Apr. 2006.

[7] T. Anderson, I. Alexeff, E. Farshi, N. Karnam, E. P. Pradeep, N. R. Pulasani, and J. Peck, "An operating intelligent plasma antenna," in *2007 16th IEEE International Pulsed Power Conference*, vol. 1, Jun. 2007, pp. 353–356.

[8] P. Russo, G. Cerri, and E. Vecchioni, "Self-Consistent Analysis of Cylindrical Plasma Antennas," *IEEE Transactions on Antennas and Propagation*, vol. 59, no. 5, pp. 1503–1511, May 2011.

Chapter 2

State of the art on plasma

This chapter deals with the state of the art on plasma in communication systems. This state of the art is divided in three parts. The fundamental of plasma is discussed in the first part of this chapter. In this part is presented the plasma theoretical dealing the laws governed the plasma and how to characterize the plasma. The second part concerns the use of plasma as reflector antenna. The state of the art of the plasma used as radiating element is presented in the third part.

2.1 Fundamentals of plasma

The plasma is the fourth state of matter in which charged particles such as electrons and atom nuclei have sufficiently high energy to move freely, rather than be bound in atoms as in ordinary matter [1]. It exist different types of plasma such the fluorescent lighting tubes, lightning, and ionosphere. The plasma state can also be reached in crystalline structures. Semiconductor materials have electrons in the conduction band and holes in the valence band that move freely. The behavior of charge carriers in semiconductor crystalline structures is analogous to the behavior of particles in gas plasma [2]. The plasma consists of free charge carriers and the interaction of particles in plasma is governed by the laws of electromagnetism and thermodynamics. The plasma is a reconfigurable medium with different conductor and dielectric properties.

2.1.1 Plasma theory

The plasma is a dispersive material. It presents some electrical properties such as electrical conductivity, electric permittivity, and magnetic permeability. The plasma obeys to the Drude model and it is defined by two main parameters, the plasma angular frequency and the electron neutral collision frequency.

2.1.1.1 Plasma conductivity

To obtain the conductivity, let's consider an electron with a charge q moving with a velocity $\mathbf{v}$ through an electric $\mathbf{E}$ and magnetic fields $\mathbf{B}$, the Lorentz force [2, 3] is expressed as:

$$m_e \frac{d\mathbf{v}}{dt} = q(\mathbf{E} + \mathbf{v} \times \mathbf{B}) \tag{2.1}$$

where m_e is the mass of electron. In general, the $\mathbf{E}$ and $\mathbf{B}$ fields are considered varying with time in the free space with the factor of $e^{j\omega t}$.

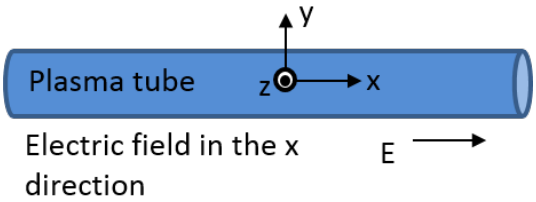

Figure 2.1: E field direction in the plasma.

We consider an incident plane wave with the electric field $\mathbf{E}$ in the x direction and the perpendicular magnetic field $\mathbf{B}$ in the y direction (see Fig. 2.1). Thus, the electric and magnetic fields can be written as:

$$\mathbf{E} = E_0 e^{j\omega t} \mathbf{a_x} \tag{2.2}$$

$$\mathbf{B} = B_0 e^{j\omega t} \mathbf{a_y} = \frac{E_0}{c} e^{j\omega t} \mathbf{a_y} \tag{2.3}$$

where c is the speed of light in free space.

In equation 2.1, the electric and magnetic fields can be substituted by these expressions in equations 2.2 and 2.3.

$$\mathbf{a} = \frac{d\mathbf{v}}{dt} = \frac{q}{m_e}(E_0 e^{j\omega t} \mathbf{a_x} + [\mathbf{v} \times \frac{E_0}{c} e^{j\omega t} \mathbf{a_y}]) \tag{2.4}$$

The equation 2.4 is written under its differential form in Cartesian coordinates (the acceleration is equal at the second differential of the displacement).

$$\frac{d^2x}{dt^2}\mathbf{a_x} + \frac{d^2y}{dt^2}\mathbf{a_y} + \frac{d^2z}{dt^2}\mathbf{a_z} = \frac{q}{m_e}(E_0 e^{j\omega t}\mathbf{a_x} + [\mathbf{v} \times \frac{E_0}{c} e^{j\omega t}\mathbf{a_y}]) = \frac{q}{m_e}(E_0 e^{j\omega t}\mathbf{a_x} - \frac{E_0}{c}\frac{dz}{dt} e^{j\omega t}\mathbf{a_x} + \frac{E_0}{c}\frac{dx}{dt} e^{j\omega t}\mathbf{a_z}) \tag{2.5}$$

Then, each of acceleration component can be expressed by:

$$\frac{d^2x}{dt^2} = \frac{q}{m_e}(1 - \frac{1}{c}\frac{dz}{dt}) E_0 e^{j\omega t} \tag{2.6}$$

$$\frac{d^2y}{dt^2} = 0 \tag{2.7}$$

$$\frac{d^2z}{dt^2} = \frac{q}{m_e}\frac{E_0}{c}\frac{dx}{dt}e^{j\omega t} \tag{2.8}$$

We can deduct the velocity component of the single charge particle from the equations 2.6, 2.7 and 2.8. The velocity in propagation direction is much smaller than the speed of light in free space ($\frac{dz}{dt} \ll c$). Therefore the acceleration component in the x direction becomes:

$$\frac{d^2x}{dt^2} = \frac{q}{m_e}E_0e^{j\omega t} \tag{2.9}$$

and the velocity in the x direction becomes also

$$\frac{dx}{dt} = \frac{q}{m_e}E_0\frac{1}{j\omega}e^{j\omega t} \tag{2.10}$$

thus the displacement in x direction is

$$x = \frac{q}{m_e}E_0\frac{1}{(j\omega)^2}e^{j\omega t} = -\frac{qE_0}{m_e\omega^2}e^{j\omega t} \tag{2.11}$$

The velocity and the displacement in the x direction are for single electron. The plasma is composed of many particles, hence the collective effect electric and magnetic fields on the particles is essential. Considering electric current produced by all the particles, the current density vector is:

$$\mathbf{J_E} = qn_e\mathbf{v}\mathbf{a_x} \tag{2.12}$$

where, n_e is the density of electrons.

By substituting equation 2.10 in 2.12, we obtain:

$$\mathbf{J_E} = qn_e[\frac{q}{m_e}E_0\frac{1}{j\omega}e^{j\omega t}]\mathbf{a_x} \tag{2.13}$$

This equation shows the current flow only in the x axis direction. Moreover the current density can be expressed as a function of the electric field and the conductivity.

$$\mathbf{J_E} = \sigma\mathbf{E} \tag{2.14}$$

According to the equations 2.13 and 2.14 , the conductivity can be formulated as:

$$\sigma E_0e^{j\omega t} = qn_e[\frac{q}{m_e}E_0\frac{1}{j\omega}e^{j\omega t}] \tag{2.15}$$

$$\sigma = -j\frac{n_eq^2}{\omega m_e} \tag{2.16}$$

2.1.1.2 Plasma angular frequency

Having the formulation of the conductivity, an investigation of the behavior of the plasma medium is done because the plasma is a medium of free charge carriers and it exhibits natural collisions that occurs due to the thermal and electrical disturbances. We are interested by the motion of electrons within the plasma. An analysis on the harmonic oscillations of the electrons and the ions are taken into account. Due to the harmonic oscillations of the electrons around the ions, we can assume that the electron density oscillates at an angular frequency ω_p and the $\mathbf{E}$ electric field intensity will also oscillate at the same angular frequency [2, 4]. The density oscillations increases the total free charge density ρ which is related to the volume current density $\mathbf{J}$. The continuity equation is written as:

$$\nabla.\mathbf{J} = -\frac{d\rho}{dt} \tag{2.17}$$

Taking $\mathbf{J}$ as in equation 2.14, the equation 2.17 becomes:

$$\nabla.(\sigma\mathbf{E}) = \sigma(\nabla.\mathbf{E}) = -\frac{d\rho}{dt} \tag{2.18}$$

The electric field and the free charge are related and are expressed as:

$$\nabla.\mathbf{E} = -\frac{\rho}{\epsilon_0} \tag{2.19}$$

By combining the equations 2.16, 2.18 and 2.19, the free charge density ρ is

$$\frac{j}{\omega_p}\frac{n_e q^2}{m_e}\frac{\rho}{\epsilon_0} = \frac{d\rho}{dt} \tag{2.20}$$

The contribution of ions to the plasma is neglected because they are much heavier than electrons, therefore its oscillation will not long last compare to the electrons. Thus the volume charge density expression in equation 2.20 can be supposed to depend only on electron oscillation. The solution of the differential equation is given by:

$$\rho = \rho_0 e^{j\frac{n_e q^2}{\omega_p m_e \epsilon_0}t} \tag{2.21}$$

The angular frequency of oscillation of the free charge density ρ is also ω_p, thus we obtain:

$$\omega_p = \frac{n_e q^2}{\omega_p m_e \epsilon_0} \Rightarrow \omega_p = \sqrt{\frac{n_e q^2}{m_e \epsilon_0}} \tag{2.22}$$

The plasma angular frequency can be also expressed as:

$$\omega_p = 8.94\sqrt{n_e} \tag{2.23}$$

where $q = 1.60217653 \times 10^{-19} C$ is the electron charge
$m_e = 9.1093826 \times 10^{-31} kg$ is the mass of electron
$\epsilon_0 = 8.8541878 \times 10^{-12} \frac{F}{m}$ free space permittivity.

The plasma frequency is noted by f_p, equal to $\omega_p/2\pi$ and its unit is Hz.

2.1.1.3 Plasma permittivity

Since the plasma is a dispersive medium, the complex electric permittivity of the plasma can be calculated by using the derived conductivity term in 2.16.

$$\nabla \times \mathbf{H} = (j\omega\epsilon_0 + \sigma)\mathbf{E} \tag{2.24}$$

$$\nabla \times \mathbf{H} = j\omega\epsilon_0(1 + \frac{\sigma}{j\omega\epsilon_0})\mathbf{E} \tag{2.25}$$

The plasma permittivity can be given for two cases, without or with the effect of the collisions. By substituting the conductivity obtained in equation 2.16, into the right hand of the equation 2.25, the equation becomes

$$j\omega\epsilon_0(1 + \frac{\sigma}{j\omega\epsilon_0})\mathbf{E} = j\omega\epsilon_0(1 - \frac{n_e q^2}{\omega^2\epsilon_0 m_e})\mathbf{E} \tag{2.26}$$

Then, the relative permittivity without collision ($\nu = 0$) is

$$\epsilon_r = (1 - \frac{n_e q^2}{\omega^2\epsilon_0 m_e}) = (1 - \frac{\omega_p^2}{\omega^2}) \tag{2.27}$$

2.1.1.4 Effects of electron neutral collision

In the previous sections (2.1.1.1 and 2.1.1.3), it was assumed that there is no loss of electron due to the collisions between electrons and other particles constituting the plasma. The mass of electron m_e in equation 2.1 becomes m (m represent more than one particle involded in the collisional) in the new equation and this equation can be written as:

$$m\frac{d\mathbf{v}}{dt} + m\mathbf{v}\nu_{col} = q(\mathbf{E} + \mathbf{v} \times \mathbf{B}) \tag{2.28}$$

where ν_{col} is the collision effect (plasma electron neutral collision frequency). When the time dependence $e^{j\omega t}$ is assumed, the left side of the the equation 2.28 gives:

$$j\omega m\mathbf{v}(1 + \frac{\nu_{col}}{j\omega}) = j\omega m\mathbf{v}(\frac{\omega - j\nu_{col}}{\omega}) \tag{2.29}$$

This result shows that by substituting the m_e in equation 2.16, by $m(\frac{\omega - j\nu_{col}}{\omega})$, the conductivity with the effects of collisions can be rewritten as:

$$\sigma = -j\frac{n_e q^2}{m(\omega - j\nu_{col})} \tag{2.30}$$

The permittivity can be also expressed in presence of effects of the collisions. Therefore, when we replace the conductivity obtained in equation 2.30 into the right side of the equation 2.26, the equation becomes:

$$j\omega\epsilon_0(1+\frac{\sigma}{j\omega\epsilon_0})\mathbf{E} = j\omega\epsilon_0(1-\frac{n_e q^2}{\omega\epsilon_0 m_e(\omega - j\nu_{col})})\mathbf{E} \tag{2.31}$$

Then the relative permittivity of the plasma with collision effect is:

$$\epsilon_r = (1-\frac{n_e q^2}{\omega\epsilon_0 m_e(\omega - j\nu_{col})}) = 1-\frac{\omega_p^2}{\omega(\omega - j\nu_{col})} \tag{2.32}$$

Having the complex permittivity and the conductivity as function of the plasma angular frequency, the wave angular frequency and the electron-neutral collision frequency, the interaction of electromagnetic waves and plasma medium will be inspected in this section by examining the propagation constant, intrinsic wave impedance and conductivity.

The propagation constant is equal to $\omega^2\mu\epsilon = \omega^2\mu\epsilon_0\epsilon_r$ from Helmholtz equation. The wave number of the propagation constant can be expressed without collision effects as:

$$k = \omega\sqrt{\mu\epsilon_0(1-\frac{\omega_p^2}{\omega^2})} \tag{2.33}$$

and with collision effects

$$k = \omega\sqrt{\mu\epsilon_0(1-\frac{\omega_p^2}{\omega(\omega - j\nu_{col})})} \tag{2.34}$$

When $\omega > \omega_p$, the propagation constant is real, the permittivity is positive and the wave propagates in plasma. In this case, the plasma medium has dielectric properties. When $\omega < \omega_p$, the propagation constant is imaginary, the permittivity is negative and the plasma medium can have conductor properties. It can reflect or absorb the incoming wave depending on the electron collision frequency.

The permittivity term defined by $\epsilon_r = \epsilon' - j\epsilon''$, shows that the conductivity depends strongly with the electron collision frequency. At high collision frequency, the plasma medium behaves as a lossy medium. The electron neutral collision participates only for loss and the plasma angular frequency participates for both (relative permittivity and loss).

2.1.2 Characterization

The section describes different manners to characterize the parameters of the plasma medium used in commercial fluorescent lamps. As the manufacturers of lamps do not give any details, the estimation of plasma parameters is necessary in order to have realistic plasma. For this reason, several techniques to estimate the plasma parameters are found in the literature. In [5] the authors characterize the plasma by using microwave interferometry which uses single fluorescent lamp as illustrated in Figure 2.2. Microwave interferometry is an established non-perturbing plasma diagnostic technique to measure plasma number density that is simple, accurate, robust, and reliable. On the another hand, the authors in [6] and [4], make a convential isolation measurement that uses several fluorescent lamps tubes arranged in parallel to form a plasma wall. The plasma slabs are shown in Figure 2.3.

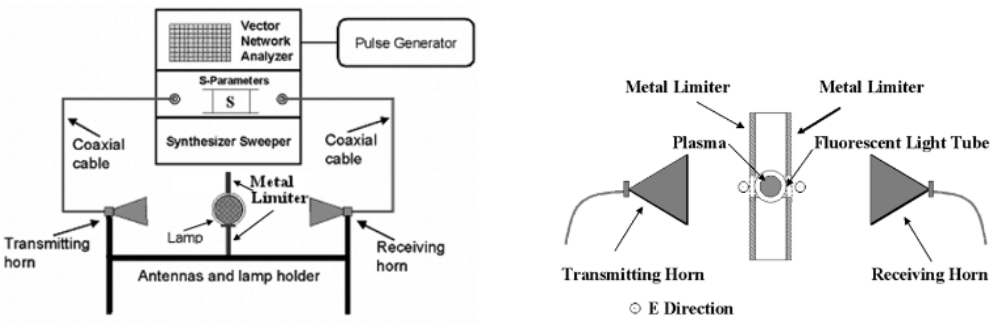

(a) (b)

Figure 2.2: Experimental setup. (a) Block diagram of the measurement system. (b) Detailed view focused on the limiter to block and control the signal through the fluorescent light tube. [5]

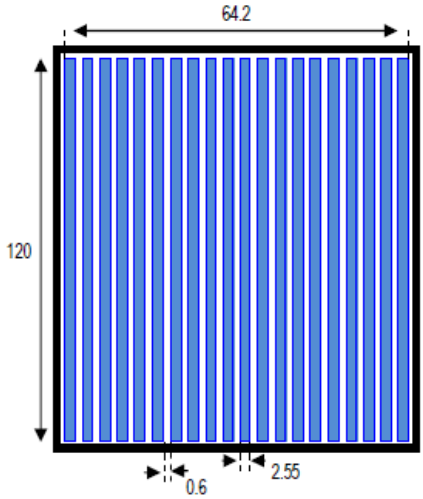

Figure 2.3: Schematic diagrams of the devices under test (DUT), plasma wall made of 20 fluorescent lamps arranged in parallel (blue color represents fluorescent lamps). (Unit in cm). [4]

This section shows the technique of measurement used in [4] in order to estimate the plasma angular frequency and the electron neutral-collision frequency. The measurements are done in small anechoic chamber. The measurement system consists of a pair of wide band antennas (2 GHz - 18 GHz), a network analyzer and the devices under test.

The plasma wall was realized by using fluorescent lamps arranged in parallel (see Fig. 2.4). The lamp socket is bi-pin G13 and regulated by electronic ballasts. The gap between two consecutive lamps is 6 mm due to the lamp socket.

Figure 2.4: Photographs of the device under test (DUT), plasma wall made of 6 fluorescent lamps arranged in parallel (measurements are conducted with 20 fluorescent lamps). [4]

The measurement setup is shown in Figure 2.5. The distance between each antenna (transmission and reception) to the devices under test is 100 cm.

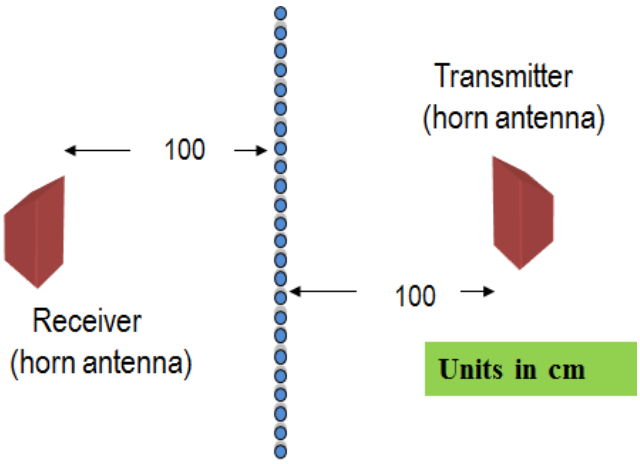

Figure 2.5: Measurement setup. [4]

The measurement in [4] was performed in three cases which are free space case, plasma OFF and plasma ON. The measured results based on the performance of plasma isolation are presented. In plasma OFF case, the isolation performance is similar to the free space case as represented in Figure 2.6(a). This result proves that the glass surrounding the plasma doesn't effect it and means that the glass is quasi transparent for the electromagnetic wave. In plasma ON case, attenuation effects are observed at the region below than 7 GHz and at the region upper to 8.8 GHz (see Fig. 2.6(b)). The transition behavior of

the plasma from reflector to dielectric is shown in Figure 2.6(c) and this transition star to 7 GHz up to 8.8 GHz.

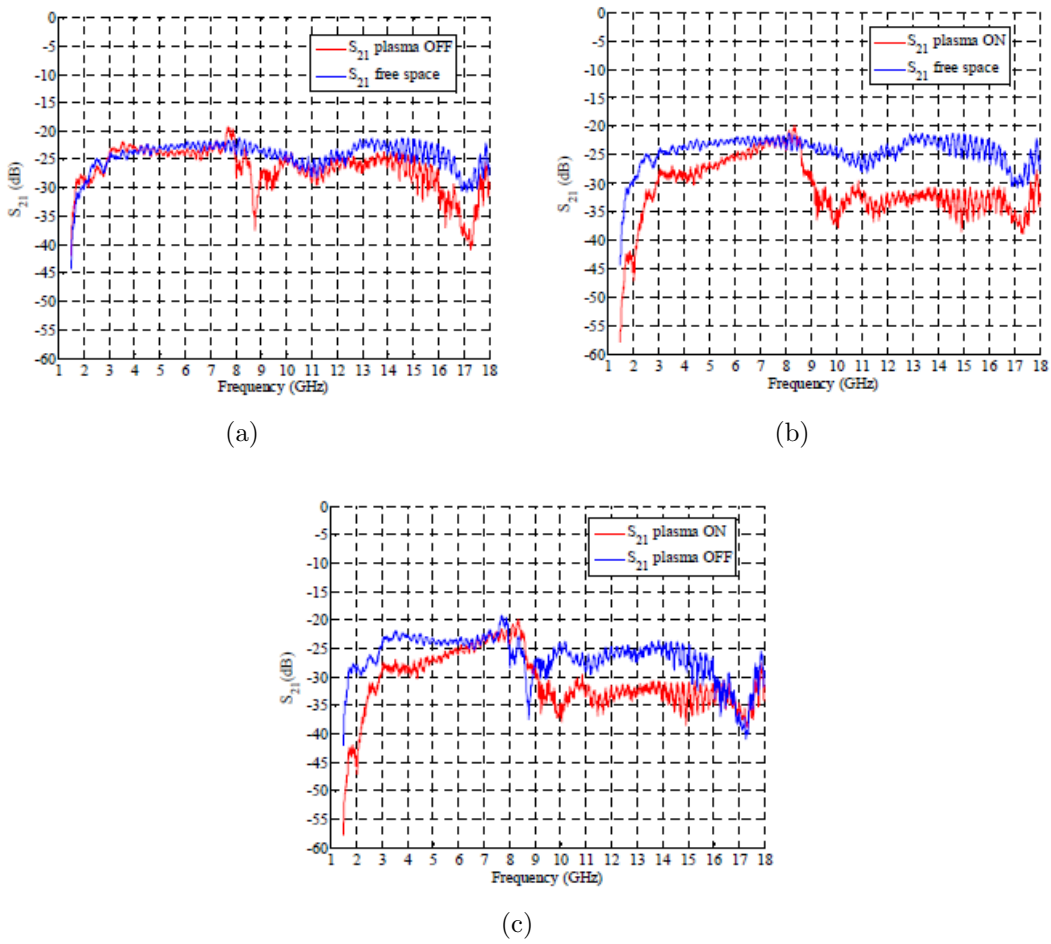

Figure 2.6: Measured transmission coefficients. (a) Plasma OFF and the free space. (b) Plasma ON and the free space. (c) Plasma ON and plasma OFF. [4]

This result shows that, the plasma frequency is estimated from 7 GHz to 9 GHz (See Fig. 2.6(c)). The approximation value of the plasma frequency chosen in [4] is 7 GHz meaning $\omega_p = 2 * \pi * 7.10^9 = 43.9823 \times 10^9$ rad/s.

In order to find the electron neutral collision frequency, a monopole operating at 4 GHz with a compact fluorescent lamp has been simulated and measured. Figure 2.7 shows the monopole with a height of 17 mm and the dimension of the ground plane is 300×300 mm^2. The compact fluorescent lamp is placed at 18.75 mm from the monopole and its height is 40 mm.

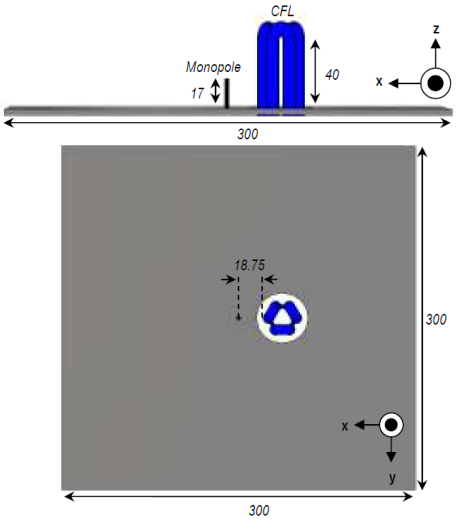

Figure 2.7: Schematic diagram of antenna used for the radiation pattern measurement. (Unit in mm). [4]

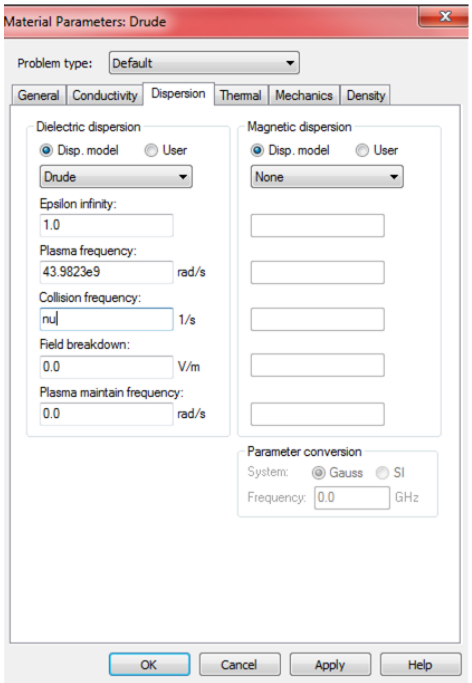

Figure 2.8: Plasma parameters defined on CST window. [7]

The radiation patterns in simulation for different plamsa electron neutral collision frequencies are compared to the measured radiation pattern. The simulated model is defined

with the plasma angular frequency $\omega_p = 43.9823 \times 10^9$ rad/s and a variable elctron neutral collision frequency. The plasma is modeled by using the Drude model in CST [7]. This Drude model is defined by two parameters which are the plasma angular frequency and the electron neutral collision frequency. The parameter setup window in CST software is presented in Figure 2.8 with $\omega_p = 43.9823 \times 10^9$ rad/s and the variable plasma electron neutral collision frequency ν_{col}.

A set of simulations by varying the electron neutral collision frequency from 100 MHz up to 3 GHz is done in order to find which value of the electron neutral collision frequency matchs the measured result. The Figure 2.9 shows that the effect of electron neutral on the simulated radiation patterns at 4 GHz is not significant when the plasma electron neutral collision frequency varies from 100 MHz to 3 GHz. The electron neutral collision frequency choose in [4] for its study is 900 MHz.

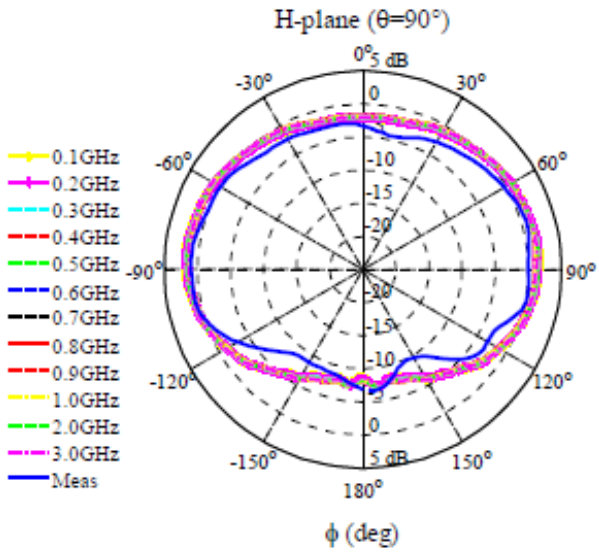

Figure 2.9: Effect of electron-neutral collision frequency on radiation pattern, E_θ components at 4 GHz. [4]

2.2 Plasma as reflector element

Since many years, an investigation on plasma reflectors called plasma mirror has been done in order to steer the beam of the antenna in particular direction expecially in radar systems [8–13]. Recently, plasma reflectors realized by using the fluorescent lamps were presented in many papers. The most utility of plasma reflector is to have a beam steering, beam scanning and beam shaping capabilities. This section is divided in two parts depending on the shape of the plasma reflectors. The first one, discusses about parabolic and corner

reflectors by using plasma fluorescent lamps and the second one presents the circular plasma reflectors using also fluorescent lamps.

2.2.1 Parabolic and corner plasma reflectors

This section describes the use of plasma system as parabolic and corner reflectors found in the literature. In [14], the authors realized a plasma parabolic reflector at 3 GHz in order to steer the beam. The realized plasma parabolic reflector is shown in Figure 2.10. The same authors in [15], enhanced the plasma parabolic concept by using commercial fluorescent lamps. The performance of this plasma parabolic reflector was compared with an identical metal parabolic reflector. The realized plasma and metal parabolic reflectors placed in an anechoic chamber are presented in Figure 2.11.

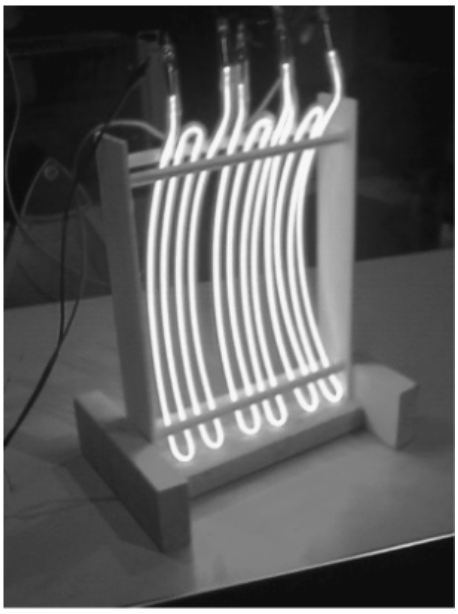

Figure 2.10: Plasma reflector. [14]

Figure 2.12 shows the radiation pattern of the plasma parabolic reflector compared with the one of metal parabolic reflector. The obtained results with plasma and metal are quite similar. It was reported that when the plasma is not excited (plasma OFF), the reflected signal is lower than -20 dB. The results show that the use of plasma reflector is capable to give similar results than with the metal reflector at 3 GHz. Another advantage is the reconfigurabilty given by the plasma reflector.

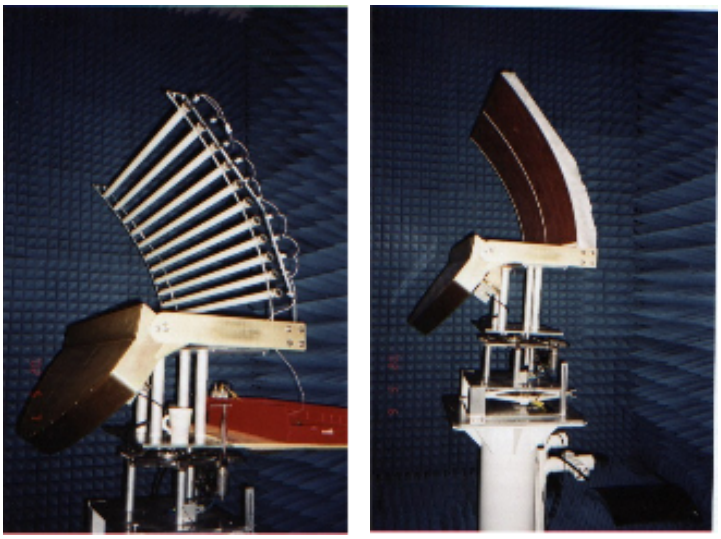

(a) (b)

Figure 2.11: Reflectors antennas. (a) Plasma reflector antenna installed in an anechoic chamber. (b) A metal reflector antenna designed to be an identical twin to the plasma reflector antenna. [15]

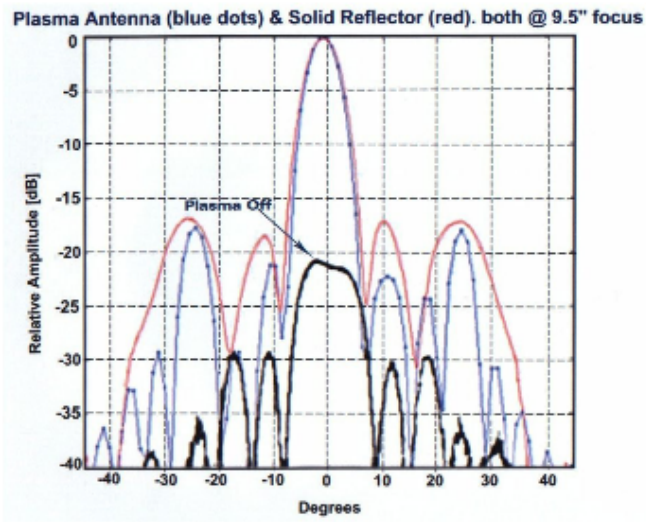

Figure 2.12: Comparison of radiation patterns for plasma reflector (blue dots) and metallic reflector (red). [15]

In [16], the authors present the performance of a reconfigurable plasma corner-reflector antenna. The designed and manufactured structure are shown in Figure 2.13. The U-shaped lamps are aligned and dual corner reflectors are made with a total of 24 lamps.

The first corner reflector is composed of 8 U-shaped lamps while the second is composed of 16 U-shaped lamps. As seen in the figure 2.13(a), the distance between the monopole and the first corner reflector is $s = 0.5\lambda$ while the distance between the monopole and the second corner reflector is $s = \lambda$. The plasma angular frequency is 43.982310^9 rad/s and the electron neutral frequency is 900 MHz.

As reported in [16], the idea was to have three switchable beam shapes, only several of the lamps were energized (ON state) in order to work as a reflector at one time.

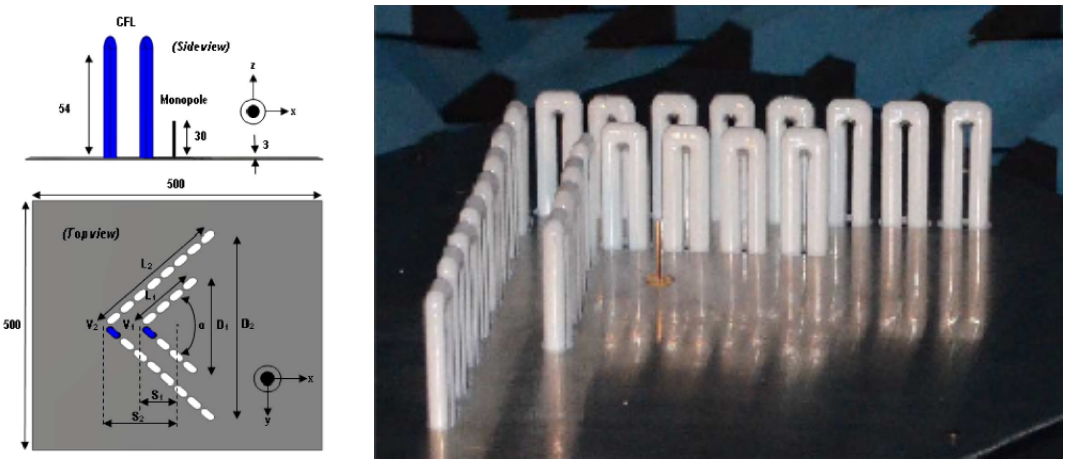

(a) (b)

Figure 2.13: Geometry of the plasma corner reflector. (a) Illustrated model (units in millimeter). (b) Realized model with 24 elements. [16]

The results obtained in simulation and measurement are shown in Figures 2.14(a) and 2.14(b) respectively. Three radiation patterns are presented:

- when all lamps are in OFF state,
- when all the lamps in the first corner reflector are in ON state while the lamps in the second corner are in OFF state,
- when all the lamps in the second corner reflector are in ON state while the lamps in the first corner reflector are in OFF state.

The presented results show that the radiation pattern of the corner reflector can be changed from single beam to dual beam configuration. The single beam is obtained when only the lamps in the first corner reflector are switched ON while the dual beam is obtained when only the lamps in the second corner reflector are switched ON. However, when all the lamps are in OFF state, the classical omnidirectional radiation pattern for the monopole is obtained.

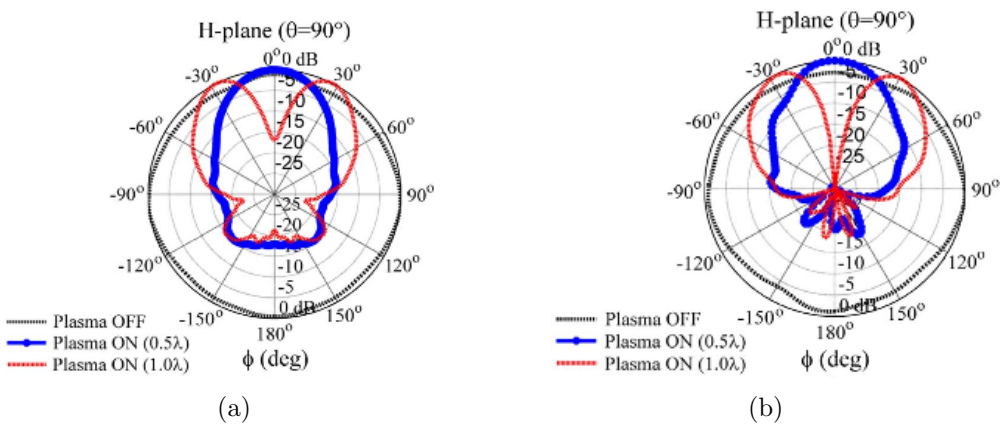

Figure 2.14: Normalized H-plane radiation patterns at 2.4 GHz.(a) Simulation. (b) Measurement. [16]

2.2.2 Circular plasma reflector

The state of the art of some circular reflectors using plasma fluorescent lamps is presented in this section. Igor Alexeff et al. presented in [17–19] important works on plasma reflectors. The plasma lamps were arranged in circular configuration in order to have a beam scanning. The design of the plasma reflector antenna at 2.5 GHz is shown in Figure 2.15. An aperture is made in order to steer the beam when any plasma lamp is in OFF state. The aperture beam depends on the number of elements switched OFF.

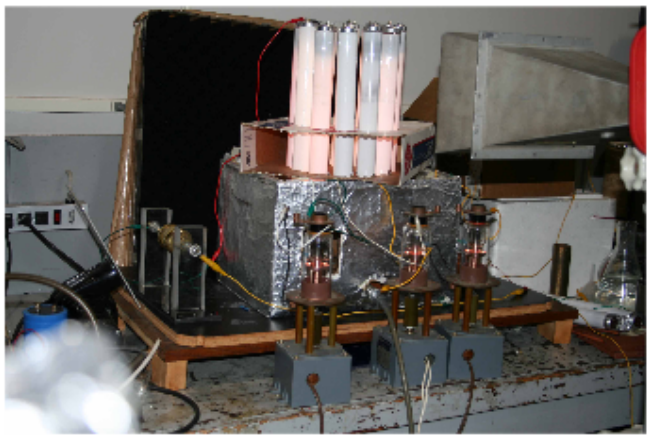

Figure 2.15: Demonstration of a prototype for an intelligent plasma antenna. A ring of plasma tubes operating beyond microwave cut-off surrounds a metal transmitting antenna. [18]

Similar arrangement was realized in [20], the plasma was arranged in circular allowing

a beam steering antenna. The geometry of the plasma beam scanning antenna is shown in Figure 2.16. The reflecting elements are supposed to be Argon gas with pressure from 1 to 5 Torr, encapsulated in T12 and T18 domestic lamps. The density of electron is 9.24×10^{17} m^{-3} and the electron neutral collision frequency equals to 6.83×10^{7} Hz. A monopole is placed at the center of the arranged reflecting elements and the distance between the monopole and each element is 0.0641 m.

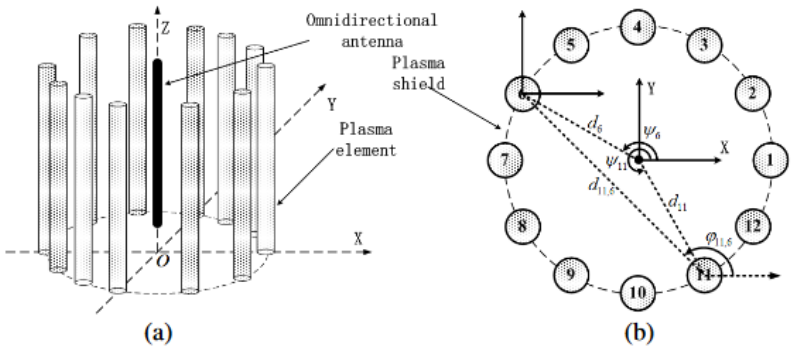

Figure 2.16: Geometry of the plasma antenna of beam scanning (12 plasma elements in this case). (a) The solid side view of the antenna.(b) The top plan view of the antenna. [20]

The numerical results are shown in figure 2.17. The results present the radiation pattern for a single beam at 4.3 GHz, 5.9 GHz and 7.2 GHz, the double beam and beam scanning at 8.1 GHz.

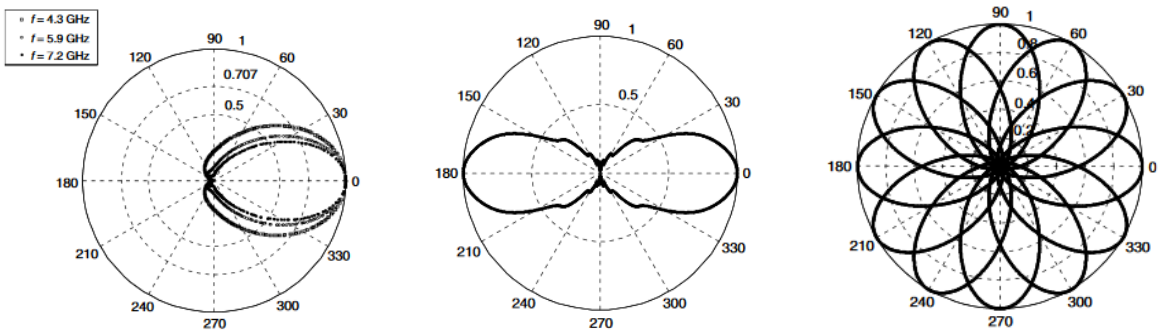

Figure 2.17: Radiation pattern for the plasma antenna. (a) Single beam at 4.3 GHz, 5.9 GHz and 7.2 GHz. (b) Double beams for the antenna at 8.1 GHz with 1st and 7th de-energized. (c) Single beam-scanning at 8.1 GHz. [20]

In [21], the simulated performance of a monopole at 4.9 GHz with circular plasma

fluorescent lamps used as reflectors have been presented. The fluorescent tube consists of a glass tube filled with mixture mercury vapor and argon gas. The plasma angular frequency is 5.634×10^{11} rad/s and the electron neutral frequency is 10^9 Hz. The structure of the monopole with fluorescent lamps is shown in Figure 2.18.

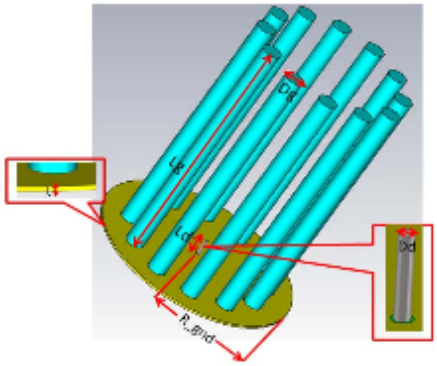

Figure 2.18: Geometry of monopole antenna with fluorescent tubes. [21]

It was reported that when the plasma tubes are switched OFF, the gain of the antenna is 1.35 dB and when the tubes are switched ON the gain becomes 6.66 dB.

Recently in [22], a round reflector antenna using U-shaped compact fluorescent lamps was presented. A monopole operating at 2.4 GHz is placed at the center of the U-shaped lamps arranged in a circular configuration (see Fig. 2.19).

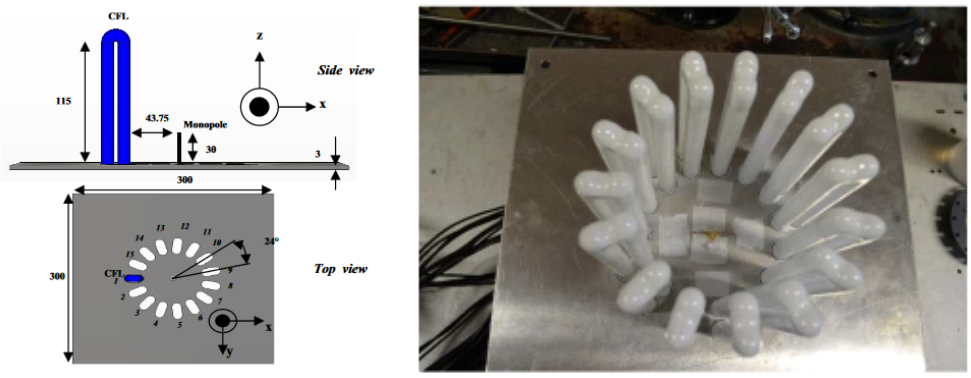

(a) (b)

Figure 2.19: (a) Geometry of a single reflective element (blue color) and a monopole antenna with finite ground plane (units in mm). Each element is numbered by its location. (b) Top view of the realized prototype with 15 elements on a finite ground plane. [22]

The angle between center axes of two adjacent elements is 24°, and it is depending on

the distance between monopole and reflector elements. In the simulations, there are 15 elements to cover 360°. The same plasma parameters than in [16] are used here.

The performance of the scanning capability of the antenna is shown in Figure 2.20. To scan the beam from 0° to 360°, only 9 lamps are need to be switched ON then we shift these 9 lamps. The smallest scanning step is 48°. As reported by the authors, the simulated and measured results were in good agreement and the beam can be directed in desired direction with appropriate numbers of elements which are switched ON.

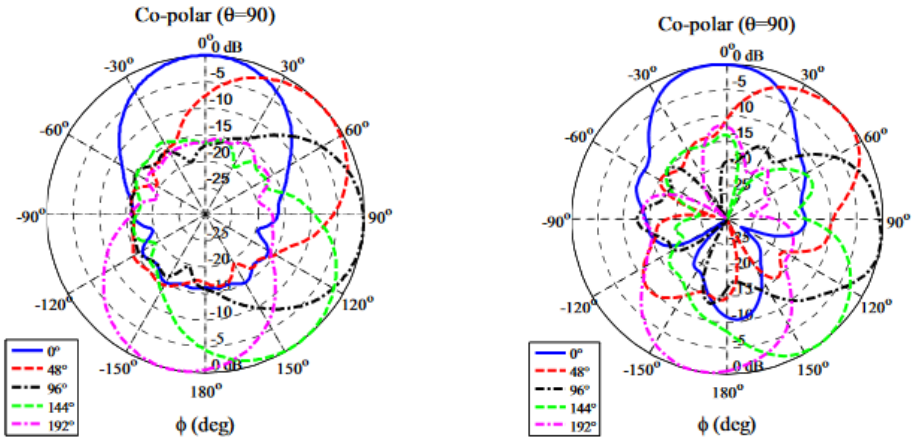

Figure 2.20: Normalized H-plane radiation patterns at 2.4 GHz. (a) Simulation. (b) Measurement. [22]

In 2016, jafar et al. proposed in [23] the same concept than in [22]. A monopole antenna operating at 2.4 GHz surrounding by round reflector plasma. This round reflector was realized using 12 commercial cylindrical shaped fluorescent tubes that contain the mixture of mercury vapor and argon gas. The height of each plasma tube from ground plane surface is 288 mm and its diameter is 16 mm. The realized prototype is shown in Figure 2.21.

As reported in [23], a number of activated elements (switched ON) defines the size of plasma window thus controlling the beam direction. In this investigation, with the optimized reconfigurable plasma antenna array, only 7 elements are activated (switched ON) at the same time while 5 elements are de-activated (switched OFF). The smallest scanning angle is 30°.

Figure 2.22 shows the simulated and measured radiation pattern in H-plane at 2.4 GHz for the two first steering angles (0° and 30°). The results show clearly that the reconfigurable radiation patterns can be pointed with twelve different steerable beam directions at 2.4 GHz (0°, 30°, 60°, 90°, 120°, 150°, 180°, 210°, 240°, 270°, 300°, and 330°). The results of the simulation seem to agree well with the measurement results.

Figure 2.21: Geometry of monopole antenna with fluorescent tubes. [23]

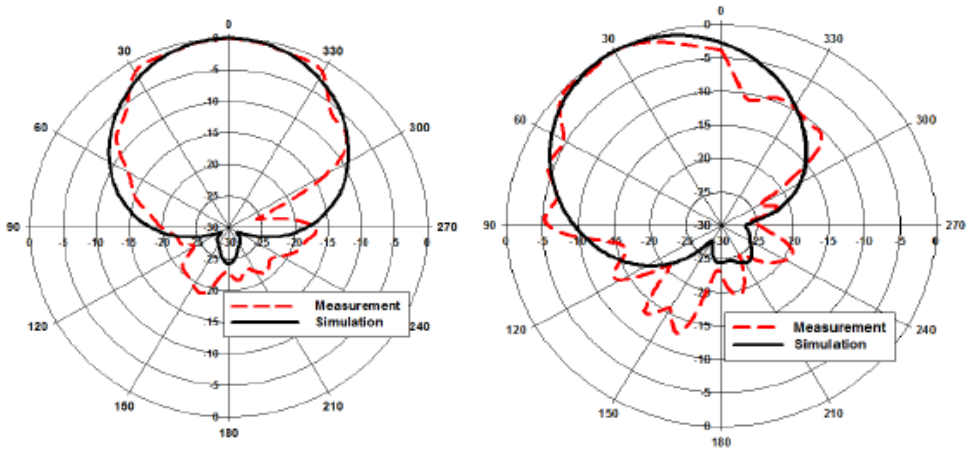

(a) (b)

Figure 2.22: (a) Simulated and measured radiation pattern in H-plane at frequency 2.4 GHz at angles. (a) 0°. (b) 30°. [23]

In [24], the authors design a monopole antenna working at 750 MHz but surrounding by a square reflector. A total of 20 U-shaped lamps have been used to realize this square reflector. The Figure 2.23 shows the designed antenna.

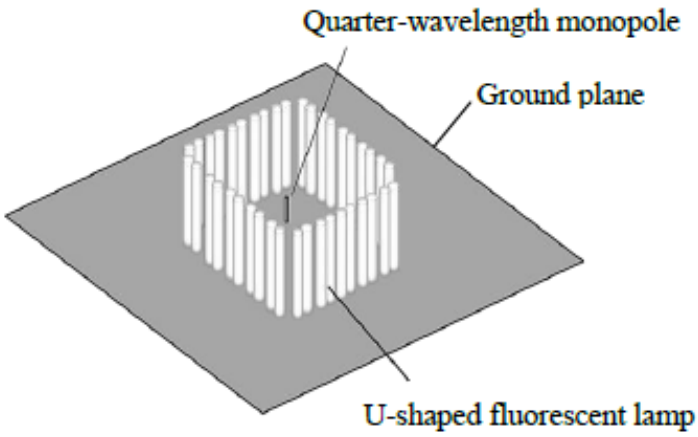

Figure 2.23: Geometry of monopole antenna surronding by fluorescent tubes arranged in a square configuration. [24]

The measured radiation patterns for different cases (lamps switched ON or OFF) are presented in Figure 2.24.

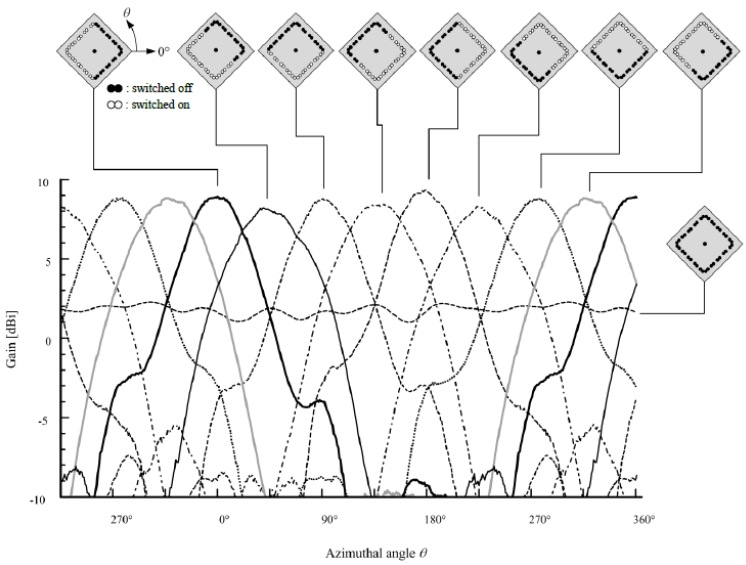

Figure 2.24: Radiation patterns for different cases. [24]

2.3 Plasma as a radiating element

This section aims to discuss the state of the art of the plasma used as a radiating element. Many investigations have been done and the study can be divided in three parts which are

the excitation techniques, the RF coupling techniques and the performance of some plasma antennas found in the literature. The excitation technique means how to generate plasma into the tube i.e. how to ionize the gas inside the tube. If radio signal is used to excite plasma, a filtering device in the receiver part is needed to filter the excitation signal. The coupling technique shows the models to have radio signal onto the plasma column.

2.3.1 Excitation techniques

Several techniques to energize the plasma exist in the literature. The most excitation techniques frequently used are: AC supply, RF discharges, Microwave discharges and laser excitation.

An AC supply is used in [15, 17, 25–29]. Generally, the fluorescent lamp tube operates with an AC supply. The fluorescent lamp differs to the incandescent lamp because it has not heating filament but it has a set of cathodes. On each side of the tube, it exists a coiled tungsten filaments as cathode that coated with an electron-emitting substance. Thus the plasma is ionized by applying an AC supply.

RF discharge is a simple technique to excite plasma in glass tube. This technique consists to have two cooper rings. The first one is reserved to the plasma excitation and pumps the RF energy and the second one is used for the information signal. A strong field is created between the first cooper ring and the ground plane. The electric lines of the electric fields penetrate inside the tube and excite the plasma media. These RF discharges are used in [30–32].

Microwaves discharges have been used [33–35] in order to excite plasma in cylindrical tube. The microwave discharges is realized by using a device called "surfaguide". In [36, 37] for instance, a numerical model similar to microwave discharges to excite the plasma was proposed.

In [38], a plasma generated by laser excitation is presented. A virtual reconfigurable plasma antenna consisting of a set of laser plasma filaments produced in air by the propagation of femtosecond laser pulses was investigated.

2.3.2 Coupling techniques

Since the plasma is encapsulated in a glass tube, it is not possible to go through this tube with a RF coaxial probe. Due to this problem, coupling techniques are necessary to have a radio signal along the plasma tube. It exists two types of coupling techniques which are capacitive or inductive. The capacitive coupling is more used in the literature due to the simplicity of implementation and all the papers presented in the rest of this chapter use this technique.

This capacitive coupling uses coupling sleeve. Some of the coupling sleeves seen in the literature are presented in Figure 2.25. A coaxial probe is placed between a metal box and the coupling sleeves.

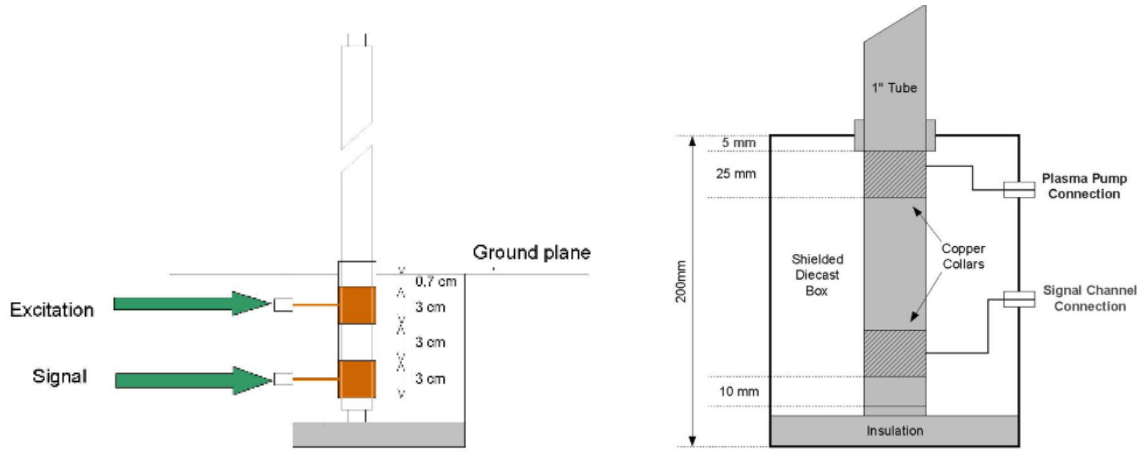

(a) (b)

Figure 2.25: Coupling sleeve in a excitation box. (a) Coupling sleeves presented in [31]. (b) Coupling sleeve presented in [30].

In [30, 31], two coupling sleeves were used, one for the RF information signal and another to energize or excite the plasma media. The measured result is presented in Figure 2.26 for the coupling between the two ports when the plasma is excited. A strong coupling can be observed between the excitation and the RF signal port.

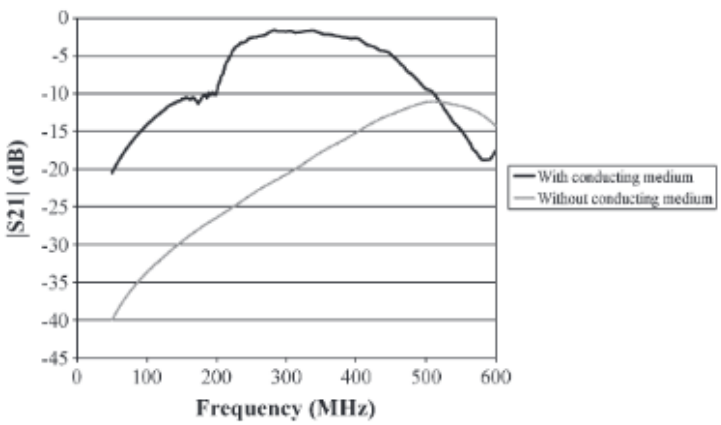

Figure 2.26: Coupling between the two ports with (black) and without (gray) the conducting medium. [31]

Due to the strong coupling between the two ports, a decoupling system was proposed in [31] to avoid the coupling effect between the excitation port and the the RF port (see Fig. 2.27).

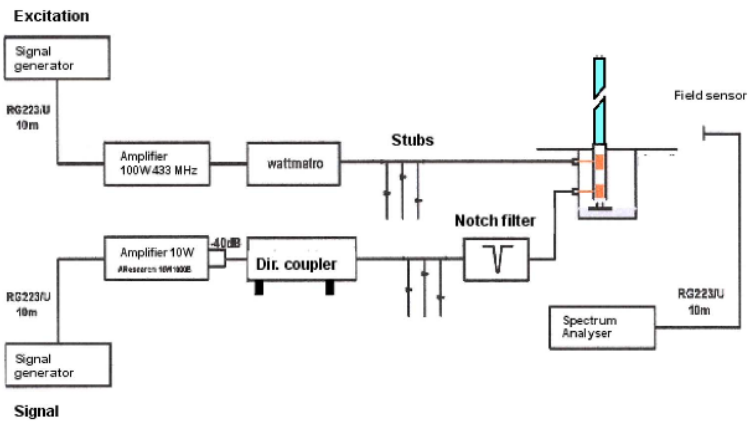

Figure 2.27: Decoupling system. [31]

2.3.3 Performance of plasma antennas in literature

In [15], Anderson et al. proposed two kind of plasma antennas. The first antenna is presented in Figure 2.28(a) with the coupling system inside the metal box and the second antenna is used for receiving radio FM and AM waves (see Fig. 2.28(b)).

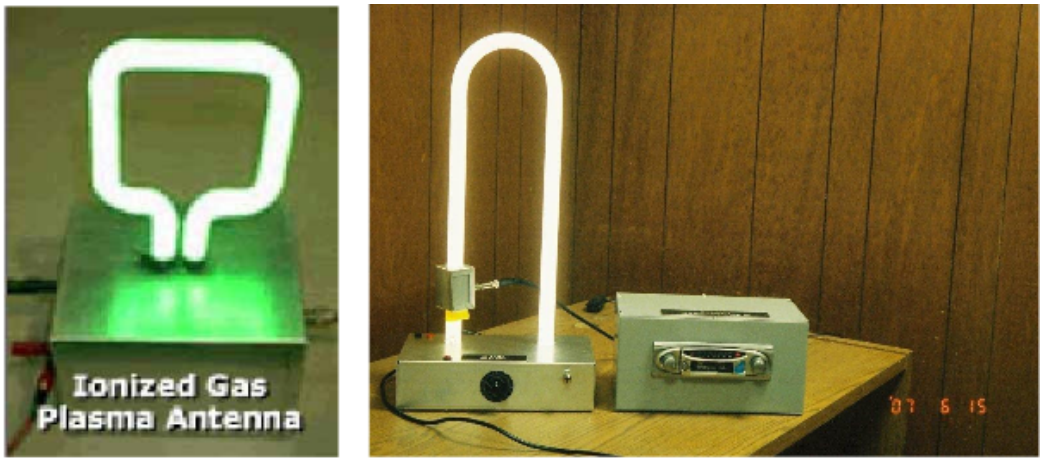

(a) (b)

Figure 2.28: Monopole antennas. (a) Plasma antenna (b) Plasma antenna connected to a radio receiver. [15]

When the density of electron in the plasma tube (U-shaped) increases, the plasma becomes more conductive and therefore the antenna works in FM. On the other hand, for lower density the antenna works in both FM and AM.

V. Kumar et al. in [39] proposed a plasma monopole antenna using a plasma commercial fluorescent lamp with a length of 20 cm and diameter of 1 cm. In order to excite the plasma, an AC supply is used by varying the frequency from 25 Hz to 200 Hz. The experimental setup is shown in Figure 2.29.

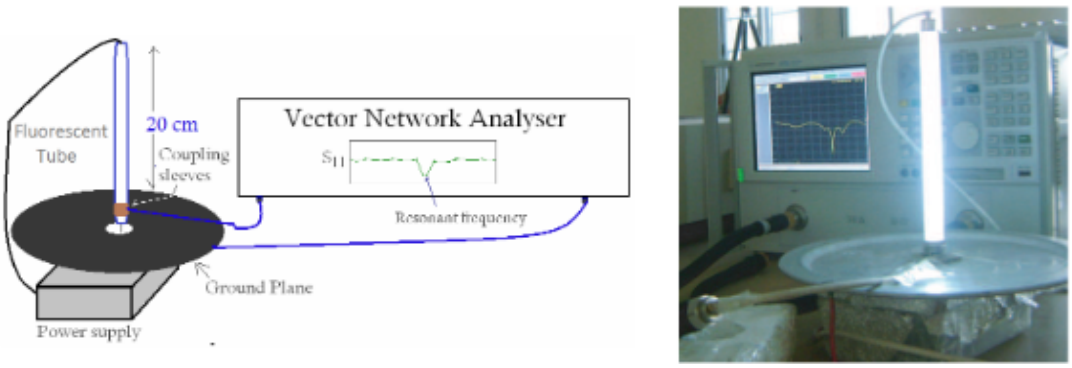

(a) (b)

Figure 2.29: Experimental setup of plasma antenna. (a) Illustration of the measurement setup. (b) Photo of the manufactured antenna. [39]

The reference return loss is named "A" which is the return loss in switch OFF mode. In a switch ON mode, two most different fluctuating results which explain the antenna loss characteristics of the fluorescent tube as plasma antenna are shown in Figure 2.30 and named curves "B" and "C".

For highest AC frequency (200 Hz AC), the measured return loss is shown in Figure 2.30 and the value is equal to -34 dB at 596.9 MHz. It is important to notice that the stability of the resonant frequency increases by increasing the frequency of the AC power supply measured up to 200 Hz.

Figure 2.30: The return loss characteristic for an AC voltage frequency of 200 Hz.[39]

Figure 2.31 shows the measured radiation of the plasma antenna in both polarization (co and cross) at 590 MHz. It is clear to see that the level in both polarization are quite similar from 0° to 60°. The authors conclude that this result is due to the scattering of the fields from the cable used to energize the plasma fluorescent lamp.

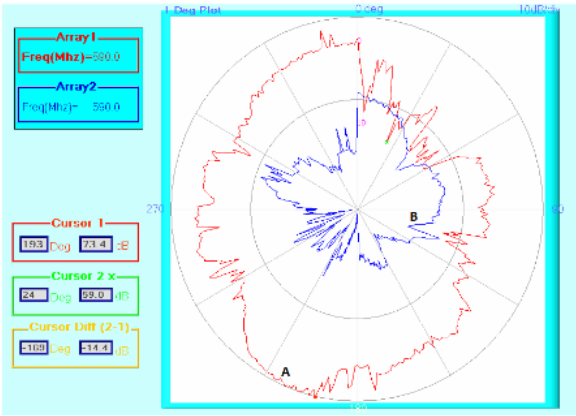

Figure 2.31: Antenna radiation pattern at 590 MHz. Co-polarization (red line) and cross-polarization (blue line). [39]

In [40], a monopole plasma antenna is presented. A commercial fluorescent lamp with 0.5 m length and 0.008 m diameter was used as radiating element. In order to energize the plasma, an electronic ballast was implemented. To couple the RF signal to the tube, an aluminum ring is placed around the tube and a SMA probe is inserted between the ring and the metallic box (coupling sleeve). The Figure 2.32 shows the antenna structure and the realized antenna.

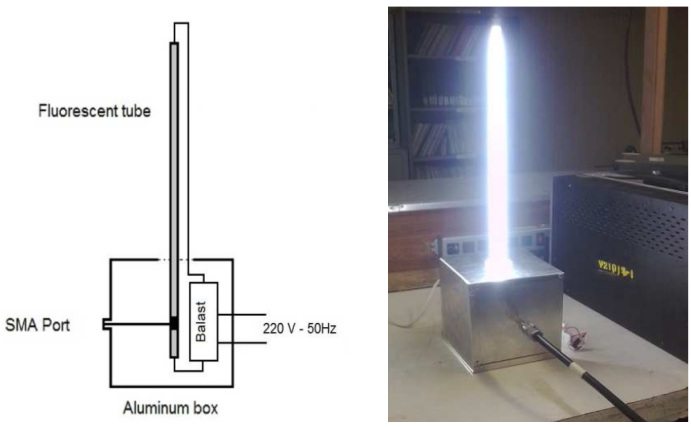

(a) (b)

Figure 2.32: Plasma antenna structure. (a) Illustrated plasma antenna. (b) Fabricated plasma antenna. [40]

The electron density is assumed to be not uniform and calculated by COMSOL Multiphysic then exported in CST. The collision frequency is fixed at 2×10^8 Hz.

The measured return loss is compared to the simulated one. The Figure 2.33 shows that the simulation and measurement results are in good agreement. The simulated resonance is at 124 MHz (-20.6 dB) and the measured resonance is at 118.4 MHz (-26.7 dB).

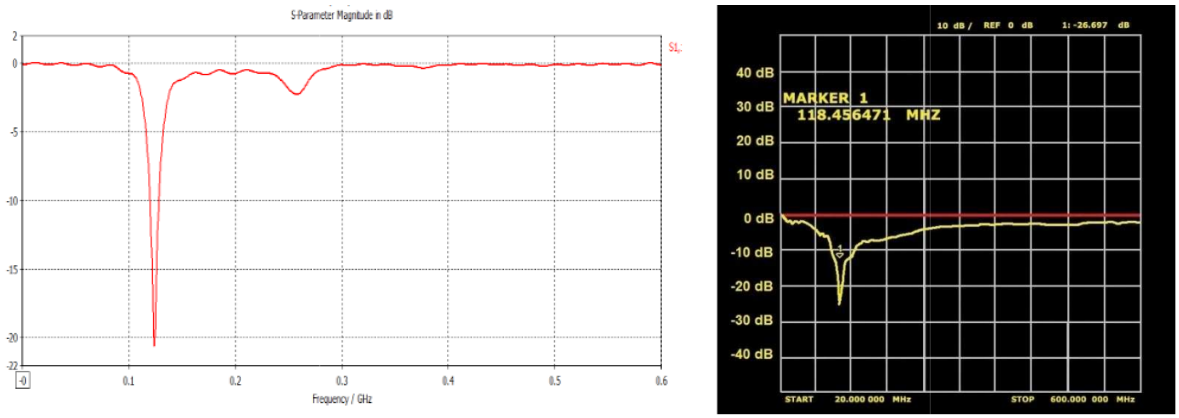

(a) (b)

Figure 2.33: Return loss. (a) Simulation. (b) Measurement. [40]

In [26], the authors built two plasma antennas of 1 m and 60 cm length respectively (see Fig. 2.34). The plasma antenna was constructed from 12 mm outer diameter and 10 mm inner diameter tube. This tube is filled with Ne gas at 2.5 Torr. The plasma frequency is equal to 8 GHz. The measured radiation pattern was done for 60 cm monopole plasma.

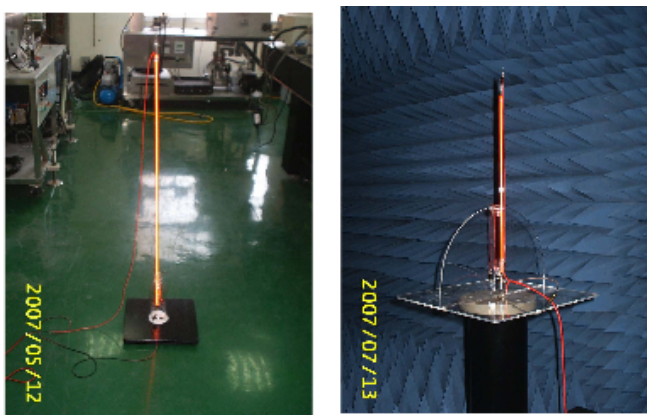

(a) (b)

Figure 2.34: Photos of the plasma antennas. (a) Plasma antenna with 1 m length. (b) Plasma antenna with 60 cm length. [26]

To energize the plasma, there are two cathode electrodes on both side of the tube. Thus, the communication signal is coupled to the antenna by using capacitive coupling as shown in Figure 2.35.

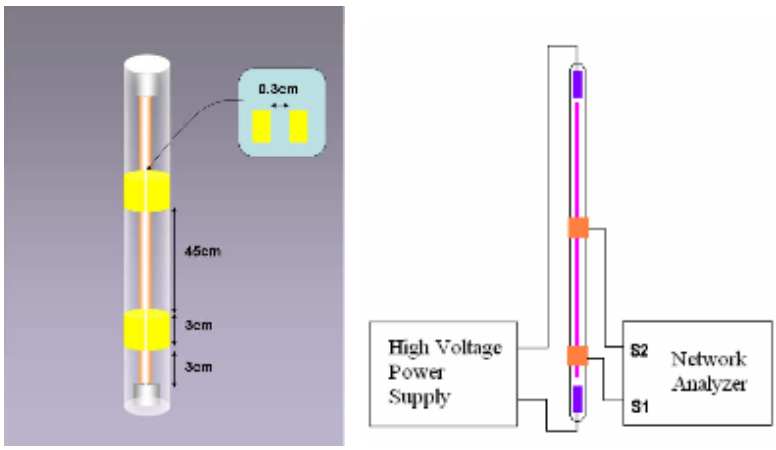

(a) (b)

Figure 2.35: (a)-(b) Two copper foils are used for signal coupling measurement with two different coupling locations at the bottom end and at the center of the tube. [26]

The return loss with and without plasma are almost similar from 1 GHz to 5 GHz (see Fig. 2.36).

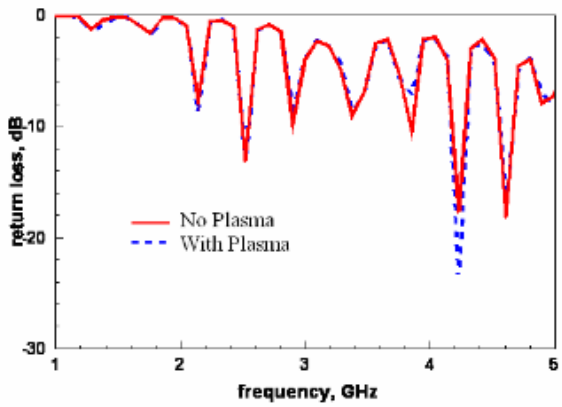

Figure 2.36: The return loss from port 1 of the 60 cm plasma antenna at 30 mA plasma conduction current. [26]

The radiation patters are shown in Figure 2.37. However it didn't show expected omnidirectional shape due to the DC wire. On the other hand, it presents many side lobes

that change with respect to frequency and direction of the antenna.

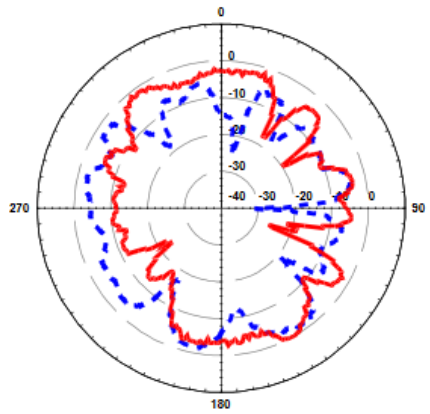

Figure 2.37: The E-plane radiation pattern of the 60 cm plasma antenna at 4.2 GHz. Red curve is co-polarization; blue curve is cross-polarization. [26]

Furthermore, in [27], the same authors than in [26] extended their study by using two gases (a neon gas (Ne) and a combination of argon and mercury vapor (Ar+Hg)) in order to see the effect of different types of low pressure gas inside the glass tube. The radiation patterns of the three antennas are basically omnidirectional but Ne plasma antenna gain starts to rise after 8 GHz and Ar+Hg plasma antenna gain starts to rise after 10 GHz.

Recently, an analysis was investigated on the return loss characteristics of plasma antenna with three different gases which are neon, argon and xenon in [41]. The measured return loss for the antennas made with these different gases are represented in Figure 2.38 and show that the return loss for all the cases are below -10 dB between 3.5 GHz and 5.5 GHz.

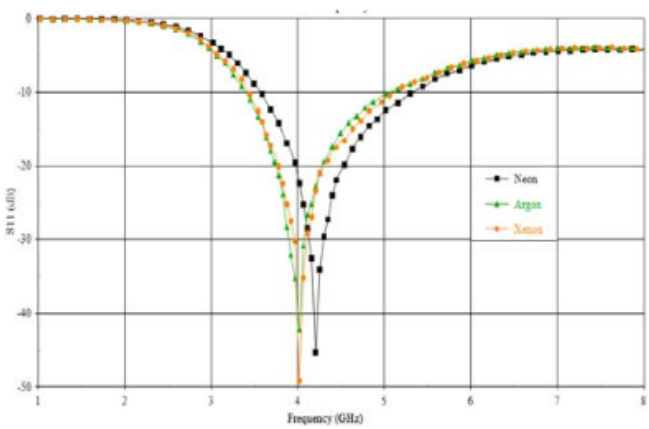

Figure 2.38: Return loss of plasma tube filled by different gases. [41]

Anshi Zhu et al. in [42] have presented plasma antennas energized by two excitation systems. The first one is an AC-biased (alternating current) plasma antenna, which has larger operation frequency scale and lower sustaining power shown in Figure 2.39(a) and the second one is a surface wave excitation plasma antenna shown in Figure 2.39(b).

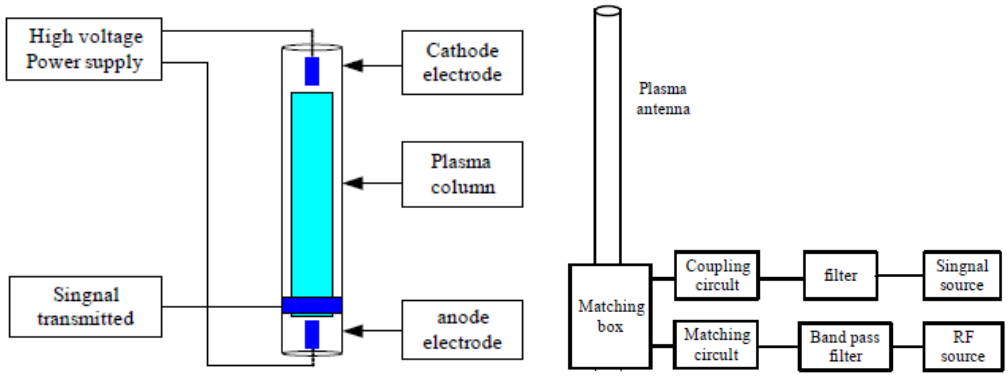

(a) (b)

Figure 2.39: Antenna structures. (a) The structure of the plasma antenna excited by high voltage. (b) The structure of the monopole plasma antenna excited by surface wave. [42]

It was reported that the plasma antenna excited by an AC-bias has larger gain (see Fig. 2.40(a)) and better directivity performance (see. Fig 2.40(b)) compared to the plasma antenna excited by a surface wave.

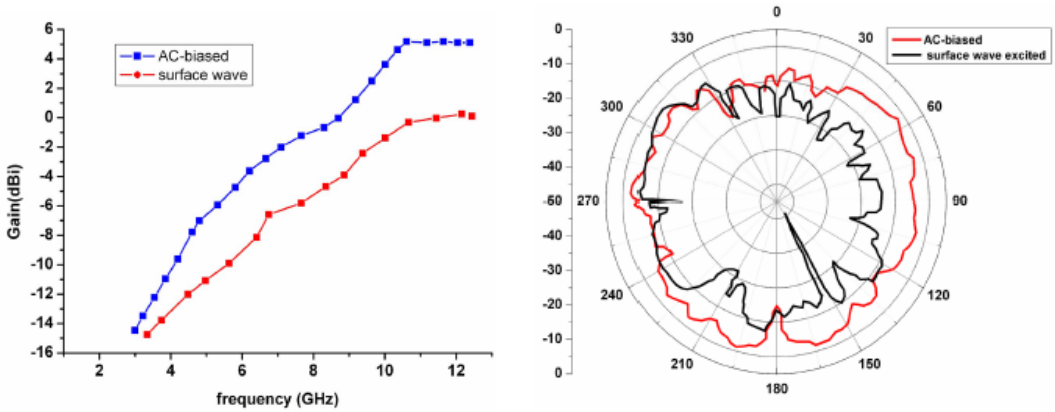

(a) (b)

Figure 2.40: Performance of the plasma antenna AC-biased and plasma antenna excited by surafce wave. (a) Gain. (b) Radiation Patterns. [42]

Jaafar et al. in [28, 29] proposed a monopole antenna using a single fluorescent lamp.

The plasma antenna tube is filled with Argon gas. The tube is energized by 12 V DC, and 0.8 A current, which is provided by a standard DC power supply. The DC power supply is connected to DC ballast before being directed to both electrodes of the fluorescent tube. This antenna is used as transmitter and receiver antenna.

The performance in terms of S_{11} and radiation patterns of the antenna is presented in Figure 2.41

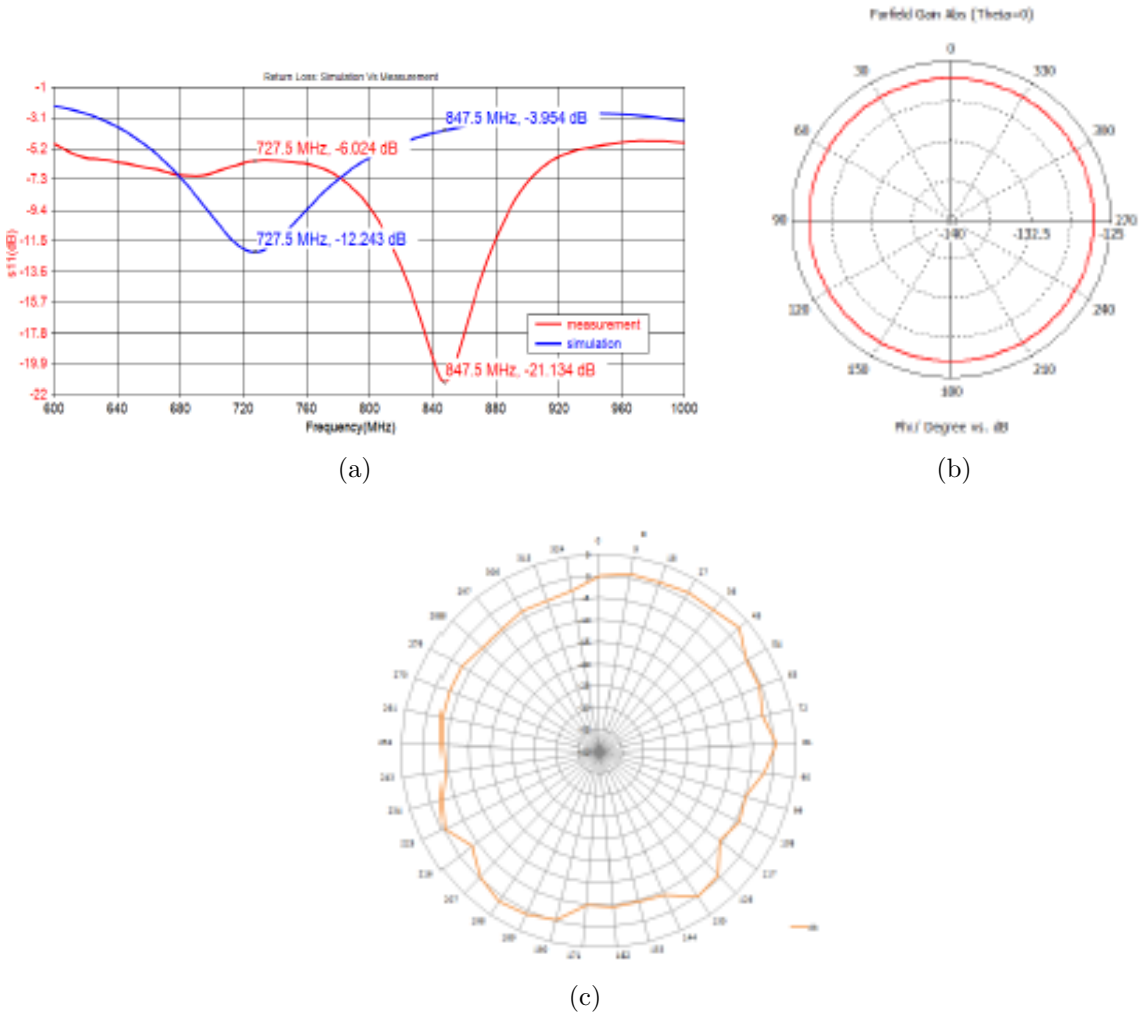

Figure 2.41: Performance of the monopole antenna. (a) Simulated and measured S_{11} magnitude. (b) Simulated radiation pattern. (c) Measured radiation pattern. [28]

The measured signal of the antenna used in transmission and reception are shown in Figure 2.42. A peak is found in both curves at 850 MHz.

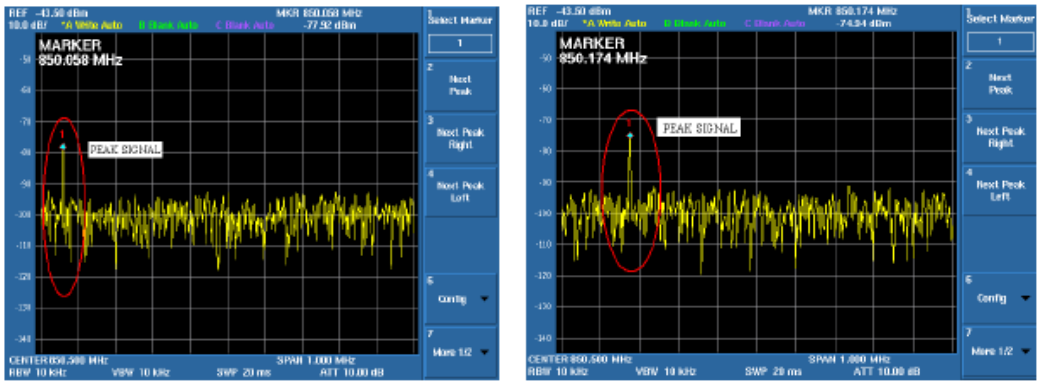

(a) (b)

Figure 2.42: Frequency spectrum of the captured signal. (a) When plasma antenna serves as transmitter. (b) When plasma antenna serves as receiver. [28]

In [43], a plasma antenna with coupling system was proposed. The coupling is made by a ring placed on center of the plasma tube and an outer cylinder surrounding the ring. The top and bottom of the outer cylinder are closed. A SMA probe is inserted between the ring and the outer cylinder. The designed and the manufactured plasma antenna with the coupling system are shown in Figure 2.43. The plasma frequency is 59.4 GHz and the collision frequency is 5×10^8 Hz.

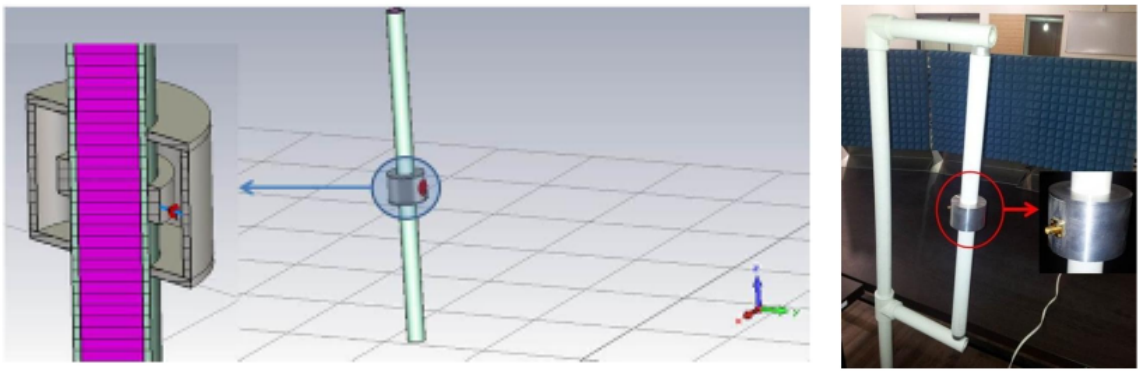

(a) (b)

Figure 2.43: Monopole antenna. (a) Simulated plasma antenna in CST. (b) Manufactured plasma antenna with F-shape leg and coupling system. [43]

The simulated S_{11} is shown in Figure 2.44(a). The resonance frequencies of this antenna are at 170 MHz and 352 MHz. The Figure 2.44(b) shows the far field pattern of the plasma antenna at 170 MHz. The maximum directivity of the antenna system is 2.45 dBi. The measured received signal is shown in Figure 2.45. This received signal is at 140 MHz.

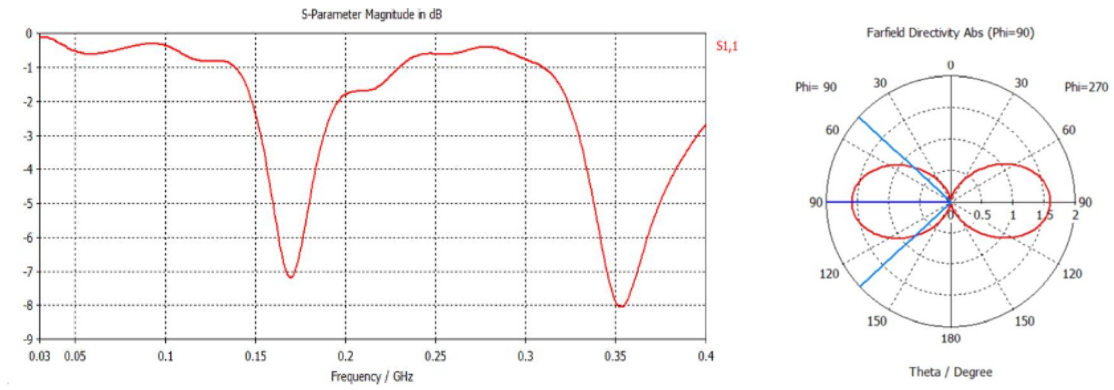

(a) (b)

Figure 2.44: Performance of the monopole antenna. (a) S_{11} parameter magnitude. (b) Simulated radiation pattern at 170 MHz. [43]

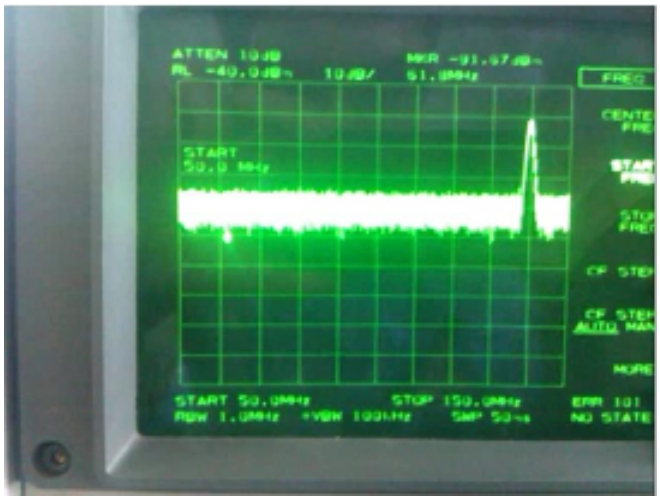

Figure 2.45: Result of the receiving signal from Helix antenna with plasma antenna in trasmission mode. [43]

In [44], a simple equivalent circuit model for plasma dipole antenna was presented. The system model is shown in Figure 2.46 with a lumped-element-equivalent circuit. The effect of the plasma frequency and the plasma collision frequency were studied in this paper and genetic algorithm technique is used to optimize the equivalent circuit for the plasma dipole antenna.

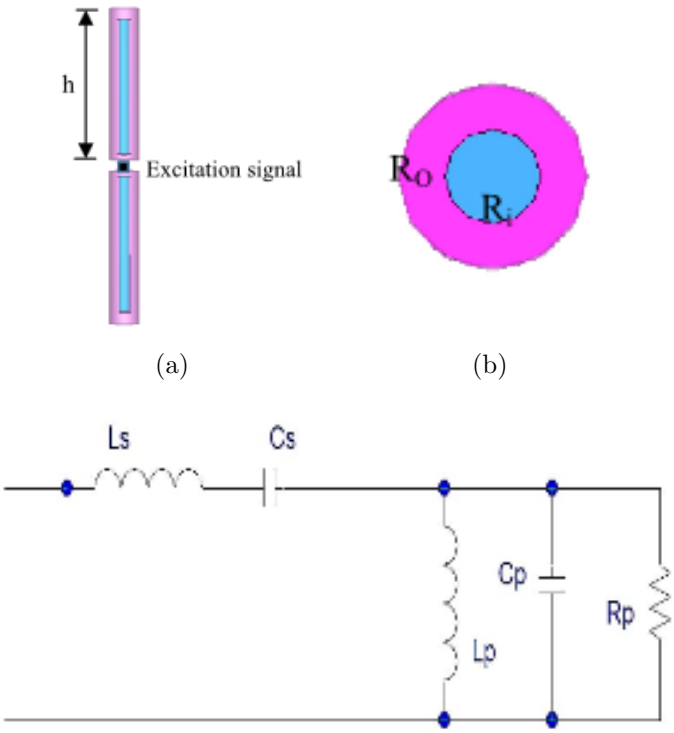

(a) (b)

(c)

Figure 2.46: Structure of the plasma dipole antenna. (a) Side view. (b) Top view. (c) Lumped-element equivalent circuit. [44]

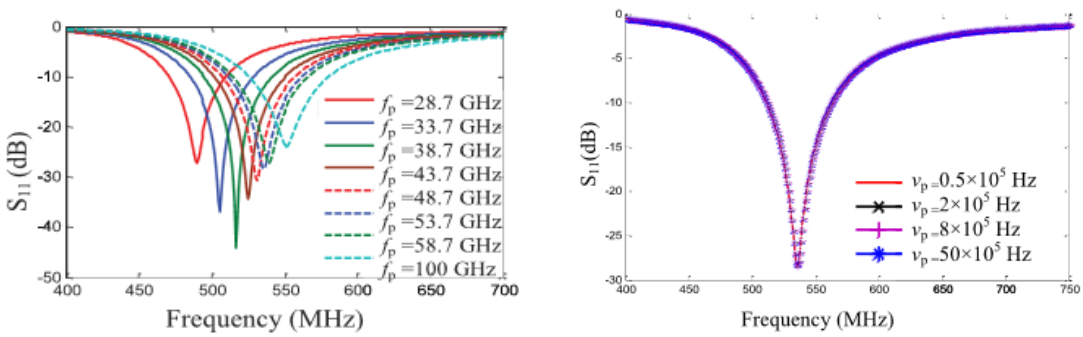

(a) (b)

Figure 2.47: Performance of the dipole antenna. (a) Variation of reflection coefficient versus frequency for different plasma frequencies. (b) Variation of reflection coefficient versus frequency for different collision frequencies. [44]

By fixing the plasma collision frequency $\nu_{col} = 2 \times 10^5$ Hz, the effect of changing the plasma frequency on the reflection coefficient is shown in Figure 2.47(a). By increasing the plasma frequency f_p, the resonant frequency shifts up to a higher frequency and the impedance matching is varied due to the change of the effective length of the plasma dipole antenna. The variation of plasma dipole reflection coefficient versus frequency for $f_p = 28.7$ GHz with different collision frequencies is shown in Figure 2.47(b). The resonant frequency, the reflection coefficient, and the impedance matching remain almost unaffected by increasing the collision frequency. Then the antenna input impedance does not change.

All the previous antennas cited use a simple cylindrical tube. But it exists also in literature some plasma antennas which have other shapes [45–48].

Longgen et al. proposed in [46] the study of the gain and VSWR of a loop plasma antenna using annular fluorescent lamp of 100 cm perimeter and 1 cm cross sectional diameter. Two excitation systems are used here. The first one is an 220 V AC source and for the second one, a RF signal was applied. A 1:4 transmission line transformer is used as balun to connect the RF power generator to the antenna. The power scale of the RF generator is about 40 W. The antenna setup with two different excitation systems are shown in Figure 2.48.

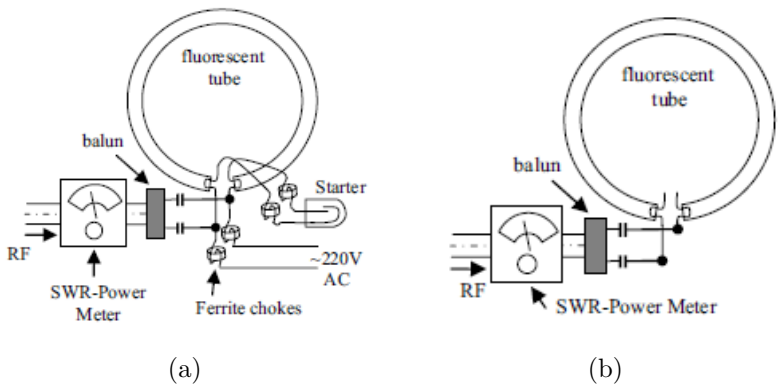

Figure 2.48: Plasma annular antenna excitation setup. (a) The 220V AC driven plasma antenna. (b) The RF driven plasma antenna. [46]

Figure 2.49(a) shows the VSRW versus the frequency. The resonant frequency of the two plasma antennas have been compared to the one given by a metal loop with similar dimension. The reference antenna resonates at 320 MHz. RF driven plasma antenna resonates at 290 MHz. The resonant frequency of 220 V AC driven plasma antenna is much lower because of the existence of unavoidable lead wires.

The relative gain of the two antennas are presented in Figure 2.49(b). The gains of the two plasma antennas are roughly at the same level. For 220V AC driven plasma antenna, the average gain is about 6 dB lower than the one of the reference metallic antenna. For RF driven plasma antenna, it is about 6.7 dB lower. we can also see that the plasma

antenna gains drop dramatically when the frequency is greater than 320 MHz. This means that the plasma antenna works better in the relatively lower frequency band.

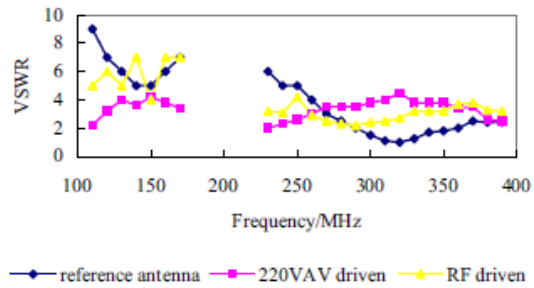

(a)

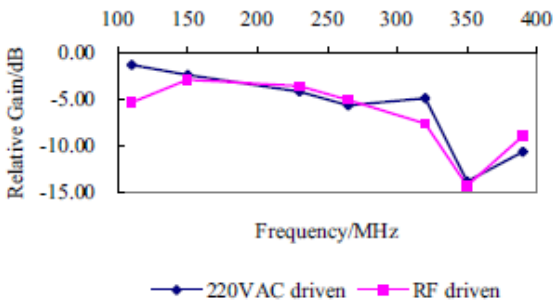

(b)

Figure 2.49: (a) VSWR curves for different antennas. (b) Plasma relative gain to the one of the reference antenna. [46]

2.4 Conclusion

This bibliography research shows different realizations and technologies in plasma domain. The two main utilizations of plasma are when it is used as radiator element in order to realize an plasma antenna and when it is used as reflector in order to steer, to scan and to shape the beam. Several techniques of excitation which are AC supply, RF discharges, microwaves discharges and laser excitation are found in literature.

The performance obtained for the plasma reflector antennas is similar to those of the metallic reflectors. The advantage of using plasma instead of metallic elements is that it allows to have an electrical control rather than mechanical one.

The results found in the literature for plasma as radiating element can be enhanced. Therefore, in the chapter 5 of this thesis, a monopole and dipole plasma antennas are studied and these antennas show acceptable performance in terms of radiations patterns, gain and S_{11} compared to ones found in the literature.

Bibliography

[1] U. S. Inan and M. Gokowski, *Principles of Plasma Physics for Engineers and Scientists*. Cambridge University Press, Dec. 2010.

[2] R. F. T REK, "An investigation on plasma antennas," Ph.D. dissertation, MIDDLE EAST TECHNICAL UNIVERSITY, 2005.

[3] J. A. Bittencourt, *Fundamentals of plasma physics*. Springer Science & Business Media, 2013.

[4] M. T. J. Tajudin, "Study and design of reconfigurable antennas using plasma medium," Ph.D. dissertation, Université Rennes 1, 2014. [Online]. Available: https://hal-univ-rennes1.archives-ouvertes.fr/tel-01060295/

[5] M. K. Howlader, Y. Yang, and J. R. Roth, "Time-resolved measurements of electron number density and collision frequency for a fluorescent lamp plasma using microwave diagnostics," *IEEE Transactions on Plasma Science*, vol. 33, no. 3, pp. 1093–1099, Jun. 2005.

[6] W. J. Vogel, H. Ling, and G. W. Torrence, "Fluorescent light interaction with personal communication signals," *IEEE Transactions on Communications*, vol. 43, no. 2/3/4, pp. 194–197, Feb. 1995.

[7] CST, "Computer simulation technonoly." [Online]. Available: https://www.cst.com/

[8] P. Linardakis, G. Borg, and N. Martin, "Plasma-based lens for microwave beam steering," *Electronics Letters*, vol. 42, no. 8, pp. 444–446, Apr. 2006.

[9] J. Mathew, R. A. Meger, J. A. Gregor, R. E. Pechacek, R. F. Fernsler, and W. M. Manheimer, "Electronically steerable plasma mirror for radar applications," in *Radar Conference, 1995., Record of the IEEE 1995 International*, May 1995, pp. 742–747.

[10] A. E. Robson, R. L. Morgan, and R. A. Meger, "Demonstration of a plasma mirror for microwaves," *IEEE Transactions on Plasma Science*, vol. 20, no. 6, pp. 1036–1040, Dec. 1992.

[11] J. Mathew, R. A. Meger, J. A. Gregor, D. P. Murphy, R. E. Pechacek, R. F. Fernsler, and W. M. Manheimer, "Electronically steerable plasma mirror," in *, IEEE International Symposium on Phased Array Systems and Technology, 1996*, Oct. 1996, pp. 58–62.

[12] J. Mathew, "Electronically steerable plasma mirror based radar-concept and characteristics," *IEEE Aerospace and Electronic Systems Magazine*, vol. 11, no. 10, pp. 38–44, Oct. 1996.

[13] R. A. Meger, R. F. Fernsler, J. A. Gregor, W. Manheimer, J. Mathew, D. P. Murphy, M. C. Myers, and R. E. Pechacek, "X-band microwave beam steering using a plasma mirror," in *, IEEE Aerospace Conference, 1997. Proceedings*, vol. 4, Feb. 1997, pp. 49–56 vol.4.

[14] I. Alexeff, T. Anderson, S. Parameswaran, E. P. Pradeep, J. Hulloli, and P. Hulloli, "Experimental and theoretical results with plasma antennas," *IEEE Transactions on Plasma Science*, vol. 34, no. 2, pp. 166–172, Apr. 2006.

[15] T. Anderson, I. Alexeff, E. Farshi, N. Karnam, E. P. Pradeep, N. R. Pulasani, and J. Peck, "An operating intelligent plasma antenna," in *2007 16th IEEE International Pulsed Power Conference*, vol. 1, Jun. 2007, pp. 353–356.

[16] M. T. Jusoh, O. Lafond, F. Colombel, and M. Himdi, "Performance and Radiation Patterns of a Reconfigurable Plasma Corner-Reflector Antenna," *IEEE Antennas and Wireless Propagation Letters*, vol. 12, pp. 1137–1140, 2013.

[17] I. Alexeff, T. Anderson, E. Farshi, N. Karnam, and N. R. Pulasani, "Recent results for plasma antennas," *Physics of Plasmas*, vol. 15, no. 5, p. 057104, 2008. [Online]. Available: http://scitation.aip.org/content/aip/journal/pop/15/5/10.1063/1.2919157

[18] T. Anderson and I. Alexeff, "Theory of plasma antenna windowing," in *The 31st IEEE International Conference on Plasma Science, 2004. ICOPS 2004. IEEE Conference Record - Abstracts*, Jul. 2004, pp. 328–.

[19] T. R. Anderson, *Plasma antennas*, ser. Artech House antennas and propagation series. Boston: Artech House, 2011, oCLC: ocn720831454.

[20] X. P. Wu, J.-M. Shi, Z. S. Chen, and B. Xu, "A new plasma antenna of beam-forming," *Progress In Electromagnetics Research*, vol. 126, pp. 539–553, 2012. [Online]. Available: http://jpier.org/PIER/pier.php?paper=12021906

[21] H. Jaafar, M. T. Ali, A. N. Dagang, H. M. Zali, and N. A. Halili, "Design monopole antenna with fluorescent tube at 4.9ghz," in *2013 Asia-Pacific Microwave Conference Proceedings (APMC)*, Nov. 2013, pp. 1049–1051.

[22] M. T. Jusoh, O. Lafond, F. Colombel, and M. Himdi, "Performance of a Reconfigurable Reflector Antenna with Scanning Capability Using Low Cost Plasma Elements," *Microwave and Optical Technology Letters*, vol. 55, no. 12, pp. 2869–2874, Dec. 2013. [Online]. Available: http://onlinelibrary.wiley.com/doi/10.1002/mop.27958/abstract

[23] H. Jaafar, M. T. Ali, A. N. Dagang, I. P. Ibrahim, N. A. Halili, and H. M. Zali, "Reconfigurable Plasma Antenna Array by Using Fluorescent Tube for Wi-Fi Application," *Radioengineering*, vol. 25, no. 2, pp. 275–282, Apr. 2016. [Online]. Available: http://www.radioeng.cz/fulltexts/2016/16_02_0275_0282.pdf

[24] T. Yamamoto and T. Kobayashi, "A reconfigurable antenna using fluorescent lamps," in *Antennas and Propagation (ISAP), 2014 International Symposium on*. IEEE, 2014, pp. 89–90. [Online]. Available: http://ieeexplore.ieee.org/xpls/abs_all.jsp?arnumber=7026544

[25] I. Alexeff, T. Anderson, S. Parameswaran, E. P. Pradeep, J. Hulloli, and P. Hulloli, "Experimental and theoretical results with plasma antennas," in *IEEE transactions on plasma science*, vol. 34. Institute of Electrical and Electronics Engineers, 2006, pp. 166–172. [Online]. Available: http://cat.inist.fr/?aModele=afficheN&cpsidt=17723037

[26] M. Chung, W.-S. Chen, B.-R. Huang, C.-C. Chang, K.-Y. Ku, Y.-H. Yu, and T.-W. Suen, "Capacitive coupling return loss of a new pre-ionized monopole plasma antenna," in *TENCON 2007 - 2007 IEEE Region 10 Conference*, Oct. 2007, pp. 1–4.

[27] M. Chung, W.-S. Chen, Y.-H. Yu, and Z. Y. Liou, "Properties of DC-biased plasma antenna," in *International Conference on Microwave and Millimeter Wave Technology, 2008. ICMMT 2008*, vol. 3, Apr. 2008, pp. 1118–1120.

[28] H. Ja'afar, M. T. Ali, H. M. Zali, N. A. Halili, and A. N. Dagang, "A monopole fluorescent tube antenna in wireless communication application," in *2013 10th International Conference on Electrical Engineering/Electronics, Computer, Telecommunications and Information Technology (ECTI-CON)*, May 2013, pp. 1–5.

[29] H. M. Zali, M. T. Ali, N. A. Halili, H. Ja'afar, and I. Pasya, "Study of monopole plasma antenna using fluorescent tube in wireless transmission experiments," in *2012 International Symposium on Telecommunication Technologies (ISTT)*, Nov. 2012, pp. 52–55.

[30] J. P. Rayner, A. P. Whichello, and A. D. Cheetham, "Physical characteristics of plasma antennas," *IEEE Transactions on Plasma Science*, vol. 32, no. 1, pp. 269–281, Feb. 2004.

[31] G. Cerri, R. D. Leo, V. M. Primiani, and P. Russo, "Measurement of the Properties of a Plasma Column Used as a Radiating Element," *IEEE Transactions on Instrumentation and Measurement*, vol. 57, no. 2, pp. 242–247, Feb. 2008.

[32] P. Russo, G. Cerri, and E. Vecchioni, "Self-Consistent Analysis of Cylindrical Plasma Antennas," *IEEE Transactions on Antennas and Propagation*, vol. 59, no. 5, pp. 1503–1511, May 2011.

[33] G. Cerri, R. D. Leo, V. M. Primiani, P. Russo, and E. Vecchioni, "2.45 GHz waveguide plasma generation in cylindrical structures," in *Microwave Symposium Digest (MTT), 2010 IEEE MTT-S International*, May 2010, pp. 1032–1035.

[34] P. Russo, V. M. Primiani, G. Cerri, R. D. Leo, and E. Vecchioni, "Experimental Characterization of a Surfaguide Fed Plasma Antenna," *IEEE Transactions on Antennas and Propagation*, vol. 59, no. 2, pp. 425–433, Feb. 2011.

[35] M. Moisan, Z. Zakrzewski, R. Pantel, and P. Leprince, "A Waveguide-Based Launcher to Sustain Long Plasma Columns through the Propagation of an Electromagnetic Surface Wave," *IEEE Transactions on Plasma Science*, vol. 12, no. 3, pp. 203–214, Sep. 1984.

[36] P. Russo, G. Cerri, and E. Vecchioni, "Self-consistent model for the characterisation of plasma ignition by propagation of an electromagnetic wave to be used for plasma antennas design," *Antennas Propagation IET Microwaves*, vol. 4, no. 12, pp. 2256–2264, Dec. 2010.

[37] ——, "Self-Consistent Analysis of Cylindrical Plasma Antennas," *IEEE Transactions on Antennas and Propagation*, vol. 59, no. 5, pp. 1503–1511, May 2011.

[38] M. Alshershby and J. Lin, "Reconfigurable plasma antenna produced in air by laser-induced filaments: Passive radar application," in *2012 International Conference on Optoelectronics and Microelectronics (ICOM)*, Aug. 2012, pp. 364–371.

[39] V. Kumar, M. Mishra, and N. K. Joshi, "Study of a Fluorescent Tube as Plasma Antenna." *Progress in electromagnetics research letters*, vol. 24, pp. 17–26, 2011. [Online]. Available: http://www.jpier.org/PIERL/pier.php?paper=11030201

[40] M. Khadir and K. Forooraghi, "Plasma Monopole Ante," 2014. [Online]. Available: http://www.isseem.ir/files/site1/user_files_c3e22c/admin-A-10-1-89-2501d27.pdf

[41] N. A. Halili, M. T. Ali, H. M. Zali, H. Ja'afar, and I. Pasya, "A study on plasma antenna characteristics with different gases," in *2012 International Symposium on Telecommunication Technologies (ISTT)*, Nov. 2012, pp. 56–59.

[42] A. Zhu, Z. Chen, J. Lv, and J. Liu, "Characteristics of AC-biased Plasma Antenna and Plasma Antenna Excited by Surface Wave," *Journal of Electromagnetic Analysis and Applications*, vol. 04, no. 07, pp. 279–284, 2012. [Online]. Available: http://www.scirp.org/journal/PaperDownload.aspx?DOI=10.4236/jemaa.2012.47039

[43] P. Darvish, A. B. Gorji, and B. Zakeri, "Design, simulation and implementation of a pre-ionized coupled plasma antenna at VHF band," in *Proceedings of 2013 URSI International Symposium on Electromagnetic Theory (EMTS)*, May 2013, pp. 452–455.

[44] M. M. Badawy, H. A. E.-A. Malhat, S. H. Zainud-Deen, and K. H. Awadalla, "A Simple Equivalent Circuit Model for Plasma Dipole Antenna," *IEEE Transactions on Plasma Science*, vol. 43, no. 12, pp. 4092–4098, Dec. 2015.

[45] F. Etesami and F. Mohajeri, "On radiation characteristics of a plasma triangular monopole antenna," in *2011 19th Iranian Conference on Electrical Engineering*, May 2011, pp. 1–1.

[46] L. Zheng, L. Cao, and Z. Zhang, "Study on the gain of plasma antenna," in *8th International Symposium on Antennas, Propagation and EM Theory, 2008. ISAPE 2008*, Nov. 2008, pp. 222–224.

[47] Z. H. Qian, K. W. Leung, R. S. Chen, and D. X. Wang, "FDTD analysis of a plasma whip antenna," in *2005 IEEE Antennas and Propagation Society International Symposium*, vol. 2B, Jul. 2005, pp. 166–169 vol. 2B.

[48] M. Liang and G. Qinggong, "FDTD analysis of a plasma helix antenna," in *International Conference on Microwave and Millimeter Wave Technology, 2008. ICMMT 2008*, vol. 4, Apr. 2008, pp. 1854–1857.

Chapter 3

Shielding

The objectives of this chapter is to discuss and explain the use of plasma lamp to have Faraday shield effect. The antenna system can be used to protect it against external undesirable signal. A Faraday cage is an enclosure formed by a conductive material or by a mesh of such material. In our case, the Faraday cage is realized by using a spiral fluorescent lamp which allows to switch ON or OFF the plasma and to obtain reconfigurable gain and radiation patterns (See Fig. 3.1). A patch antenna with a broadside radiation pattern or a monopole antenna with an end-fire radiation pattern, operating at 2.45 GHz, is placed inside the Faraday cage. The performance of the reconfigurable system is observed in terms of input reflection coefficient, gain and radiation pattern via simulations and measurements. It is shown that by switching ON the fluorescent lamp, the gain of the antenna can be decreased in particular direction and reconfigurable radiation patterns can be observed.

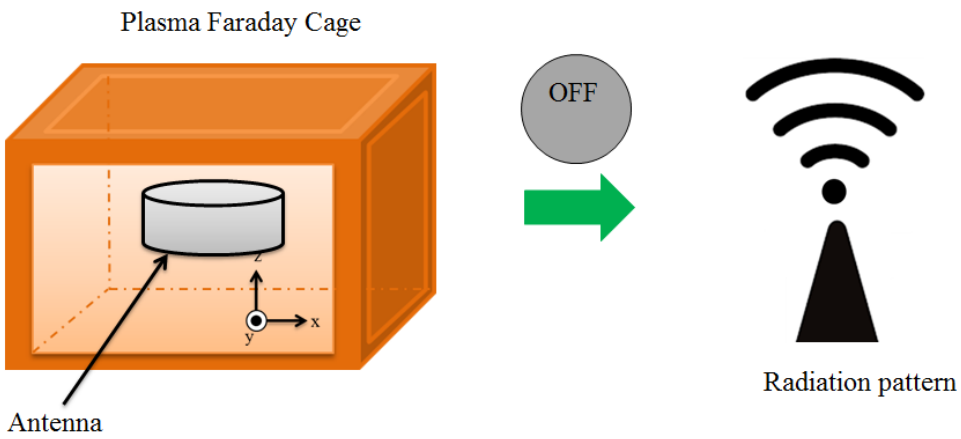

(a)

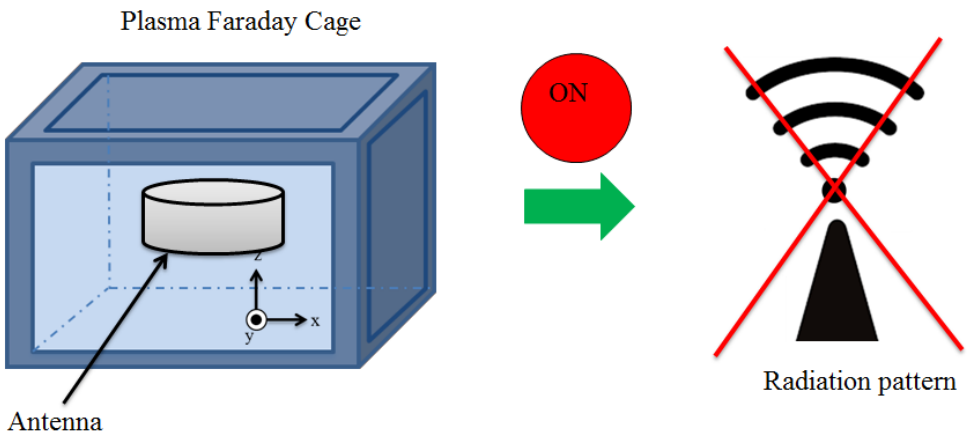

(b)

Figure 3.1: Faraday cage principle. (a) Plasma OFF. (b) Plasma ON.

3.1 Illustration of the closed plasma Faraday cage

In this section, we simulated a patch operating at 2.45 GHz inside a closed plasma Faraday (see Fig. 3.2) in order to demonstrate that the closed plasma can be used as a Faraday cage.

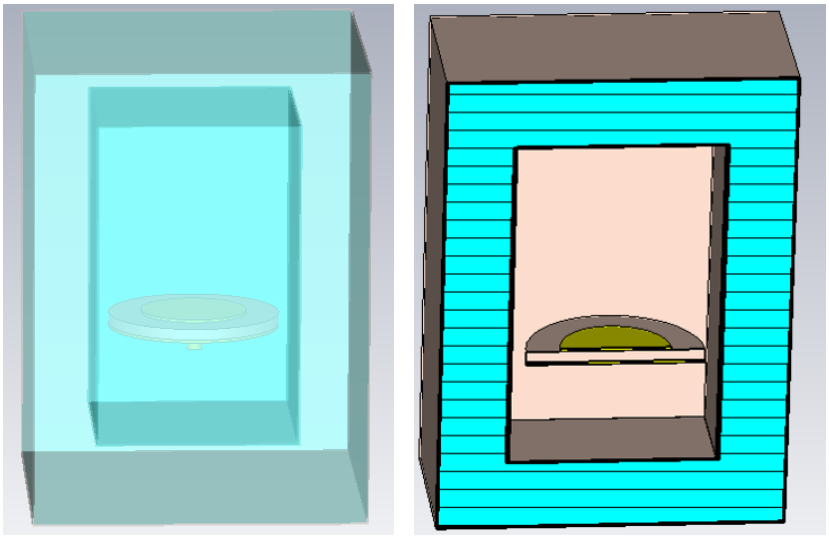

(a) (b)

Figure 3.2: Closed plasma Faraday cage. (a) global view. (b) Cut view.

The Figure 3.3 shows the simulated radiation patterns of the antenna inside the plasma Faraday cage for the plasma OFF and ON cases. When plasma is switched ON, we can observe that a stronger reduction of the radiation and its level is lower than -35 dB. This result confirms that the closed plasma cage can be an efficient Faraday cage.

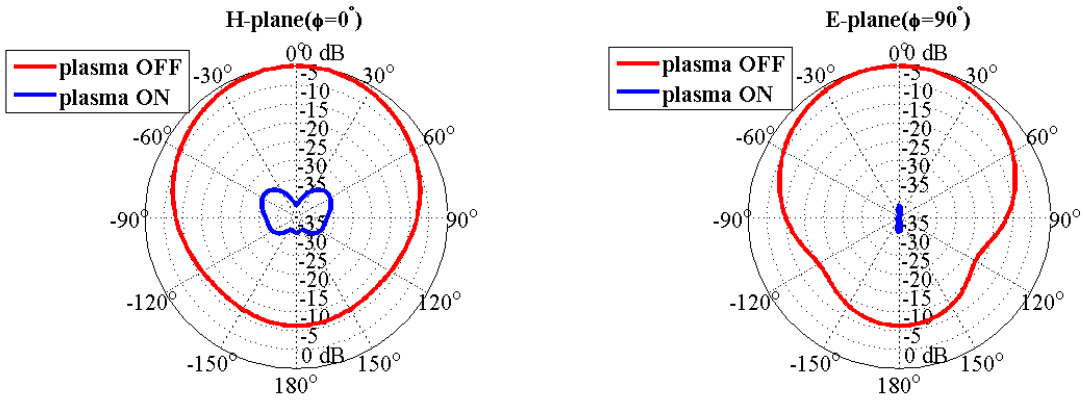

(a) (b)

Figure 3.3: Normalized radiation patterns at 2.45 GHz for the patch inside the closed plasma Faraday closed. (a) H-plane. (b) E-plane.

Unfortunately, this case is theoretical because it does not exist complete closed commercial plasma lamp that can be used as a Faraday cage. Nevertheless, we found a commercial lamp with a spiral shape that could have quite the same behavior.

3.2 Lamp Description

The lamp used in this study is a fluorescent lamp with a spiral shape [1] shown in Figures 3.4(a) and 3.4(b). The height of the lamp is 134 mm, the inner diameter is 60 mm, the spiral diameter is 19 mm, the outer diameter is 98 mm and the gap between the turns is 3.64 mm. An electronic ballast with specification of 220-240 V, 50 Hz is used to energize the 85 Watts spiral lamp. A reflector plane with a size of $200 \times 200\ mm^2$ is used on the bottom of the lamp in order to mask the electronic devices used to energize the plasma. As we see in the Figure 3.4(b), the lamp is composed of two parts (spiral part and end of the lamp part), justifying why we use two kind of antennas (patch and monopole) operating at the same frequency (2.45 GHz) in order to evaluate the impact of polarization on the radiation patterns of the antenna surrounded by the lamp.

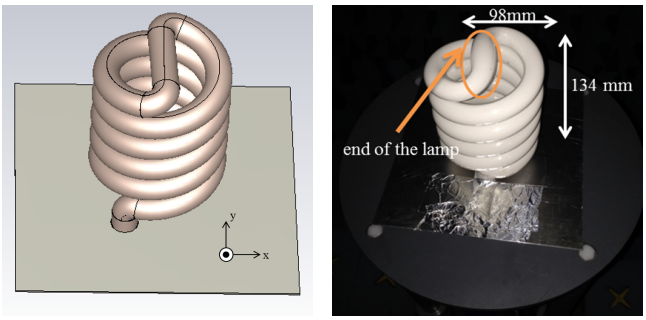

(a) (b)

Figure 3.4: Lamp description. (a) Design of simulated lamp. (b) Commercial lamp.

3.3 Patch antenna case

3.3.1 Patch antenna alone

3.3.1.1 Design and Realization

We design a circular patch antenna operating at 2.45 GHz which will be enclosed in a compact fluorescent lamp. The geometry of the proposed patch antenna fed by a coaxial line is shown in Figure 3.5. This circular patch with a 31 mm diameter is printed on FR4 substrate with a thickness h = 3.2 mm, ϵ_r = 4.4 and $\tan\delta$ = 0.025. The diameter of the dielectric substrate is 50 mm. The feed point is located along the y-axis, at a distance d = 5 mm from the center of the patch in order to match the antenna at 50 Ω. The antenna is polarized along the y-axis and the ground plane is on the bottom of the substrate. The Figures 3.5(a), 3.5(b) and 3.5(c) show respectively the simulated patch antenna, top and bottom view of the manufactured patch antenna.

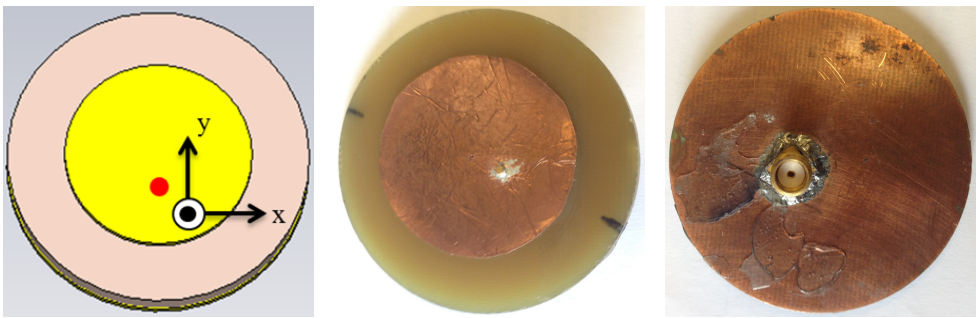

(a) (b) (c)

Figure 3.5: Patch antenna. (a) Simulated patch antenna. (b) and (c) Top and Bottom views respectively for the manufactured patch antenna.

3.3.1.2 Performance of the patch antenna

This section describes the performance of the patch antenna in simulation and measurement in terms of S_{11} and radiations pattern. The simulated and measured magnitude of the S_{11} parameters are shown in Figure 3.6 for the patch antenna. The measured result is in good agreement with the simulated one. The resonant frequency is close to 2.45 GHz in simulation and measurement.

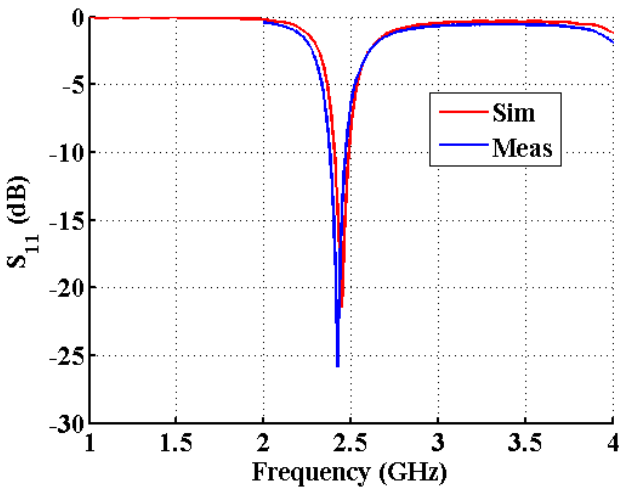

Figure 3.6: Simulated and measured magnitude of S_{11} parameters for the patch alone.

Radiation patterns have been measured in order to validate the simulation results. Measurements have been performed in a SATIMO anechoic chamber (near field setup) with a peak gain accuracy equals to ±0.8 dBi for 800 MHz to 6 GHz operating frequencies. The SATIMO anechoic chamber is composed of 32 bi-polarized receving antennas located on an arch in circular shape arrangement with an internal diameter of 1.5 m. A software allows automation measurement sequences, the acquisition and processing of data. This measurement technique makes it possible to obtain 3D radiation pattern and very fast procedure compared to a conventional system. The Figure 3.7 shows the SATIMO measurement setup.

The Figures 3.8(a) and 3.8(b) show the H and E-planes measured and simulated radiation patterns at 2.45 GHz respectively. For both simulation and measurement results, each radiation pattern is normalized to its maximum value of the electric-field. We can clearly observe that the radiation patterns in measurement and simulation are similar. The level of measured patch cross-polarization is below than -15 dB and its simulated cross-polarization in E and H-planes is below than -30 dB (not able to be seen in Figures 3.8(a) and 3.8(b)). The measured realized gain is 4 dBi which is almost 1 dB lower than the simulation one. This difference is due to the measurement setup accuracy.

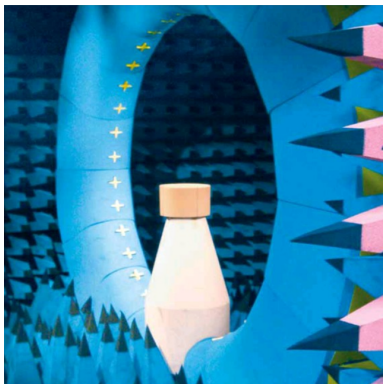

Figure 3.7: Radiation pattern measurement setup (SATIMO).

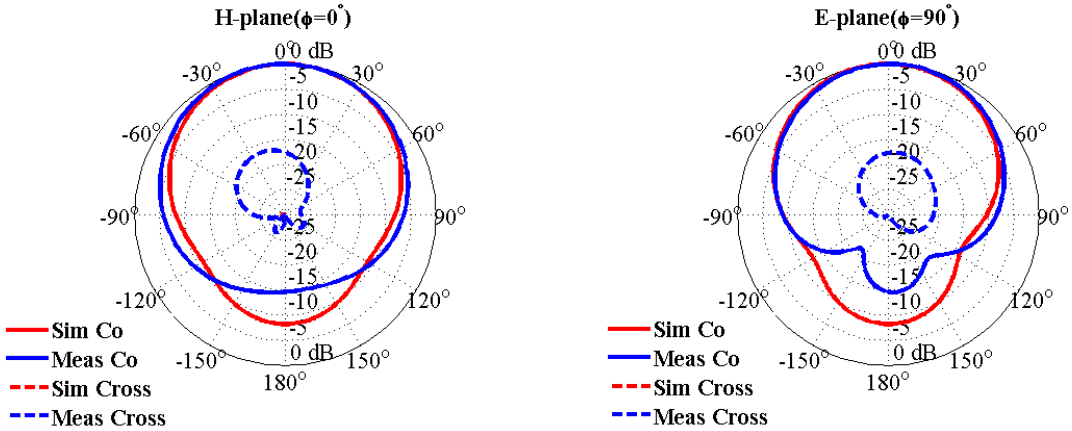

(a) (b)

Figure 3.8: Normalized radiation patterns at 2.45 GHz for the patch. (a) H-plane. (b) E-plane.

3.3.2 Simulated metallic spiral lamp

In the first time, simulations have been done by considering a metallic (perfect electrical conductor (PEC)) spiral lamp as shown in Figure 3.9 in order to see the shielding effect. The patch antenna is inserted inside this metallic spiral lamp. Depending of the geometry of the lamp, two cases are investigated: in the first case, the electric field polarization (y-axis) is parallel to the end of the lamp, while in the second one the electric field polarization (x-axis) is orthogonal to the end of the lamp. The S_{11} parameter of the patch alone is compared to the S_{11} results obtained for antenna system (patch + metal) in both cases.

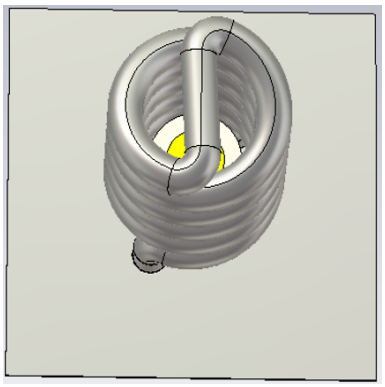

Figure 3.9: Simulated lamp replaced by PEC.

The Figure 3.10 shows the S_{11} magnitude comparison between patch alone and patch inside metallic spiral lamp. It is important to notice that the antenna system is not well matched at the operating frequency (-2.89 dB at 2.45 GHz). The presence of the metallic spiral lamp deteriorates the matching of the patch antenna. However, the S_{11} in first case (Fig. 3.10(a)) is similar to the S_{11} in second case (Fig. 3.10(b)).

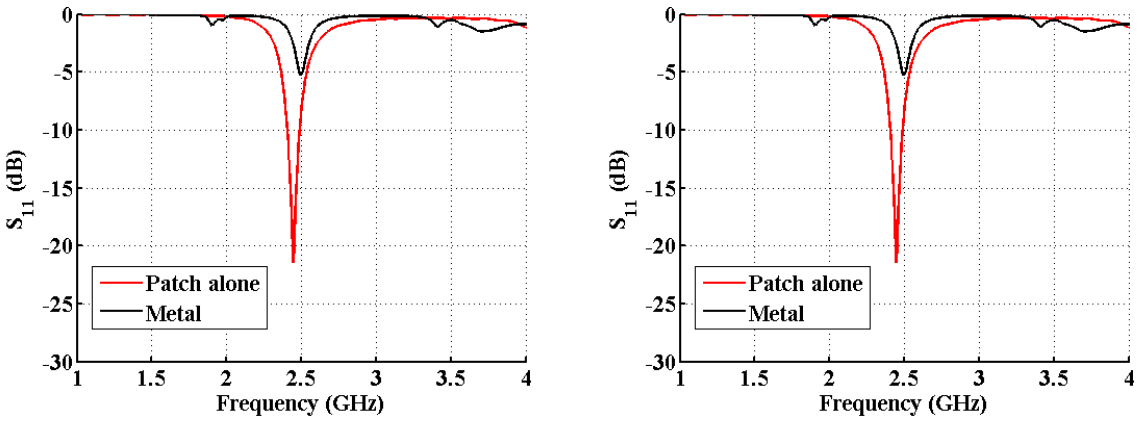

Figure 3.10: Simulated S_{11}. (a) First case. (b) Second case.

- **First case: the electric field polarization is parallel to the end of the lamp**

The Figures 3.11(a) and 3.11(b) present respectively the H and E-planes of the radiation patterns for patch alone and the patch inside the metallic lamp. These results show that the metallic lamp is efficient for shielding but the antenna system is not matched.

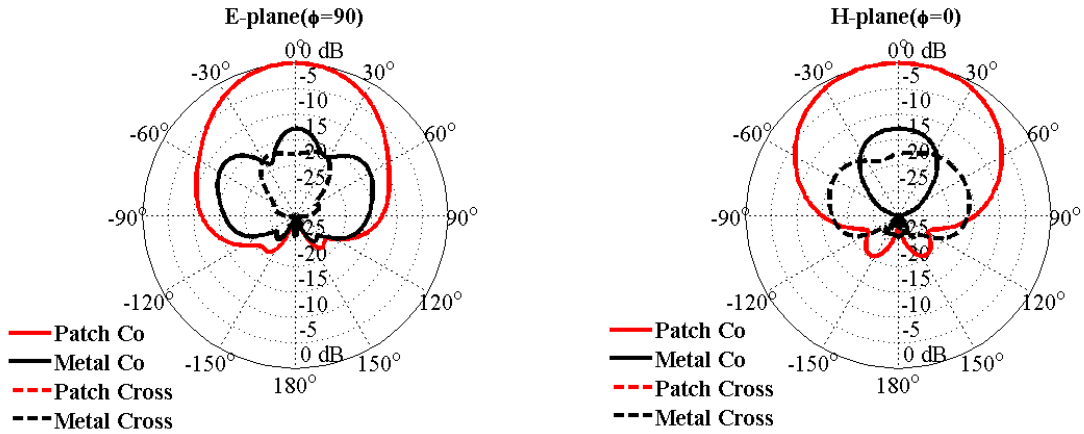

(a) (b)

Figure 3.11: Normalized radiation patterns at 2.45 GHz for patch alone and patch inside the metallic lamp in the first case. (a) E-plane. (b) H-plane.

- **Second case: the electric field polarization is orthogonal to the end of the lamp**

In this case, the patch antenna is rotated to 90°, thus the electric field polarization is along the x-axis and becomes orthogonal to the end of the lamp.

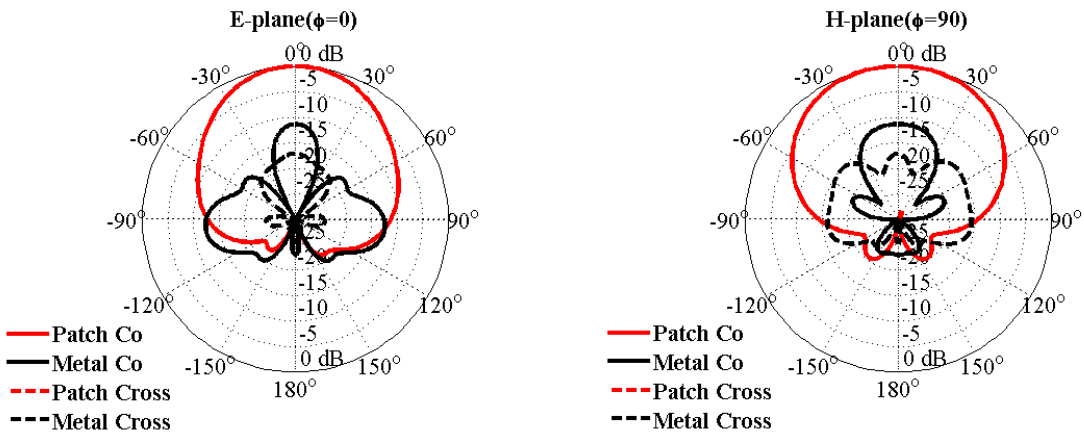

(a) (b)

Figure 3.12: Normalized radiation patterns at 2.45 GHz for patch alone and patch inside the metallic lamp in the second case. (a) E-plane. (b) H-plane.

The Figures 3.12(a) and 3.12(b) show respectively the H and E-planes of the radiation patterns for patch alone plane and the patch inside the metallic lamp. In this second case,

the shielding is effective but a little bit less than for the first case than. Therefore, the shielding seems depend of the antenna polarization versus the end of the lamp.

The real plasma media inside the spiral lamp is not a perfect conductor, so in the following part we simulated the case with the true plasma to see the impact on the S_{11} and radiation pattern of the patch antenna.

3.3.3 Patch inside the plasma spiral lamp

3.3.3.1 Parametric study

We begin by a parametric study concerning the distance between the patch and the reflector plane used to mask the electronic devices (see Fig.3.13). Several simulations have been performed by varying the distance from 20 mm to 70 mm in order to find which distance gives us more efficient effect between plasma ON and plasma OFF in term of gain in the broadside direction and matching at 2.45 GHz.

In simulation (performed using CST Microwave studio [2]), the tubes containing the gas are made from lossy glass Pyrex with $\epsilon_r = 4.82$, $\tan\delta = 0.005$ and thickness of 0.5 mm. The plasma obeys to the Drude model. We used the same Drude model as in [3, 4], with the same parameters ($\nu = 900$ MHz and $\omega_p = 43.9823\ 10^9$ rad/s corresponding to 7 GHz in frequency). These values of plasma parameters were characterized by a previously PhD student in our laboratory [5].

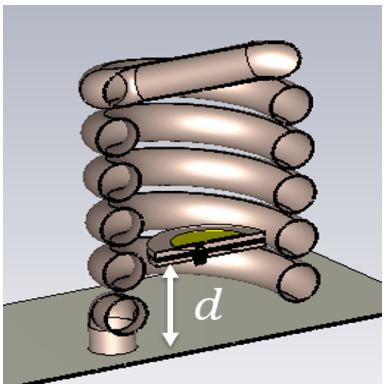

Figure 3.13: Parametric Study.

Here also two cases are considered, in the first case, the electric field polarization (y-axis) is parallel to the end of the lamp, while in the second one the electric field polarization (x-axis) is orthogonal to the end of the lamp. In this parametric study, we present only the first case i.e. when the electric field polarization is parallel to the end of the lamp.

The Figure 3.14 shows the S_{11} magnitude for all the distances. We can notice that the S_{11} is always the same whatever the distance for plasma OFF case (Fig. 3.14(a)). This result confirms that, the glass surrounding the plasma has no significant effect on the S_{11}. For plasma ON case (Fig. 3.14(b)), we can also notice that for all the distances, the

matching at 2.45 GHz is better than -10 dB. The S_{11} is not significantly affected by the plasma and also by the variation of the distance.

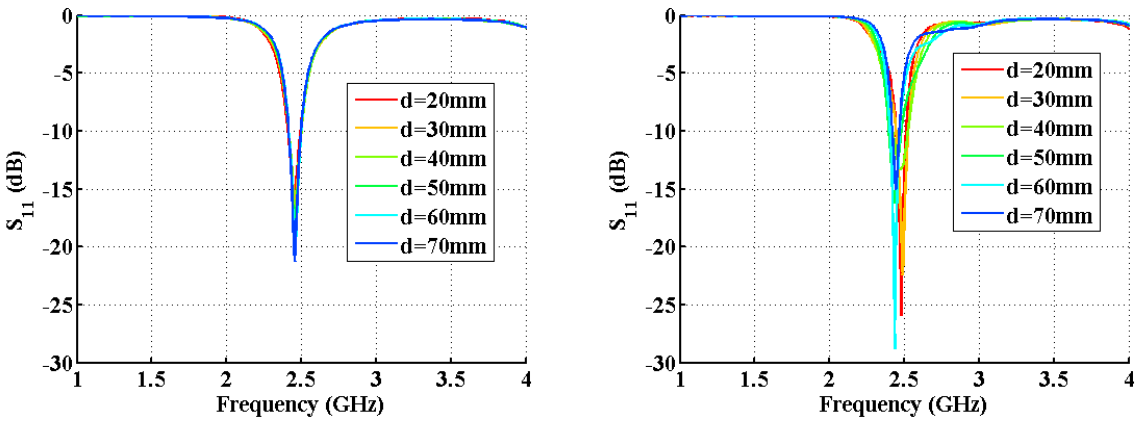

(a) (b)

Figure 3.14: S_{11} magnitude comparison. (a) Plasma OFF. (b) Plasma ON.

The simulated H and E-planes normalized radiation patterns for different values of the distance d are shown respectively in the Figures 3.15 and 3.16. Each radiation pattern is normalized to its maximum value of the electric-field for the plasma OFF. Referring to the Figures 3.15 and 3.16, the difference between plasma ON and plasma OFF in both planes (E-plane and H-plane) is almost 15 dB in the broadside direction (angular sector $\theta = \pm 20°$) for $d = 20$ mm and $d = 30$ mm. For $d = 40$ mm, $d = 50$ mm and $d = 60$ mm, the difference is 10 dB. At $d = 70$ mm the radiation patterns for plasma OFF is significantly disturbed.

It is important to notice that when the plasma is ON, the radiation patterns are reconfigurable. The radiation pattern switches from a conventional radiation pattern of a patch (plasma OFF) to another radiation pattern (plasma ON).

We can notice that the distances $d = 20$ mm and $d = 30$ mm give better performance in terms of gain reduction (shielding) between OFF and ON state. We remark also that $d = 40$ mm, $d = 50$ mm and $d = 60$ mm give quite same results. Therefore, by a issue of manufacturing, the two first distances ($d = 20$ mm and $d = 30$ mm) cannot be achieved because it is not possible to put the antenna inside the lamp. Thus, in our study, a trade-off is done by choosing the distance $d = 50$ mm rather than $d = 40$ mm in order to have more freedom by inserting the antenna inside the lamp.

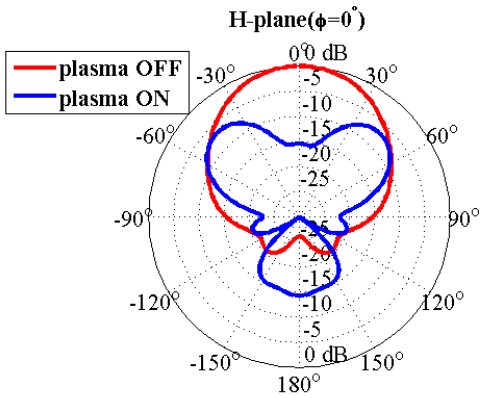

(a) d = 20 mm

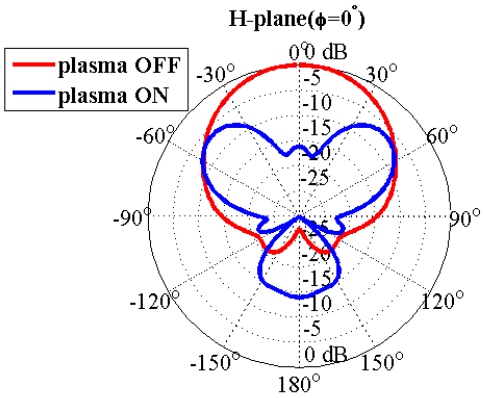

(b) d = 30 mm

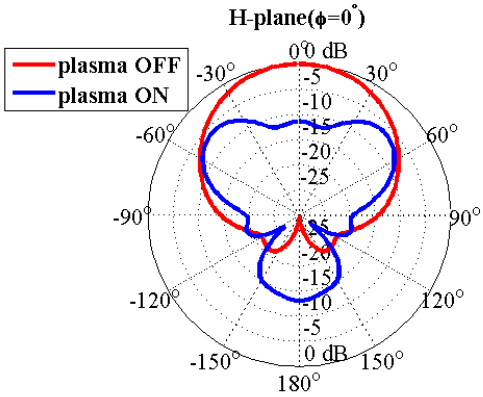

(c) d = 40 mm

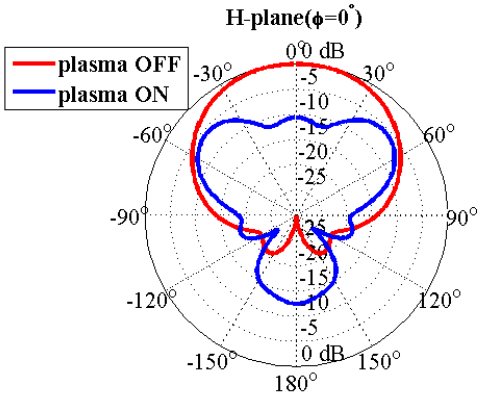

(d) d = 50 mm

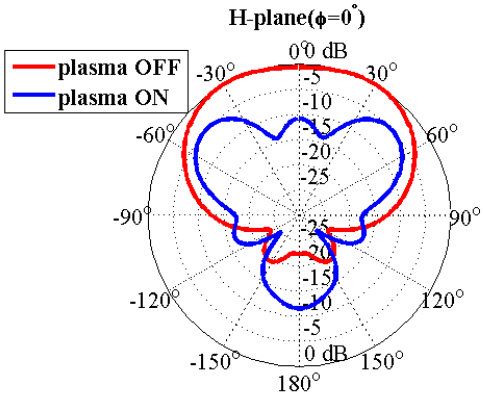

(e) d = 60 mm

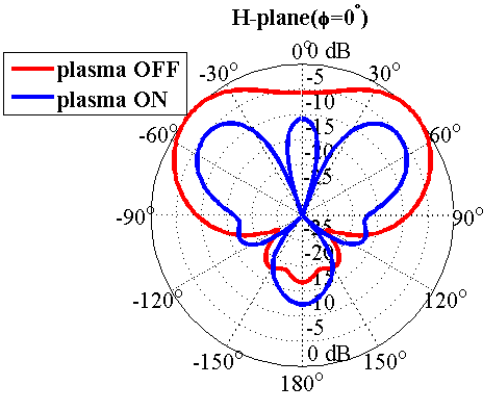

(f) d = 70 mm

Figure 3.15: Simulated H-plane radiation patterns.

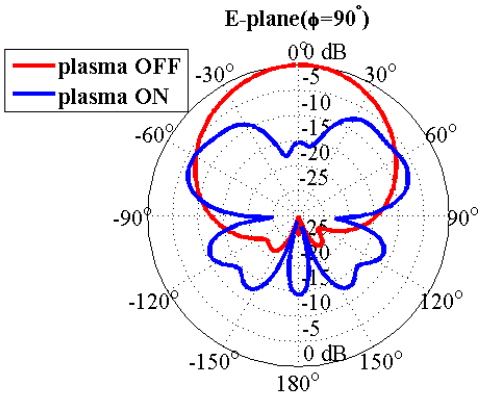

(a) d = 20 mm

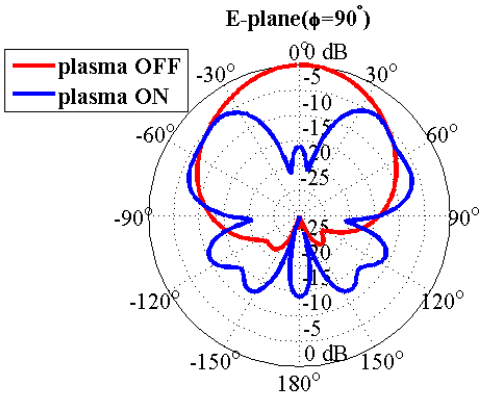

(b) d = 30 mm

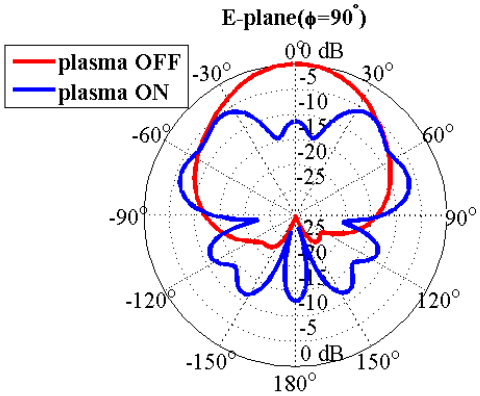

(c) d = 40 mm

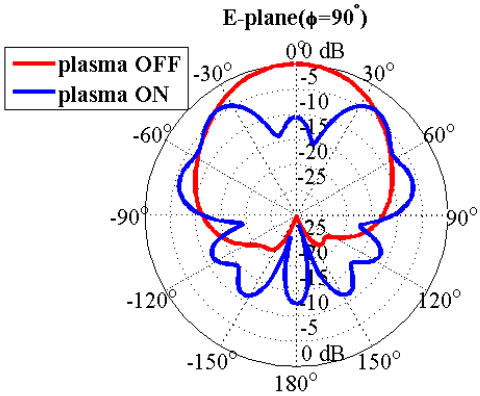

(d) d = 50 mm

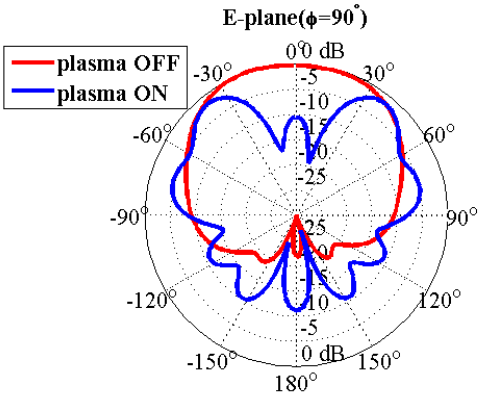

(e) d = 60 mm

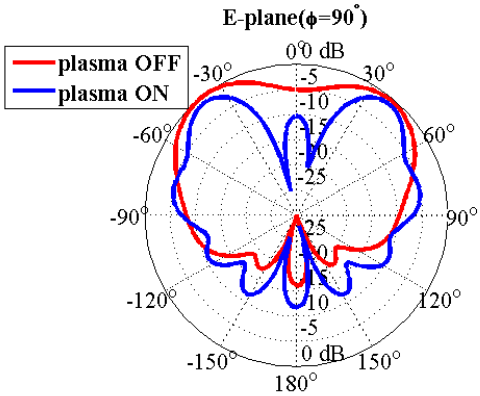

(f) d = 70 mm

Figure 3.16: Simulated E-plane radiation patterns.

3.3.3.2 Fabrication of plasma shield effect

The fabricated prototype and the antenna support for the patch antenna are shown in Figure 3.17. There are 4 pins screwed to support the antenna (see Fig. 3.17(b)). As seen in Figure 3.17(c), two substrates have been superposed, then 4 holes have been made on the second substrate in order to connect the 4 pins used as support for the patch antenna. The patch antenna is put inside the lamp at a height equals to 50 mm from the reflector plane used to hide the electronic devices.

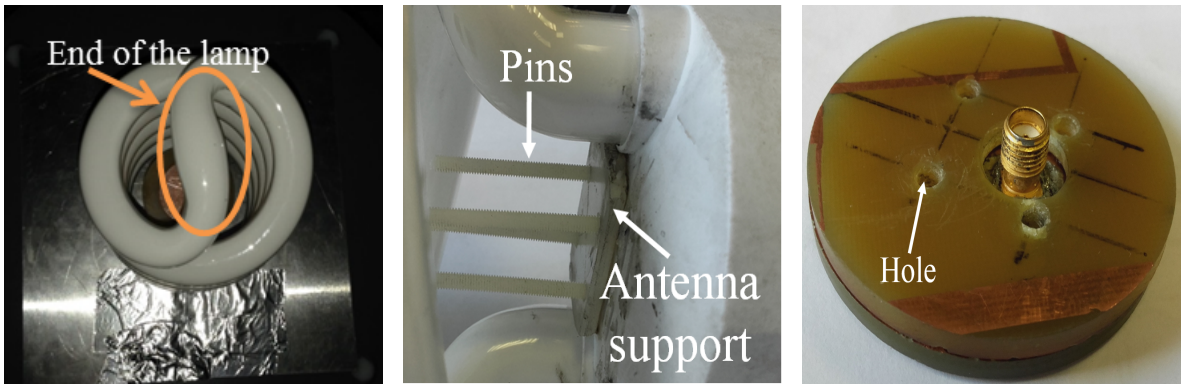

(a) (b) (c)

Figure 3.17: Realized models. (a) The plasma lamp. (b) Antenna support. (c) Second subtrate as support.

3.3.3.3 Results and Discussion

As for simulation, the results are considered for two cases in order to understand the interaction between the patch antenna and the lamp. In the first one, the electric field polarization is parallel to the end of the lamp (y-axis), while in the second one the electric field polarization is orthogonal to the end of the lamp (x-axis). In fact, the antenna inside the lamp is just rotated compared to the lamp.

- **First case: the electric field polarization is parallel to the end of the lamp**

The simulated and measured magnitude of S_{11} parameters are shown in Figure 3.18 for the patch alone and by switching ON or OFF the fluorescent lamp (plasma ON / plasma OFF). The measured results are in a good agreement with the simulated ones. For all configurations (patch alone, plasma OFF, plasma ON), the resonant frequency is close to 2.45 GHz in both simulation and measurement (Fig. 3.18(a) and 3.18(b)). The frequency shift between the configurations is almost equal to 1.2%.

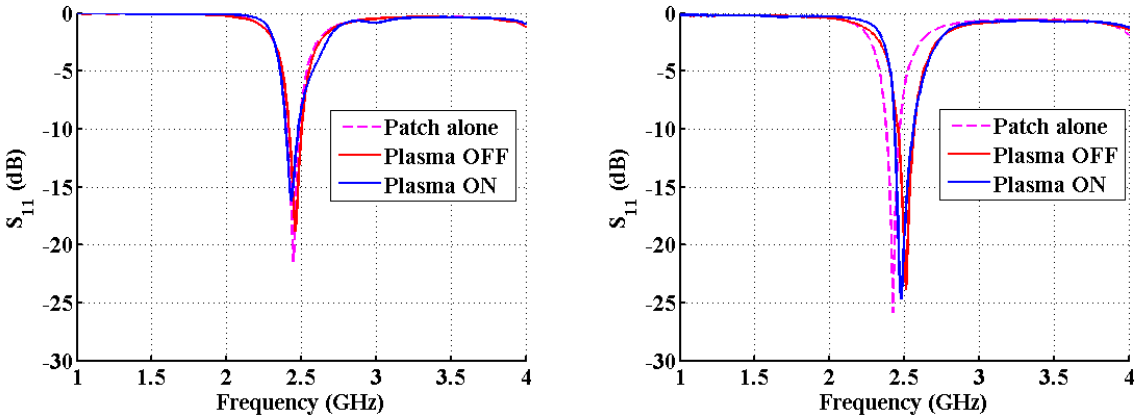

(a) (b)

Figure 3.18: S_{11} magnitude comparison in the first case. (a) Simulation. (b) Measurement.

The Figures 3.19 and 3.20 show the measured and simulated radiation patterns at 2.45 GHz, respectively for the co- and the cross-polarization. For both simulation and measurement results, each radiation pattern is normalized to the maximum value of the electric-field for the plasma OFF. Regarding the gain, we can notice a difference of 10 dB in simulation and 12 dB in measurement between plasma OFF and plasma ON on the angular sector $\theta = \pm 20°$ in co-polarization (Fig. 3.19(a) and 3.19(b)) and a difference of 5 dB for the measured cross-polarization (Fig. 3.20(a) and 3.20(b)).

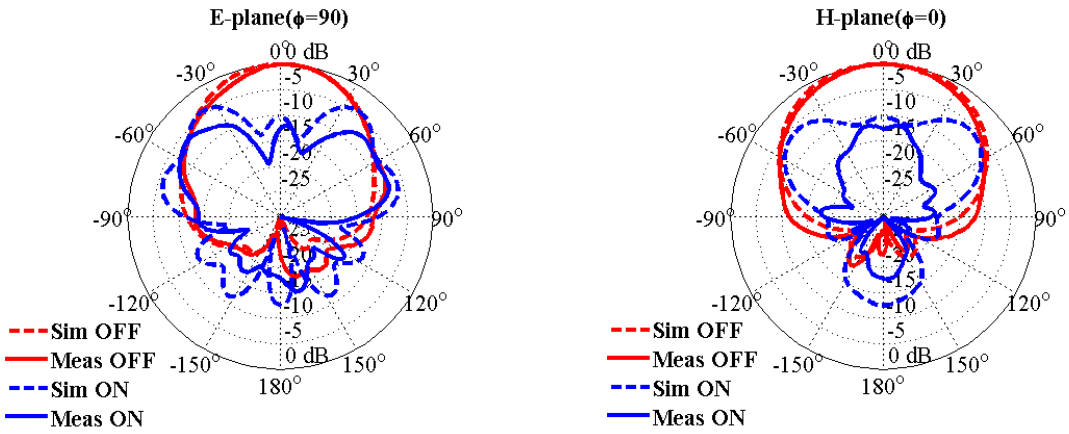

(a) (b)

Figure 3.19: Normalized co-polarization radiation patterns at 2.45 GHz for plasma OFF and plasma ON in the first case. (a) E-plane (b) H-plane.

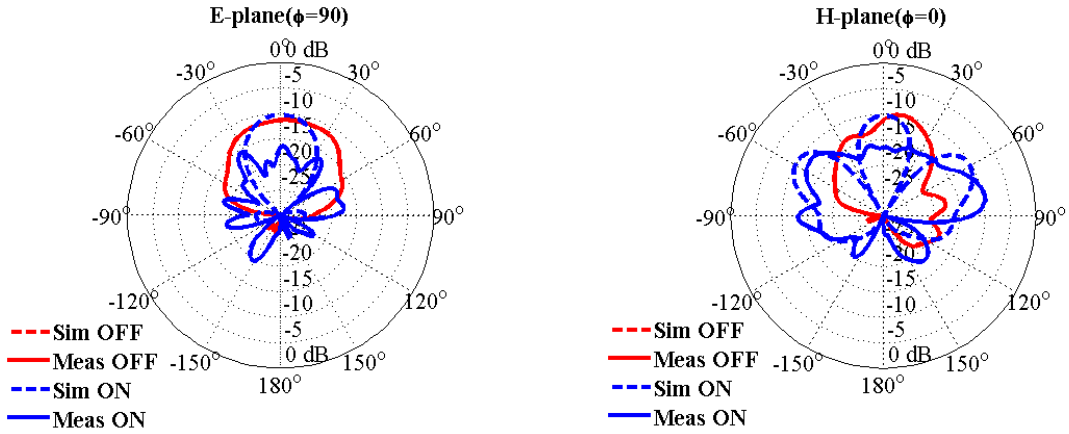

(a) (b)

Figure 3.20: Normalized cross-polaristion radiation patterns at 2.45 GHz for plasma OFF and plasma ON in the first case. (a) E-plane. (b) H-plane.

In co-polarization, the antenna gain decreases strongly when the plasma is ON. The simulated and measured radiation patterns for plasma OFF are similar to the radiation pattern for a classical patch, confirmed that the glass surrounding the plasma has not significant affect on the antenna. But when the lamp is switched ON (plasma ON), the radiation patterns change. In plasma ON case, the measured results are not in good agreement to the simulated ones especially in the H-plane (see Fig. 3.19(b)) due to the inadequate knowledge of the exact plasma parameters.

Contrary of the metal, the using of plasma lamp allows to keep a good matching for the antenna at the operating frequency and the radiation patterns are also reconfigurable.

- **Second case: the electric field polarization is orthogonal to the end of the lamp**

As shown in the Figure 3.21, the simulated and measured magnitude of S_{11} parameters for patch alone, plasma OFF and plasma ON are in good agreement. The resonant frequency is close to the operating frequency for all the configurations.

Furthermore, the Figures 3.18 and 3.21, show that the magnitude of S_{11} parameters are independent to the electric field polarization cases.

The Figure 3.22 and 3.23 represent the measured and simulated radiation patterns at 2.45 GHz for plasma OFF and plasma ON cases (co- and the cross-polarization respectively). The difference of gain is almost 3 dB in simulation and 5 dB in measurement on the angular sector $\theta = \pm 20°$ between plasma OFF and plasma ON in co-polarization (Fig. 3.22(a) and 3.22(b)) and almost 15 dB for the measured cross-polarization (Fig. 3.23(a) and 3.23(b)). In this case, the radiation patterns are not reconfigurable. Furthermore, simulation and measurement results are not in good agreement.

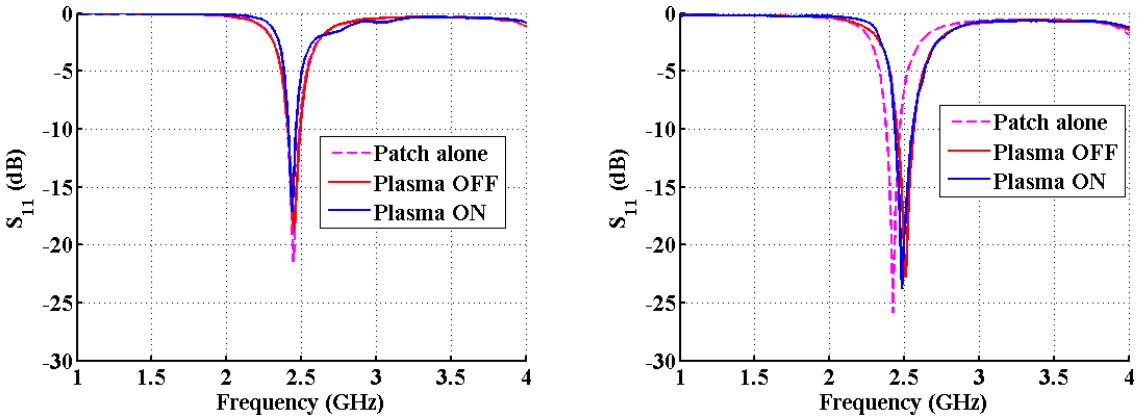

(a) (b)

Figure 3.21: S_{11} magnitude comparison in the second case. (a) Simulation. (b) Measurement.

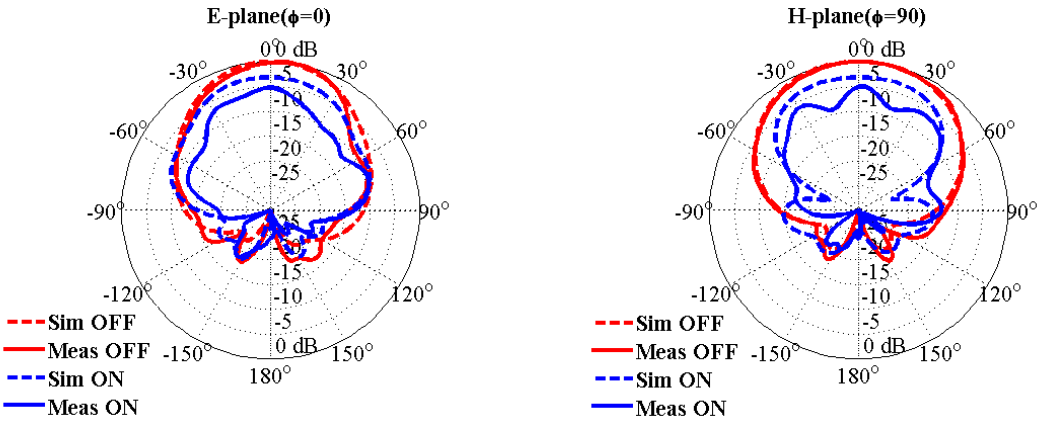

(a) (b)

Figure 3.22: Normalized co-polarization radiation patterns at 2.45 GHz for plasma OFF and plasma ON in the second case. (a) E-plane. (b) H-plane.

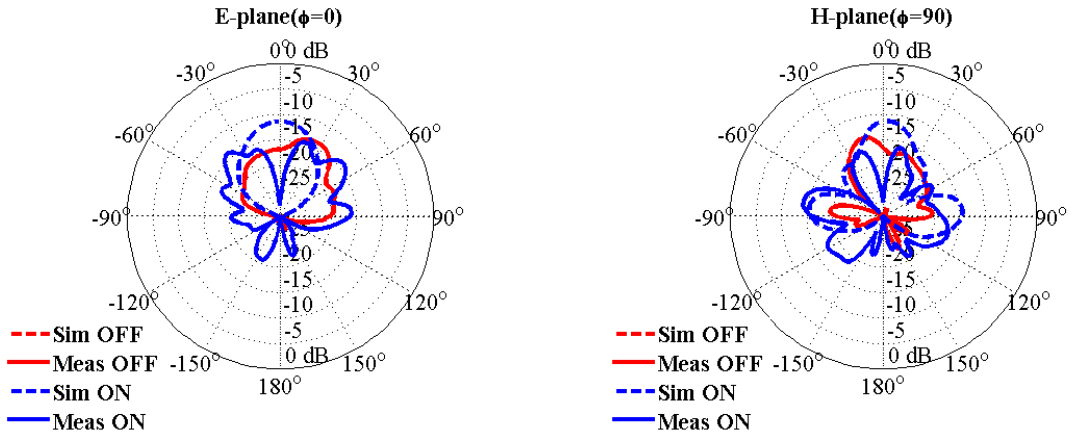

(a) (b)

Figure 3.23: Normalized cross-polarization radiation patterns at 2.45 GHz for plasma OFF and plasma ON in the second case. (a) E-plane. (b) H-plane.

As measurement and simulation are not always in good agreement especially in H-plane, we tried to enhance the model by changing ω_p and ν. After several simulations, the characteristics of the plasma which give the best agreement with the simulations are when ω_p = 62.8318 10^9 rad/s (corresponding to 10 GHz in frequency) is considered and ν is kept equal to 900 MHz. Without any of information from the manufacturer, the retro-simulation was necessary in order to have realistic plasma data for this kind of lamp. In this section, the new results are given for the two cases of polarization.

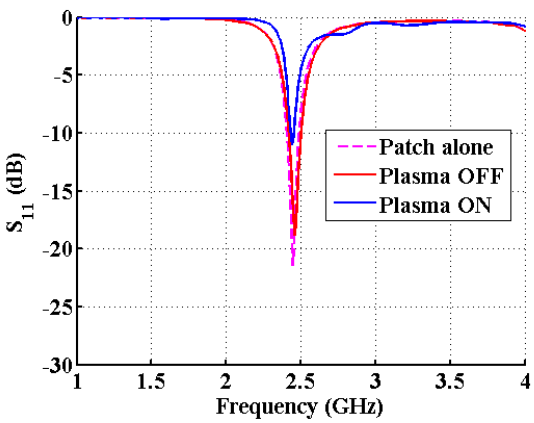

Figure 3.24: Simulated S_{11} magnitude.

The simulated and measured magnitude of S_{11} parameters are shown in Figure 3.24 for the patch, plasma OFF and plasma ON. The measured results are in a good agreement

with the simulated ones. For all configurations (patch alone, plasma OFF, plasma ON), the resonant frequency is close to 2.45 GHz in both simulation and measurement. The S_{11} results are similar in both polarization cases and similar also to the results obtained when ω_p = 43.9823 10^9 rad/s. These results have confirmed that the variation of the plasma angular frequency from ω_p = 43.9823 10^9 rad/s to ω_p = 62.8318 10^9 rad/s has not affected the magnitude of S_{11}.

- **First case: the electric field polarization is parallel to the end of the lamp**

By Referring to Figures 3.25 and 3.26, the simulated radiation patterns are compared to the measured ones. They show the measured and simulated radiation patterns at 2.45 GHz, for respectively the co- and the cross-polarization. For both simulation and measurement results, each radiation pattern is normalized to the maximum value of the electric-field for the plasma OFF. We can clearly observe that the measured and simulated radiation patterns are similar. In term of gain, a difference of 12 dB ($\theta = \pm 20°$) for both simulation and measurement between plasma OFF and plasma ON is observed in E and H-planes for co-polarization (Fig. 3.25(a) and 3.25(b)) and 5 dB in the measured E and H-planes for cross-polarization (Fig. 3.26(a) and 3.26(b)). In co-polarization, the antenna gain decreases strongly when the plasma is ON.

Table 3.1 presents the maximum simulated and measured gain at 2.45 GHz. We show also the simulated directivity in plasma OFF and ON cases. In plasma OFF case, the directivity is 7.5 dBi while it is 5.2 dBi for the plasma ON case. In term of maximum realized gain, we obtain respectively 6.4 dBi for plasma ON and 0.3 dBi for plasma OFF case. The difference between the directivity and the gain in plasma ON case is due to the loss introduced by the plasma because it is not a perfect metal. The measurement confirms the simulation. The obtained results show a strong reduction between plasma OFF and ON. Furthermore, the antenna is reconfigurable in terms of radiation patterns by switching ON the plasma.

Table 3.1: Directivity and maximum realized gain for the patch in the first case

States	Plasma OFF	Plasma ON
Simulated directivity (dBi)	7.5	5.2
Maximum simulated gain (dBi)	6.4	0.3
Maximum measured gain (dBi)	6	0.2

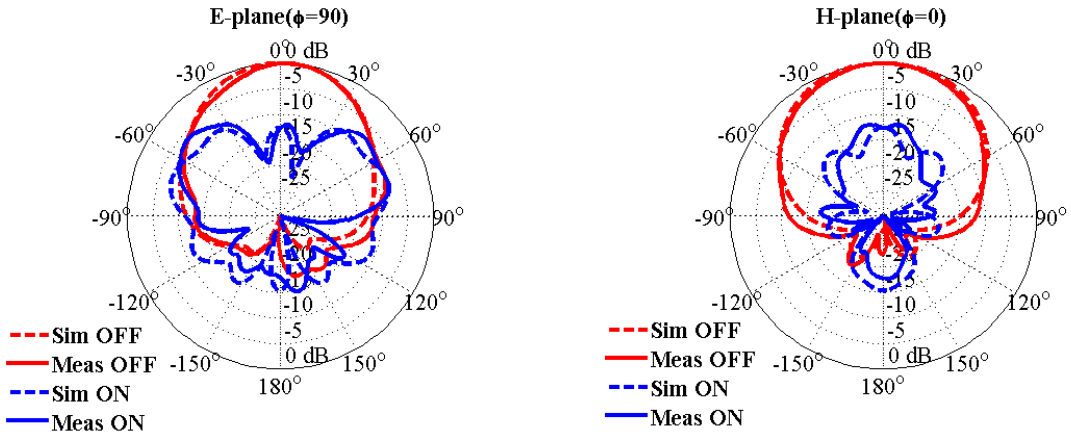

(a) (b)

Figure 3.25: Normalized co-polarization radiation patterns at 2.45 GHz for plasma OFF and plasma ON in the first case with $\omega_p = 62.8318\ 10^9$ rad/s. (a) E-plane. (b) H-plane.

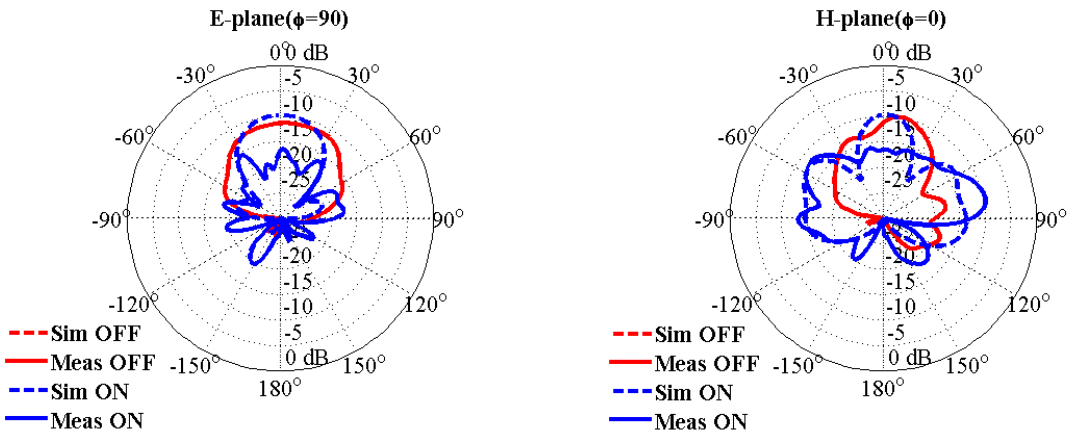

(a) (b)

Figure 3.26: Normalized cross-polarization radiation patterns at 2.45 GHz for plasma OFF and plasma ON in the first case with $\omega_p = 62.8318\ 10^9$ rad/s. (a) E-plane. (b) H-plane.

- **Second case: the electric field polarization is orthogonal to the end of the lamp**

The Figures 3.27 and 3.28 show the normalized radiation patterns respectively for the co- and cross-polarization. For the co-polarization (Fig. 3.27(a) and 3.27(b)), the difference of gain is 7 dB in simulation and 5 dB in measurement for $\theta = \pm 20°$ between plasma OFF and plasma ON.

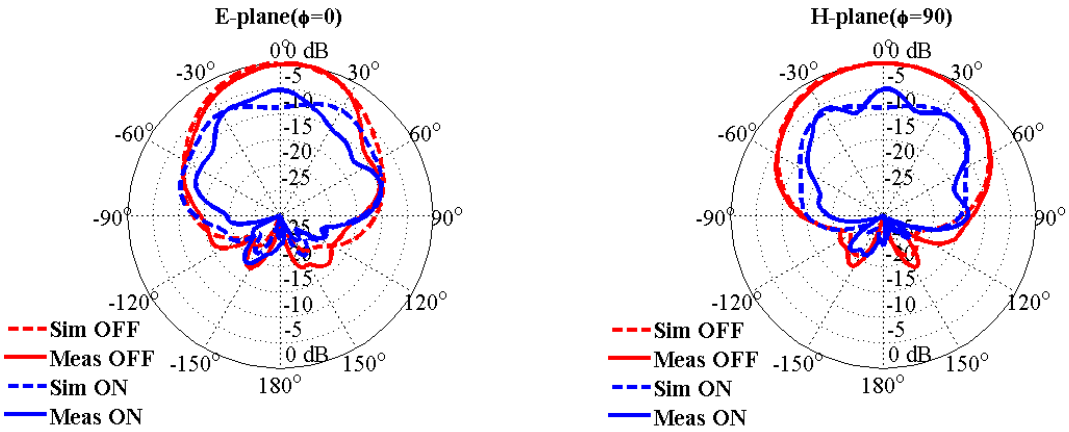

(a) (b)

Figure 3.27: Normalized co-polarization radiation patterns at 2.45 GHz for plasma OFF and plasma ON in the second case with ω_p = 62.8318 10^9 rad/s. (a) E-plane. (b) H-plane.

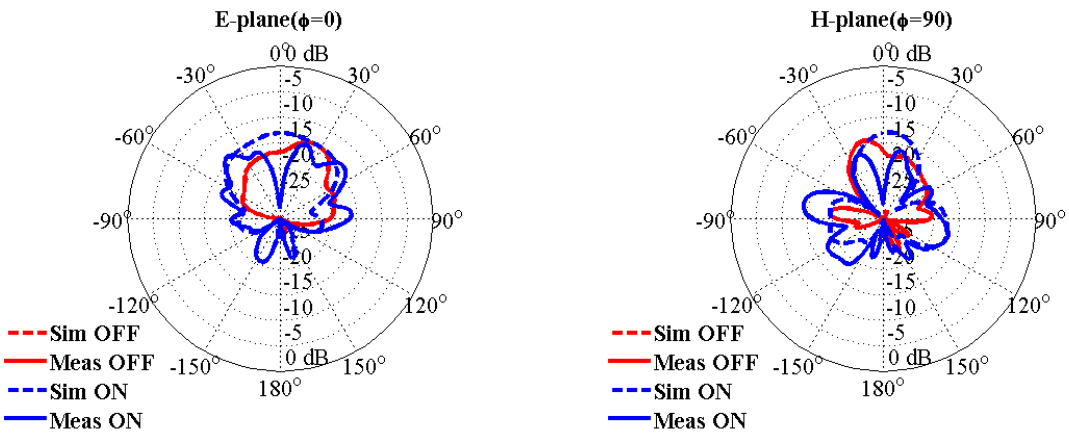

(a) (b)

Figure 3.28: Normalized cross-polarization radiation patterns at 2.45 GHz for plasma OFF and plasma ON in the second case with ω_p = 62.8318 10^9 rad/s. (a) E-plane. (b) H-plane.

Table 3.2 shows the directivity and the maximum realized gain at 2.45 GHz. The results obtained present a slight reduction between plasma OFF and ON and the antenna is not reconfigurable in terms of radiation patterns by switching ON the plasma. The measurement is in good agreement with the simulation.

Table 3.2: Directivity and maximum realized gain for the patch in the second case

States	Plasma OFF	Plasma ON
Simulated directivity (dBi)	7.5	5.4
Maximum simulated gain (dBi)	6.4	1.4
Maximum measured gain (dBi)	5.9	0.7

In the Figures 3.26(a), 3.26(b), 3.28(a) and 3.28(b) the levels of simulated plasma OFF cross-polarization are very low in E and H-planes and do not appear in the figures.

The results for the first case (polarization of patch along y axis) are more interesting because the decreasing of gain is more significant and the radiation patterns of the antenna are reconfigurable.

3.3.3.3.1 Influence of the part of the lamp

After, we tried to understand which part of the lamp affects the radiation patterns. Thus, in the simulations, the lamp is separated in two parts, the end of the lamp (without spiral part, see Fig. 3.29(a)) and the spiral part (without the end of the lamp, see Fig. 3.29(b)).

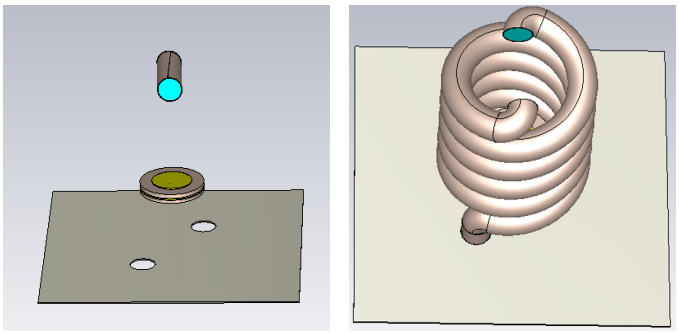

(a) (b)

Figure 3.29: Parts of the lamp. (a) End of the lamp only. (b) Spiral part only.

- **First case: the electric field polarization is parallel to the end of the lamp**

Figure 3.30 shows the co-polarization normalized radiation patterns in E-plane (Figs. 3.30(a)) and H-plane (Figs. 3.30(b)) of the end of the lamp and the spiral part compared to the plasma OFF and plasma ON. This curves are normalized to the maximum value of the electric-field for the plasma OFF. We notice that, the radiation patterns are affected by the combination of both parts and not only by the end of the lamp. In fact, the lamp and the patch are relatively near to each other, so the impact of lamp must be seen in

near fields conditions that can explain why the two parts of the lamp (end and spiral ones) affect the electric field of the patch antenna.

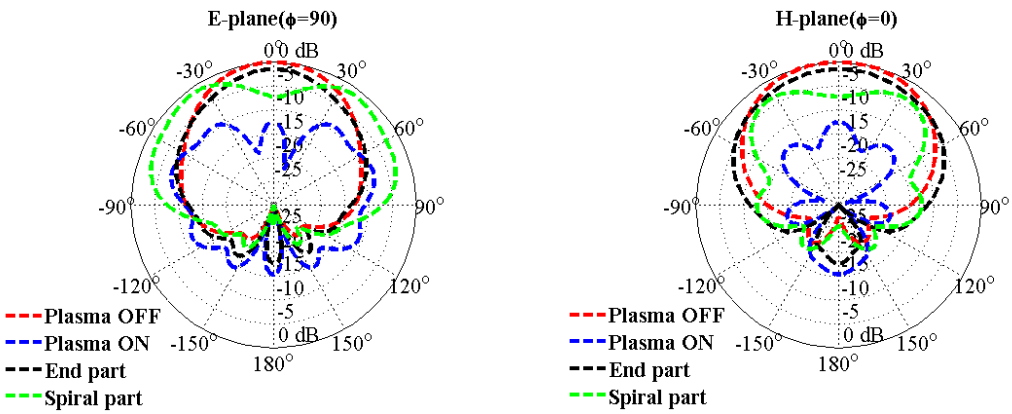

(a) (b)

Figure 3.30: Normalized co-polarization radiation patterns at 2.45 GHz for plasma OFF, plasma ON, the end of the lamp and spiral part in first case. (a) E-plane. (b) H-plane.

- **Second case: the electric field polarization is orthogonal to the end of the lamp**

The co-polarization normalized radiation patterns in E-plane (Figs.3.31(a)) and H-plane (Figs. 3.31(b)) of the end of the lamp and spiral part compared to the plasma OFF and plasma ON is presented in Figure 3.31.

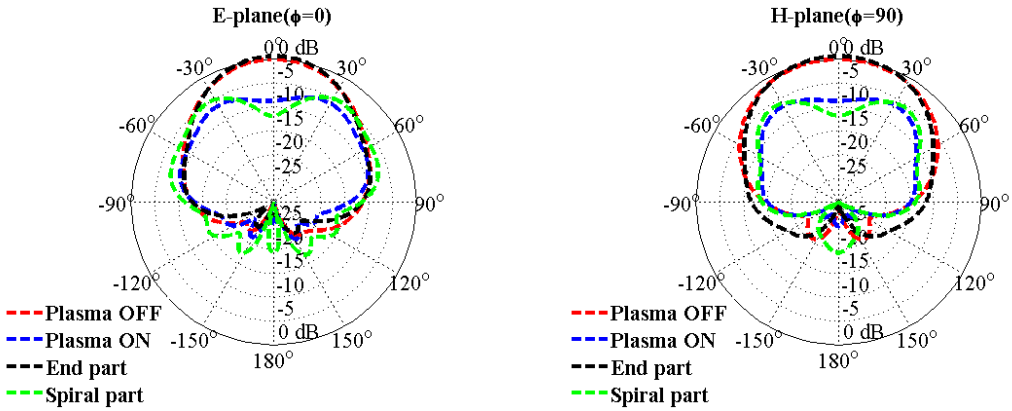

(a) (b)

Figure 3.31: Normalized co-polarization radiation patterns at 2.45 GHz for plasma OFF, plasma ON, the end of the lamp and spiral part in the second case. (a) E-plane. (b) H-plane.

It is clearly to observe that, in this second case, the spiral part affect mostly the radiation patterns since as the radiation patterns of the end of the lamp and the plasma OFF are quite similar.

3.4 Monopole Antenna case

3.4.1 Monopole alone

In this part, we replace the patch antenna by a quarter-wavelength monopole. The diameter is 2 mm and the height is 30 mm. This monopole is placed in the center of a ground plane with a diameter of 50 mm. The Figures 3.32(a) and 3.32(b) present the simulated and manufactured monopole. The four holes seen in the ground plane (Fig. 3.32(b)) are used to connect the four pins in order to fix the monopole inside the lamp.

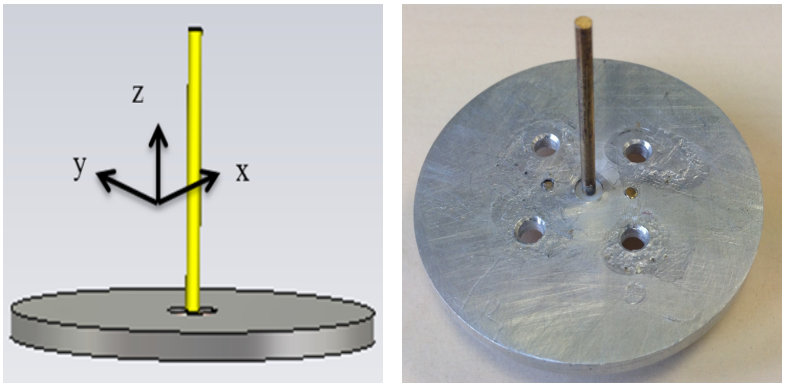

(a) (b)

Figure 3.32: Monopole antenna. (a) Simulated monopole. (b) Manufactured monopole.

The performance of the monopole antenna in terms of S11 and radiations patterns is represented respectively in the Figures 3.33 and 3.34.

The obtained results in measurement and simulations are in good agreement. The monopole is matched at the operating frequency.

The normalized radiation patterns shown in Figures 3.34(a) and 3.34(b), demonstrate that the level of measured cross-polarization is below than -20 dB and the simulated cross-polarization in E and H-planes is below than -30 dB that's why it does not appear in the Figures. The realized gains in simulation and measurement are 1.1 dB and 0.5 dB respectively. These gains are small due to the reduced size of the ground plane.

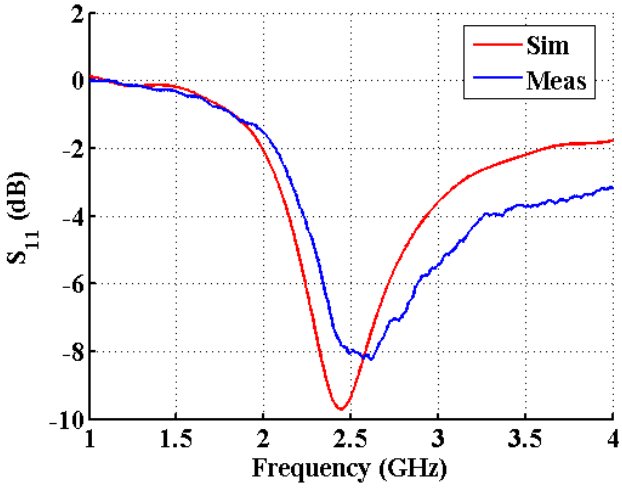

Figure 3.33: Simulated and measured S_{11} for the monopole.

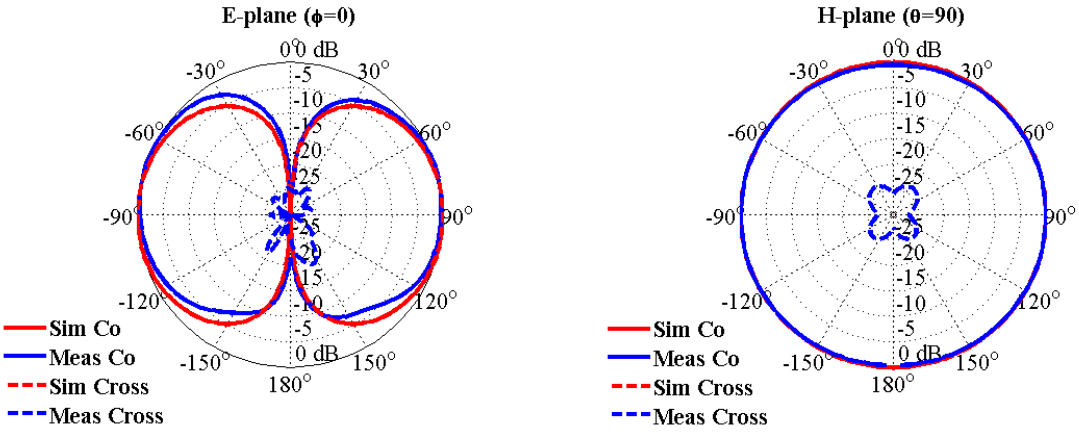

(a) (b)

Figure 3.34: Normalized radiation patterns at 2.45 GHz. (a) E-plane. (b) H-plane.

3.4.2 Monopole inside the lamp

3.4.2.1 Modeling and Simulation

As previously for the patch, the monopole is put inside the lamp at the distance $d = 50$ mm from the reflector plane used to hide the electronic devices (see Fig. 3.35). The monopole is polarized along the z-axis.

Figure 3.35: Monopole inside the lamp.

3.4.2.2 Results and discussion

The Figures 3.36(a) and 3.36(b) show the magnitude of S_{11} for simulation and measurement respectively. The antenna is not well matched at the operating frequency in plasma ON case. The resonant frequency is shifted in plasma ON case at 3.5 GHz in measurement and almost at 4 GHz in simulation. Therefore, the plasma affects the resonant frequency of the antenna.

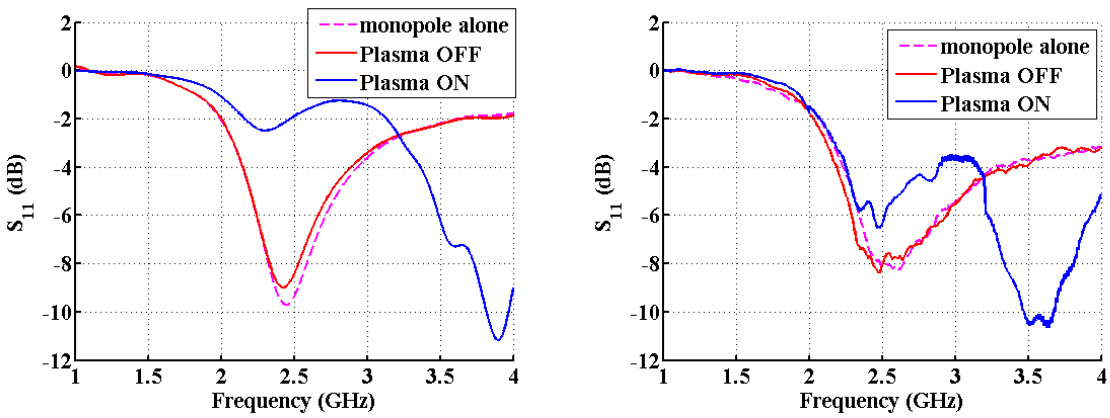

(a) (b)

Figure 3.36: S_{11} magnitude parameter comparison. (a) Simulated S_{11} monopole antenna. (b) Measured S_{11} monopole antenna.

Figures 3.37 and 3.38 present the normalized radiation patterns in E and H-planes for co and cross-polarization respectively. For the co-polarization (Figs. 3.37(a) and 3.37(b)), the difference of gain between plasma OFF and plasma ON is low, almost 5 dB, because the electric field polarization of monopole is orthogonal to the spiral part of the lamp. So the electromagnetic waves coming from the monopole are weakly attenuated. The cross-polarization levels (Figs. 3.38(a) and 3.38(b)) are lower than -10 dB in measurement and simulation. For plasma ON case, we obtain a classical radiation patterns of a monopole antenna. Therefore the antenna is not reconfigurable.

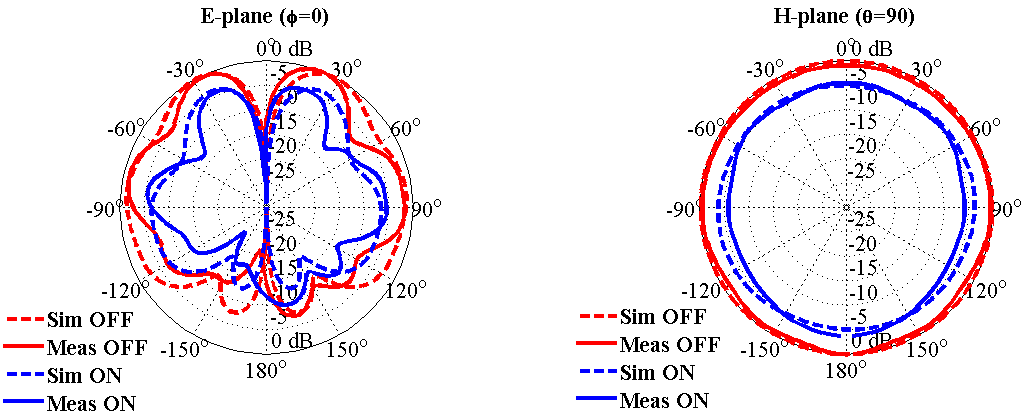

(a) (b)

Figure 3.37: Normalized co-polarization radiation patterns at 2.45 GHz for plasma OFF and plasma ON. (a) E-plane. (b) H-plane.

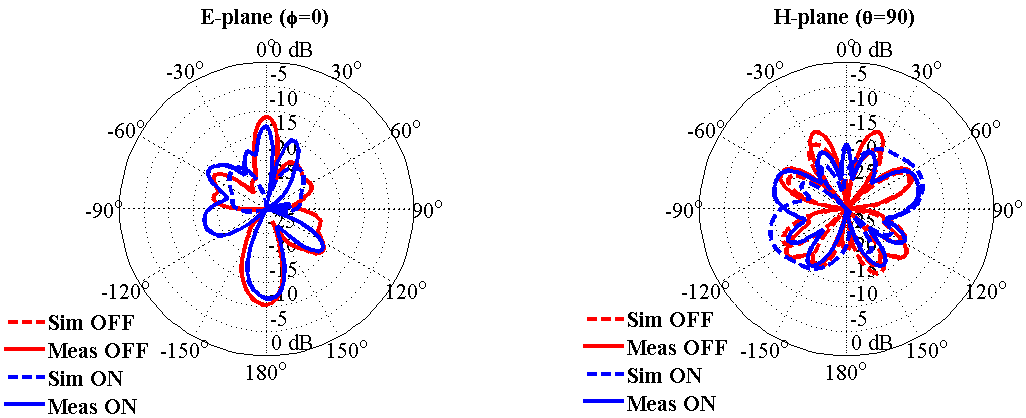

(a) (b)

Figure 3.38: Normalized cross-polarization radiation patterns at 2.45 GHz for plasma OFF and plasma ON. (a) E-plane. (b) H-plane.

Table 3.3 shows the directivity and the maximum realized gain at 2.45 GHz for the monopole antenna. The directivity is similar for plasma OFF and ON. The simulation and measurement are in good agreement and the gain decreases slightly when the plasma is switched ON.

Table 3.3: Directivity and maximum realized gain in the monopole case

States	Plasma OFF	Plasma ON
Simulated directivity (dBi)	3.8	4
Maximum simulated gain (dBi)	3.4	-1.3
Maximum measured gain (dBi)	3	-0.7

Simulations with a metallic lamp have been done to compare with the plasma lamp configuration. The figure 3.39 shows the normalized radiation patterns for the plasma OFF and metallic lamp. Thus the difference between plasma OFF and metal is 5 dB. These results confirm that the monopole is not very affected by shielding using spiral lamp.

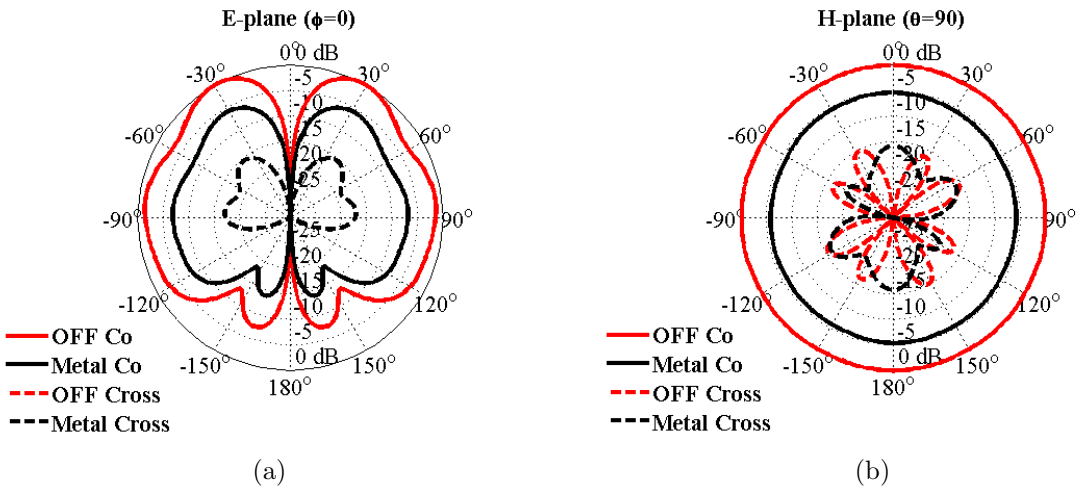

(a) (b)

Figure 3.39: Simulatd normalized radiation patterns at 2.45 GHz for plasma OFF and metal. (a) E-plane. (b) H-plane

3.5 Conclusion

In this chapter, a shielding cage using commercial fluorescent lamp (plasma) was presented. Two types of antennas were considered inside the lamp to show the impact of this cage on antenna radiation pattern and polarization. It is interesting to note that the radiation patterns of the patch (first case) can be strongly reduced when the plasma is ON and they are reconfigurable due to the presence of the plasma lamp. The results show that the shielding depends to the polarization. This behavior can be suitable to protect the antenna against external undesirable signal.

Bibliography

[1] Maxi Helitron, 220-240V/ 50Hz, Beneito and Faure, Lighting S.L., http://www.beneito-faure.com/.

[2] CST, "Computer Simulation Technology," http://www.cst.com/

[3] M. T. Jusoh, O. Lafond, F. Colombel, and M. Himdi, "Performance of a reconfigurable reflector antenna with scanning capability using low cost plasma elements," *Microwave and Optical Technology Letters*, vol. 55, no. 12, pp. 2869-2874, 2013.

[4] M. T. Jusoh, M. Himdi, F. Colombel, and O. Lafond, "Performance and radiation patterns of a reconfigurable plasma corner-reflector antenna," *IEEE Antennas and Wireless Propagation Letters*, no 99, pp. 1137-1140, 2013.

[5] M. T. Jusoh, "Study and design of reconfigurable antennas using plasma medium," *Thse de doctorat - Universit Rennes 1*, Avril 2014.

Chapter 4

Reconfigurable antenna arrays

Since many years, reconfigurable antenna arrays have been studied due to their ability to do multipurpose function. There are three types of reconfigurable antennas which are frequency, radiation pattern and polarization. In this chapter, we present reconfigurable antennas using plasma tubes allowing to obtain reconfigurable Half-Power-Beam-Width (HPBW) of the radiation patterns.

Two original structures have been studied:

- A printed four patches array operating at 2.45 for which one we put above each radiating element a plasma tube allowing to weight the different radiating elements and therefore to reconfigure the HPBW of the radiation pattern.

- A slot antenna array operating at the same frequency for which plasma flaps are used to close the aperture of the slots in order also to reconfigure the HPBW of the radiation pattern.

4.1 Patches array at 2.45 GHz

In this section we present a reconfigurable patches array using plasma tubes. There are different types of microwave switches, based on different technologies to have reconfigurable patches array in the literature. In [1–3], the authors proposed a reconfigurable system by using available commercial transistors, easily integrable and working in one direction (transmission or reception). On the other hand, a reconfigurable system was proposed in [4] using MEMS (Micro-Electro-Mechanical-Systems) offering very interesting performance, but still requires technological maturity. For all these systems, the main difficulty is to keep a good matching whatever the number of fed antennas in the array. The main advantage using plasma tubes compared to microwave switches resides in the possibility to keep a good matching level whatever the number of active patches in the array. So the matching of antenna can be good for all configurations.

4.1.1 Patches array alone

The patches array geometry based on four-elements spaced by $0.5\lambda_0$ and operating at 2.45 GHz is shown in Figures 4.1 and 4.2. Each radiating element is a rectangular patch whose length and width are equal to 34.8 mm and 25 mm respectively. The four patches are fed through a 1:4 power divider. The patches are printed on Neltec (NX9300) substrate with a thickness h = 0.786 mm, ϵ_r = 3 and $\tan\delta$ = 0.002. The antenna is polarized along the y-axis and the ground plane is printed on the bottom side of the substrate. The Figures 4.1 and 4.2 show respectively the design of simulated patches array and the manufactured patches array.

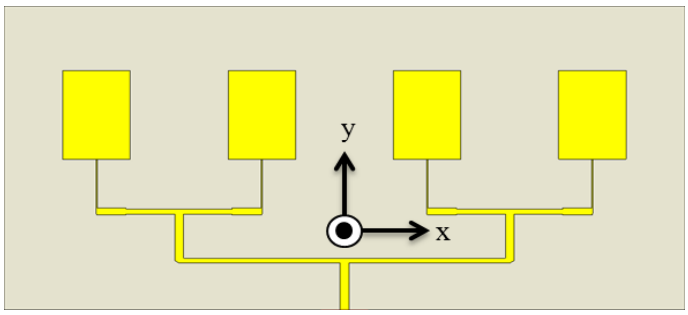

Figure 4.1: Design of simulated patches array.

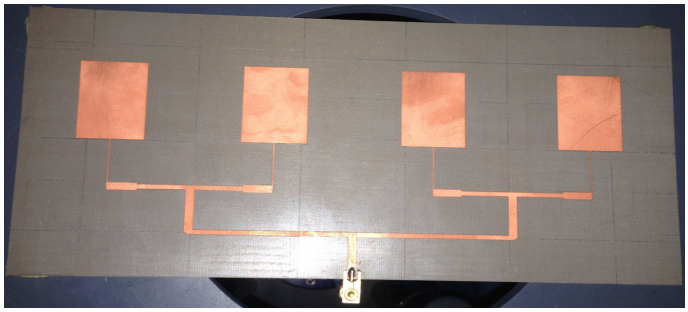

Figure 4.2: Manufactured patches array.

The performance of the patches array is presented in the Figures 4.3 and 4.4 in terms of S_{11} and radiation patterns. The Figure 4.3 shows the simulated and measured magnitude of S_{11} parameter for the array. The simulated S_{11} parameter is matched at the operating frequency (2.45 GHz) but there is a little bit shift for the measured S_{11} and the antenna is matched at 2.48 GHz (shift of 30 MHz corresponding to 1.2%).

Radiation patterns have been measured in order to validate the simulation results. Measurements have been performed in a SATIMO anechoic chamber (near fields setup) with a peak gain accuracy equals to ±0.8 dBi. The simulated radiation patterns are presented at

2.45 GHz and the measured radiation patterns are given at 2.48 GHz in agreement with the best matching frequency.

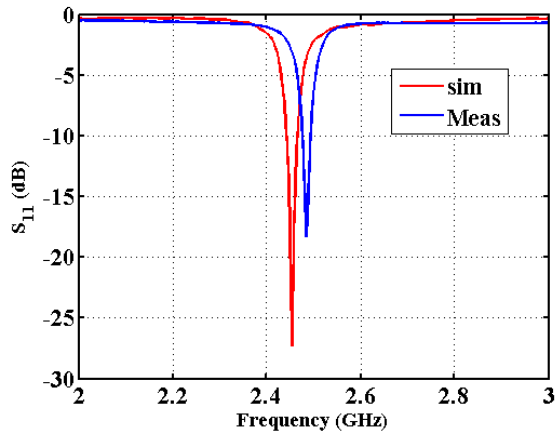

Figure 4.3: Simulated and measured of the magnitude of S_{11} parameter for the patches array.

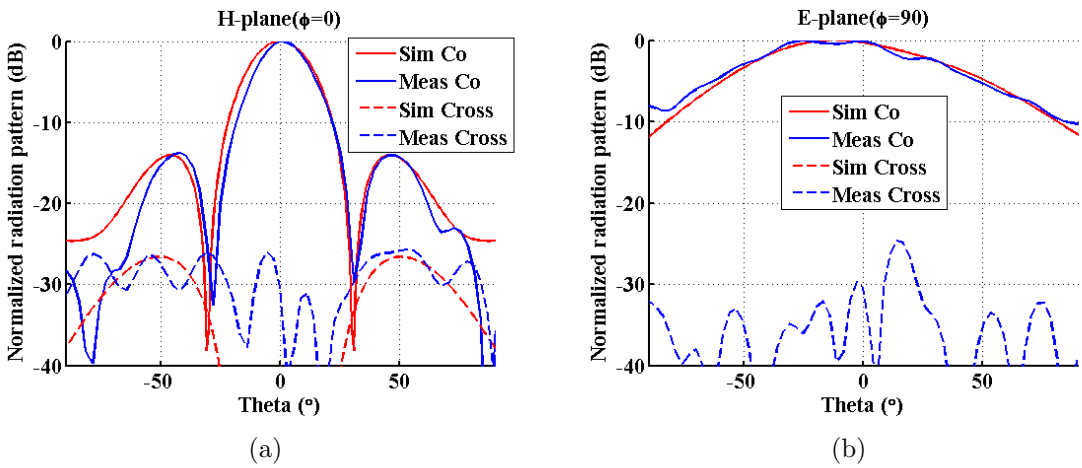

Figure 4.4: Normalized radiation patterns of patches array, simulation at 2.45 GHz and measurement at 2.48 GHz. (a) H-plane. (b) E-plane.

The Figure 4.4 shows the simulated and measured normalized radiation patterns in both planes (H-plane and E-plane) for the patches array. For both simulation and measurement results, each radiation pattern is normalized to the maximum value of its electric-field. We can clearly observe that the measured and simulated radiation patterns are similar. The results obtained are similar to the results for a classical four patches array. In the H-plane

(Fig. 4.4(a)), the simulated HPBW is equal to 25.6° and the measured HPBW is 23°. The simulated and measured realized gain are respectively 10 dBi and 9 dBi. The side lobe level (SLL) is almost -13 dB in simulation and measurement. The cross polarization level is lower than -20 dB for simulation and measurement in both planes. The simulated E-plane cross-polarization does not appear because its level is very low.

4.1.2 Antenna system (patches array with plasma wall)

The main idea is to reconfigure the radiation patterns. For that, we use plasma commercial fluorescent lamps and each lamp is put above a radiating element. Depending to the number of energized plasma tubes, it will be possible to change the beamwidth of radiation pattern because each switched ON tube acts like a "quasi metallic cover" for radiating patch.

4.1.2.1 Modeling and Simulations

The designed and manufactured patches array with the plasma wall made with four commercial fluorescent lamps (T8 type) is shown in Figures 4.5, 4.6 and 4.8. The height of each lamp is 590 mm, the tube diameter is 26 mm, and the gap between two adjacent lamps is $0.5\lambda_0$ in order to respect the inter-element distance in the array. Each tube is put above a radiating element and the distance between the antenna and the plasma wall is d (Fig. 4.5).

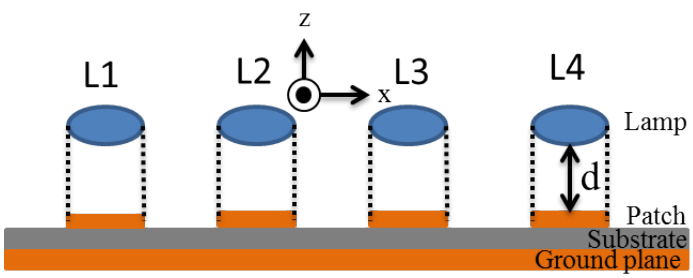

Figure 4.5: Geometry of the system.

For simulations performed with CST Microwave Studio [5], the tubes containing the gas are made from lossy pyrex glass with ϵ_r = 4.82, $\tan\delta$ = 0.005 and thickness of 0.5 mm. Furthermore, we used the same Drude model as in [6], with the same parameters (ν = 900 MHz and ω_p = 43.9823 10^9 rad/s). The simulated antenna system is shown in Figure 4.6.

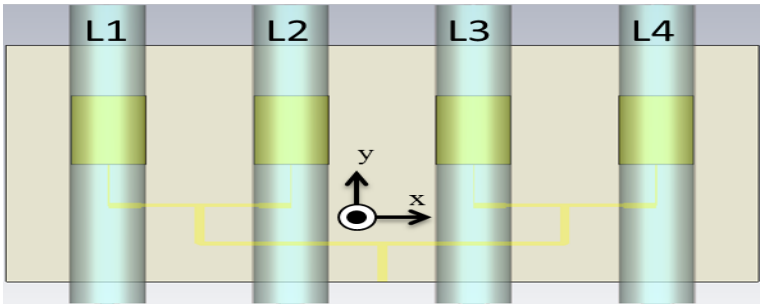

Figure 4.6: Simulated model: The patches array with plasma wall.

Plasma wall was build using fluorescent lamps (4000K color temperature) which are arranged in parallel. The lamp sockets are bi-pin G13 and are regulated by electronic ballasts. The power to energize the 18-W commercial fluorescent lamps is supplied by a set of electronic ballasts with specification of 220-240 V, 50-60 Hz (see Fig. 4.7). The realized prototype is shown in Figure 4.8.

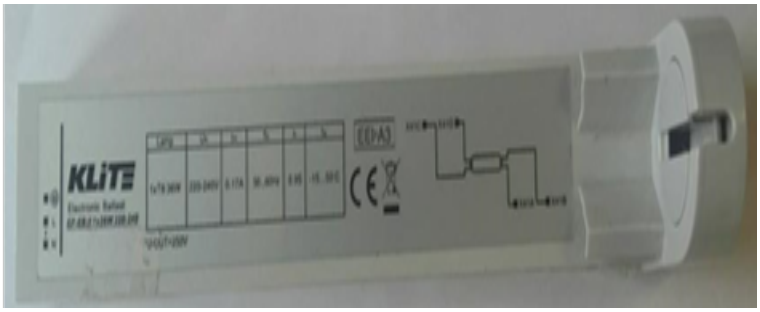

Figure 4.7: Electronic ballast.

Figure 4.8: Realized model: The patches array with plasma wall.

In this study, many configurations have been tested by switching OFF or ON state (energized) the lamps. The table 4.1 summarizes the tested configurations. It exists others

configurations when two lamps are ON (L1 and L2, L1 and L3, L2 and L3, L3 and L4). But some of them give dissymetric radiation patterns (L1 and L2, L3 and L4) or induce grating lobes in the radiation patterns (L1 and L3, L2 and L3) because the inter-element distance is equal or higher than λ. So these configurations are not considered here.

Table 4.1: Configurations

Configurations	**C0**	**C1**	**C2**	**C3**	**C4**
Switching ON	-	L4	L1 and L4	L1, L3 and L4	L1, L2, L3 and L4

4.1.2.2 Parametric study

First, we start to do a parametric study for d (distance between the patch and the wall of plasma. see Fig. 4.5) in order to find which distance gives us the best trade-off for good matching for all the configurations.

- **distance** $d = 0$ **mm**

The simulated and measured S_{11} magnitude for the distance d = 0 mm and for all the configurations are shown respectively in Figures 4.9(a) and 4.9(b). We can notice that, some configurations are not well matched nor in simulation and in measurement. For example, the C4 configuration is not matched (-4 dB in measurement and -7 dB in simulation).

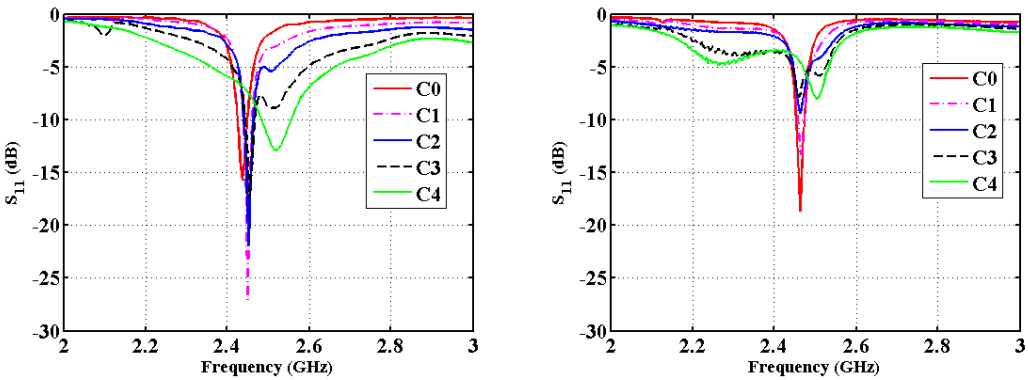

(a) (b)

Figure 4.9: S_{11} magnitude comparison for $d = 0$ mm. (a) Simulation. (b) Measurement.

- **distance** $d = 3$ **mm**

The Figures 4.10(a) and 4.10(b) show respectively the simulated and measured magnitude of the S_{11} parameter for all the configurations. A good matching at 2.45 GHz for all configurations is remarked in simulation but the matching is not perfect for all the configurations in measurement.

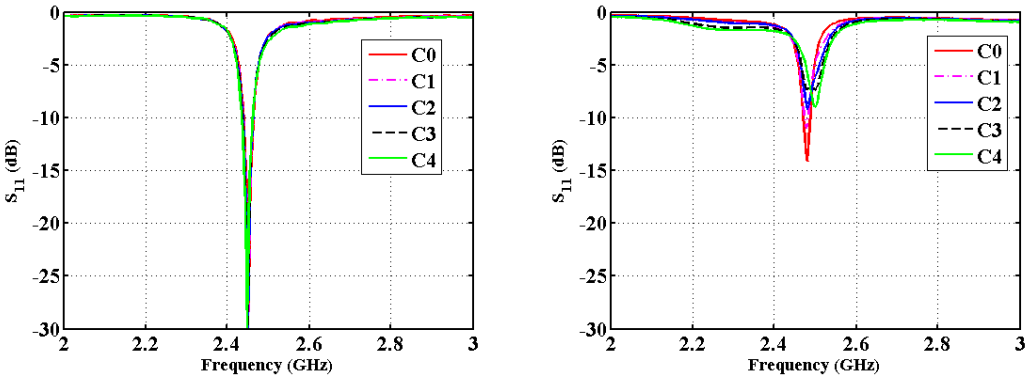

(a) (b)

Figure 4.10: S_{11} magnitude comparison for $d = 3$ mm. (a) Simulation. (b) Measurement.

- **distance $d = 6$ mm**

We extend our parametric study at $d = 6$ mm. The simulated and measured magnitude of the S_{11} and for all the configurations are shown respectively in Figures 4.11(a) and 4.11(b). The measured results are in a good agreement with the simulated ones and for all configurations, the resonant frequency is 2.45 GHz in simulation (Fig. 4.11(a)) and 2.48 GHz in measurement (Fig. 4.11(b)).

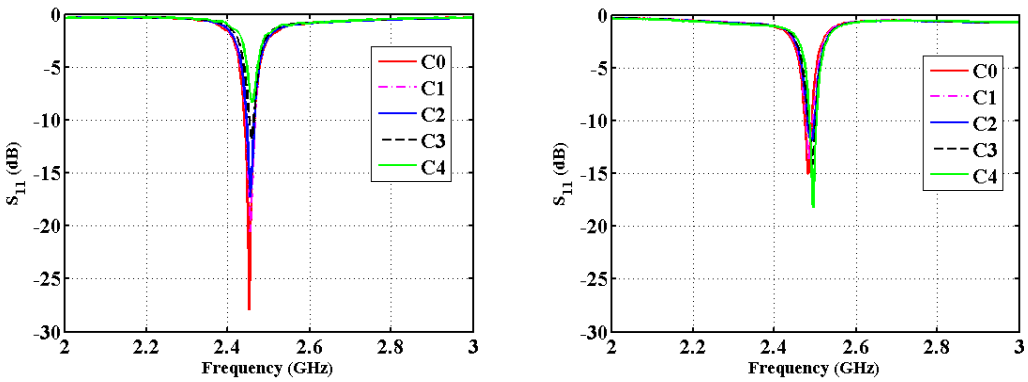

(a) (b)

Figure 4.11: S_{11} magnitude comparison for $d = 6$ mm. (a) Simulation. (b) Measurement.

The obtained results for d = 6 mm show that the simulation and measurement are similar and all the configurations are matched. Therefore, the results presented in the rest of the section 4.1.2 is for d = 6 mm. These results show also that the matching of the patches array is not significantly affected by the plasma tubes (ON or OFF). In fact, this result is obtained thanks to the plasma tubes because they don't act like perfect conductors.

4.1.2.3 Results and Discussion

The Figures 4.12 and 4.13 show the H-plane and E-plane of simulated and measured radiation patterns respectively for the configurations C0, C1, C2 and C3. For both simulation and measurement results, each radiation pattern is normalized to the maximum value of its electric-field. We can clearly observe that the radiation patterns in measurement and simulation are similar.

In the H-plane (Fig. 4.12), the simulated HPBW (Fig. 4.12(a)) is equal to 25.6° for C0 configuration, 30° for C1, 37.1° for C2 and 37.4° for C3 and the measured HPBW (Fig. 4.12(b)) is equal to 23° for C0 configuration, 28° for C1, 37° for C2 and 38° for C3. The simulated maximum realized gains are 10.1, 9.2, 7.6 and 5.5 dBi for C0, C1, C2 and C3 configurations respectively and the measured maximum realized gains are respectively equal to 9.3, 7.7, 5.6 and 3.2 dBi for the same configurations. The simulated side lobe level (SLL) is good whatever the configuration, both in simulation and measurement. The level of the cross polarization component for all configurations is lower than -20 dB in simulation and -15 dB in measurement.

In the E-plane (Fig. 4.13), all configurations give quite the same radiation patterns because they are not affected by the array factor (Fig. 4.13(a) and Fig. 4.13(b)).

Moreover, some simulations have been performed to demonstrate that the Pyrex glass of the lamps has no effect on radiation patterns when all the lamps are OFF.

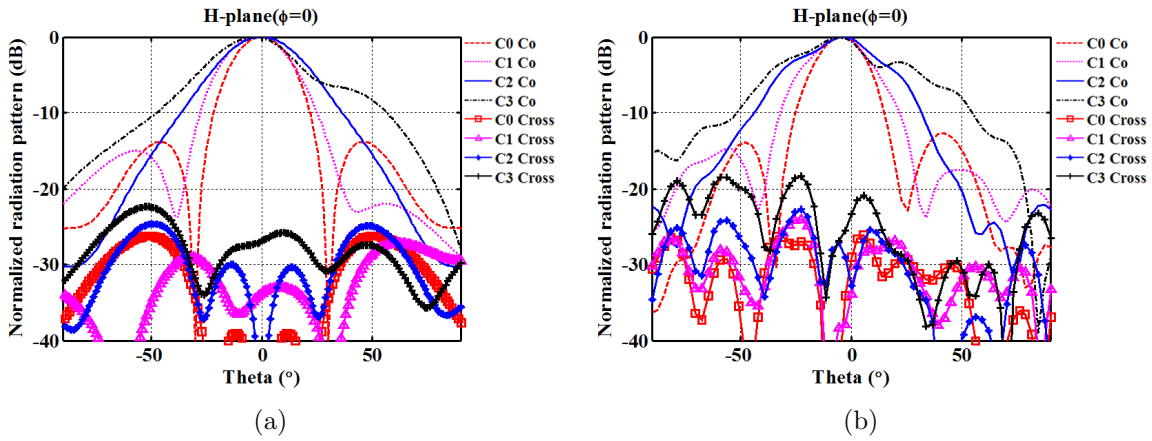

Figure 4.12: Normalized H-plane radiation patterns. (a) Simulation at 2.45 GHz. (b) Measurement at 2.48 GHz.

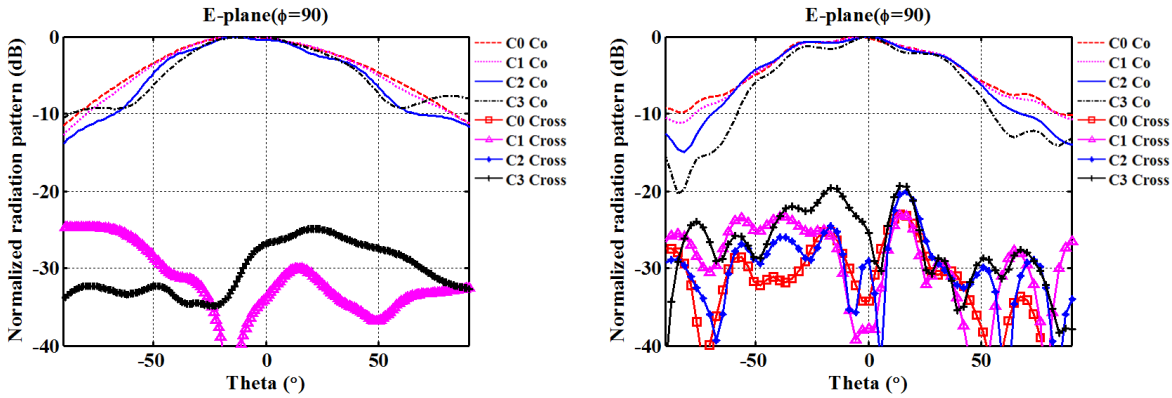

(a) (b)

Figure 4.13: Normalized E-plane radiation patterns.(a) Simulation at 2.45 GHz. (b) Measurement at 2.48 GHz.

In a second time, we compared C0 and C4 configurations in order to find out the gain reduction when all the plasma tubes are switched ON. The Figures 4.14 and 4.15 show the simulated and measured radiation patterns respectively for the C0 and C4 configurations and for the two planes (E and H). For both simulation and measurement results, each radiation pattern is normalized to the maximum value of the electric field for C0 case.

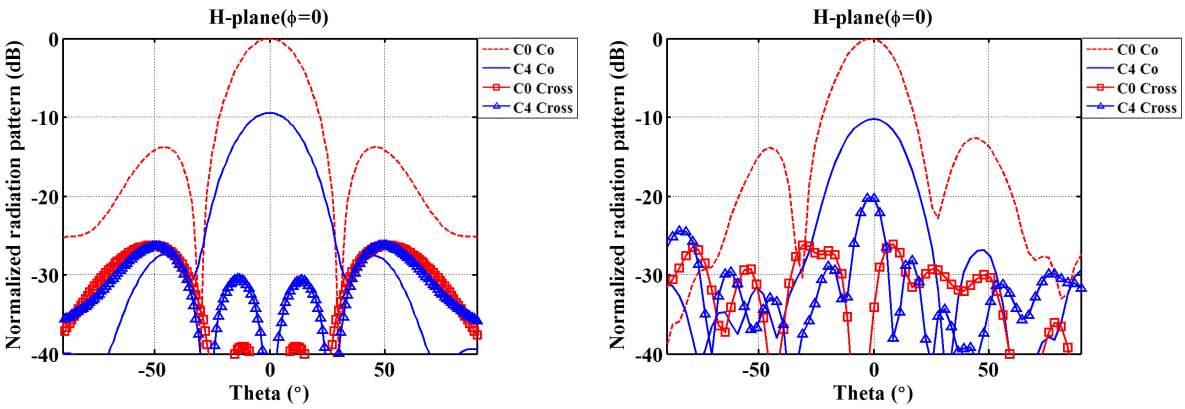

(a) (b)

Figure 4.14: Normalized H-plane radiation patterns. (a) Simulation. (b) Measurement.

We can clearly observe that the radiation patterns in measurement and simulation are quite similar. Regarding the gain, we can notice a difference of 10 dB for both simulation and measurement between C0 and C4 configurations. The antenna gain decreases strongly when all the lamps are ON, and radiation patterns of C0 and C4 configurations are almost

the same in terms of HPBW and SLL because for both cases all the patches radiate the same electromagnetic field (amplitude and phase).

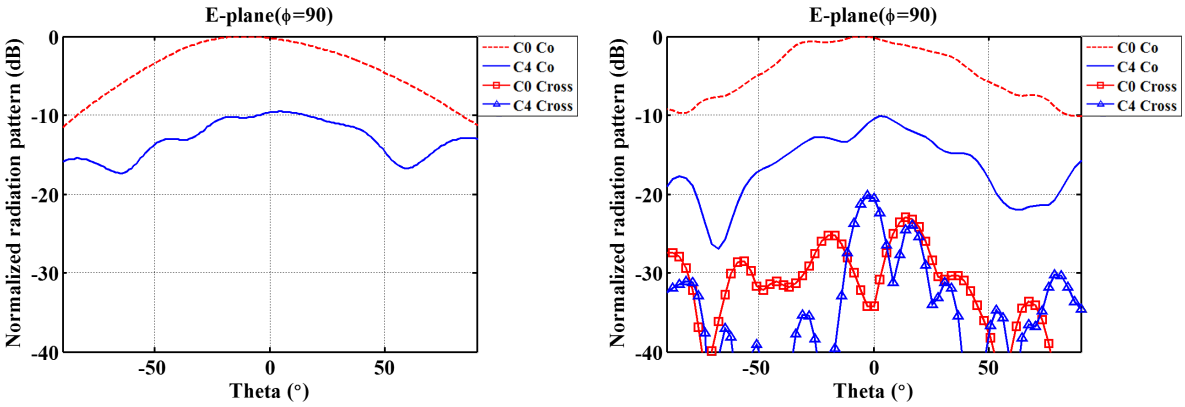

(a) (b)

Figure 4.15: Normalized E-plane radiation patterns. (a) Simulation. (b) Measurement.

The cross-polarization components in E-plane for C0, C2 and C4 configurations do not appear in the Figures (Fig. 4.13(a) and Fig. 4.15(a)) because their levels are very low and correspond to a null of radiation in H-plane for $\theta = \phi = 0°$ (see Figures 4.12(a) and 4.14(a)).

The simulated and measured results for all configurations are summarized in the table 4.2.

Table 4.2: Results for all configurations at 2.45 GHz in simulation and 2.48 GHz in measurement

Plasma ON	**C0**		**C1**		**C2**		**C3**		**C4**	
	Simu	Meas	Simu	Meas	Simu	Meas	Simu	Meas	Simu	Meas
HPBW (°)	25.6	23	30	28	37.1	37	37.4	37	27	25
Maximum realized gain (dBi)	10.1	9.3	9.2	7.7	7.6	5.6	5.5	3.2	0.1	-0.8
SLL (dB)	-13.6	-12.7	-15	-14.7	-22.6	-22.4	-19.4	-15	-14.7	-16.7

4.1.2.4 Weighted patches array

The plasma is not a perfect switch, it just acts like a amplitude taper for the signal coming from the radiating element. Hence, in order to understand the result of radiation

pattern in terms of beamwidth and side lobe level, we tried to find the weighted value (isolation of plasma lamp) which allows to validate the results. So the Figure 4.16 shows the simulated classical 4 patches array with one power source for each single antenna. We changed the weights of the different power sources to find back the equivalent result for the measured HPBW with plasma tubes and for the different configurations. The retro-simulated weighted value is 0.2 when the lamp is ON and 1 when the lamp is OFF. The table 4.3 shows the simulated HPBW results for the weighted patches array compared to the measured HPBW with plasma tubes.

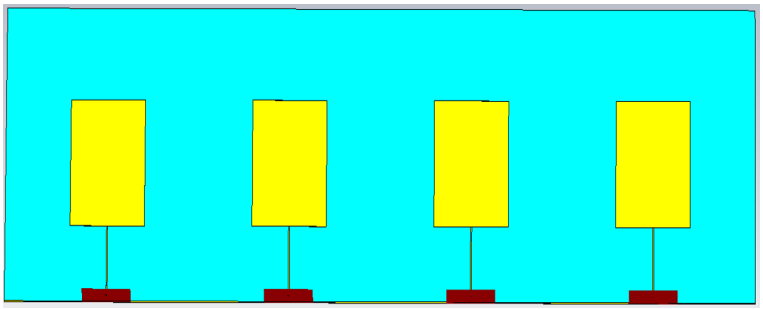

Figure 4.16: Simulated Weighted patches array.

Table 4.3: Simulated HPBW results for weighted patches array at 2.45 GHz compared to the measured HPBW results with plasma tubes

Configurations	**C0**	**C1**	**C2**	**C3**
Weights	**1 1 1 1**	**1 1 1 0.2**	**0.2 1 1 0.2**	**0.2 1 0.2 0.2**
HPBW (°)	25.5	30.9	38.1	36.2
Measured HPBW (°)	23	28	37	37

The obtained results in term of HPBW for the weighted array are quite similar to the results for the patches array with plasma wall.

4.1.2.5 Received power

In this section, we use the reconfigurable patches array to do a link budget between it an a transmitter horn antenna. This measurement has been done to evaluate the noise level induced by the plasma antenna system. The measurement setup is shown in the Figure 4.17. A wide band horn antenna [2-18 GHz] is used for the transmission antenna with a transmitted power equals to 10 dBm delivered by a power generator. Then, by using a spectrum analyzer, we measure the received power with our antenna for all the configurations.

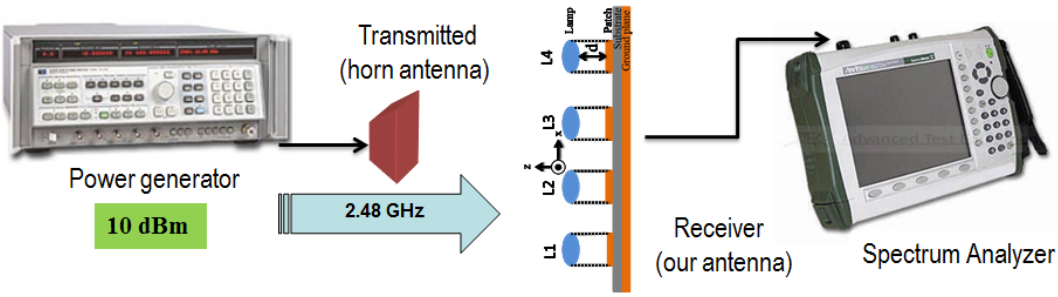

Figure 4.17: Measurement setup for the link budget between a horn antenna and our reconfigurable antenna array with plasma lamps.

When the plasma is ON, it appears a very low modulation at ±100 KHz from the carrier frequency (see Fig. 4.18). This modulation is due to the energizing system of the plasma, but the level (-80 dBm) is very low compared to the carrier level (-34 dBm for C4). We can also notice that the signal power decreases from C0 to C4 configuration and we find back the 10 dB difference in gain between C0 and C4 cases.

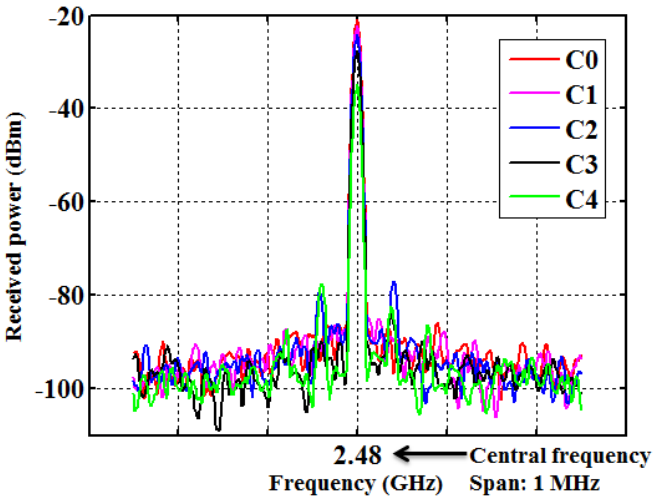

Figure 4.18: Measured received power.

The table 4.4 shows the measured received power compared to the calculated received power using the free space equation (see equation 4.1):

$$P_r = P_t + G_t + G_r + 20\log_{10}(\frac{\lambda}{4\pi R}) \tag{4.1}$$

where P_t is the transmitted power, G_t and G_r are the antenna gains of the transmitting and receiving antennas respectively, λ is the wavelength, and R is the distance between the

antennas. The fourth factor in the equation 4.1 is the so-called free-space path loss. In our case, the distance between the transmitted and received antenna is almost equal to 4 m. The transmitted power is equal to 10 dBm. The transmitted antenna gain is 12 dBi. The received power for one given configuration is calculated according to its gain of receiving antenna (see Table 4.2). The measured results are in good agreement with the calculated ones. Some small differences appear and can be explained by the non ideal environment (not ideal free space).

Table 4.4: Received power for all the configurations

Configurations	**C0**	**C1**	**C2**	**C3**	**C4**
Measured Received power (dBm)	-21	-22.5	-25	-28	-34
Calculated Received power (dBm)	-21	-22.6	-24.7	-27.2	-31.2

4.1.2.6 Application

This section describes the use of our antenna as receiving antenna for a WIFI application. The idea is to demonstrate that the antenna can be used as receiving antenna for WIFI and also to prove that the plasma is not so noisy. To realize the study, an USB WIFI card with a software is plugged in a computer. The antenna is connected to the USB card via a SMA cable and is placed at 7 to 8 m from the access point. The measurement setup is shown in Figure 4.19.

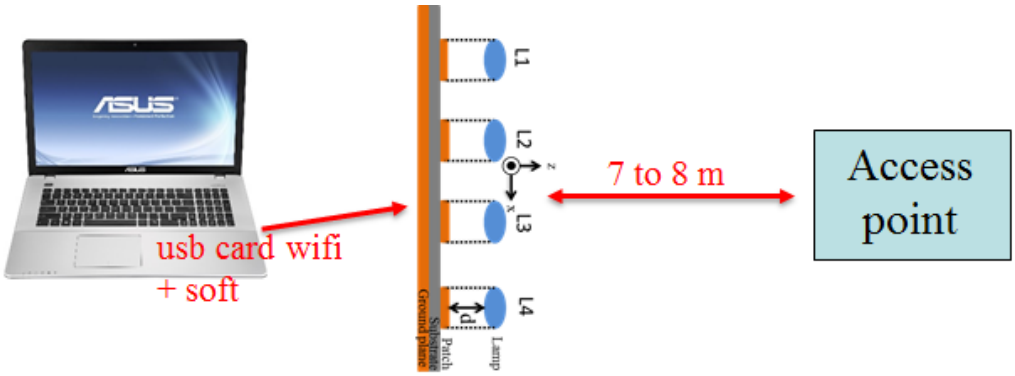

Figure 4.19: Measurement setup of our antenna as receiving antenna for a WIFI application.

The level of the signal is given by the software embedded in the laptop. The Figure 4.20 shows the level of the signal (in %) for all the configurations. The level of the signal (see table 4.5) is equal to 100% for C0, 98% for C1, 96% for C2, 84% for C3 and 74% for C4. For all the configurations with the antenna system, we can connect to internet even in C4 configuration where the gain is lower (-0.8 dB) and the level of the signal is

74%. This result proves that the plasma is not so noisy and can be used to realize original reconfigurable structures.

Table 4.5: Level of the signal in %

Configurations	**C0**	**C1**	**C2**	**C3**	**C4**
Intensity of the signal (%)	100	98	96	84	74

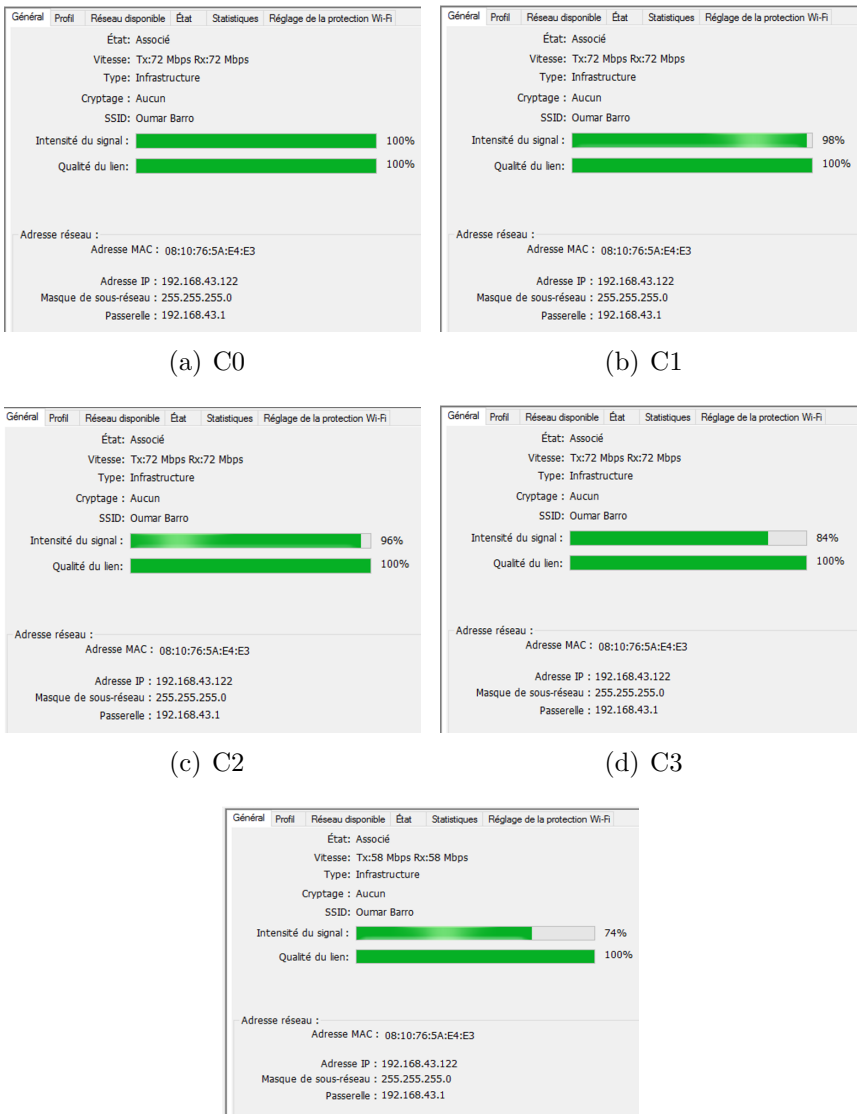

(a) C0 (b) C1

(c) C2 (d) C3

(e) C4

Figure 4.20: Level of the signal in %.

4.2 Slot Antenna Array at 2.45 GHz

High Power Microwave (HPM) antennas are well suited for high pulsed power application [7] like no lethal weapon or drones interception. In this field of applications, antennas must provide good efficiency, low loss and low back side radiation. Radiation pattern control and so Half-Power-Beam-Width reconfiguration is important to focus only on the target. However, there is a challenge to maintain a suitable power handling with reconfiguration radiation pattern. Two particular ways are possible to design reconfigurable radiation pattern with variable HPBM. The first one is based on electronic devices to electronically control the radiation pattern [2, 8]. Another way is to use a mechanical system as in [9] with a defocusing system on a parabolic antenna.

In this section, a H-plane mechanically actuated radiation pattern antenna is presented firstly. The HPBW reconfiguration between 17.8° and 63.1° is provided by physically moving two parasitic flaps. Secondly, electrically flaps using plasma tubes are considered to obtain a electronically reconfigurable HPBW antenna. For the two designed, the same slot waveguide antenna is considered.

The E-plane pattern is fixed by a 3 slots array distributed by a power splitter [10] fed by a horn antenna. A set of measurements including reflection coefficient and radiation patterns is presented, and compared to the simulation results.

4.2.1 Antenna Design

The proposed antenna is based on a radiating aperture with the illustrated uniform E-Field amplitude and phase distribution (Fig. 4.21). The objective of the design is to mechanically and electrically change the physical aperture length in order to obtain the reconfigurable radiation pattern in the H-plane. According to the equation 4.2, the mathematical relation between the physical aperture length and the corresponding HPBW ($\theta_{H(-3\ dB)}$ in degrees) can be expressed as follow (for uniform electric field distribution along the aperture):

$$\theta_{H(-3\ dB)} = \lambda_0 \times 180/(a \times \pi) \tag{4.2}$$

Where λ_0 is the wavelength in the free space and a the length of the aperture. In order to be compliant with a HPBW variation in the H-plane from 20° to 60°, it is deduced that the antennas aperture length a should evolve from 351 mm to 117 mm respectively (at 2.45 GHz). Therefore the initial length a is chosen to be 400 mm. To provide the constant amplitude and phase distribution along the aperture, a H-plane sectorial horn antenna is used [11]. The length of the horn is fixed to be 390 mm to guarantee the constant phase. To provide the amplitude and phase distribution in each aperture (E-plane), a power splitter in the E-plane is used after the horn antenna. The global design is presented in Figure 4.22.

The details of the power splitter are shown in Figure 4.23. To design it, an optical approach is first used to theoretically determine the dimensions. To provide the same phase in all apertures, the equations 4.3 and 4.4 must be respected.

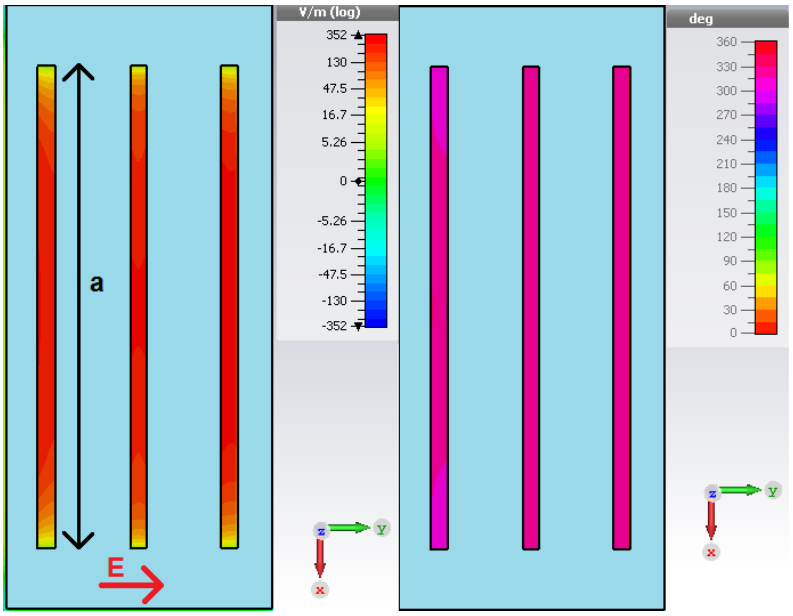

Figure 4.21: Radiating aperture with the E-Field amplitude and phase distribution.

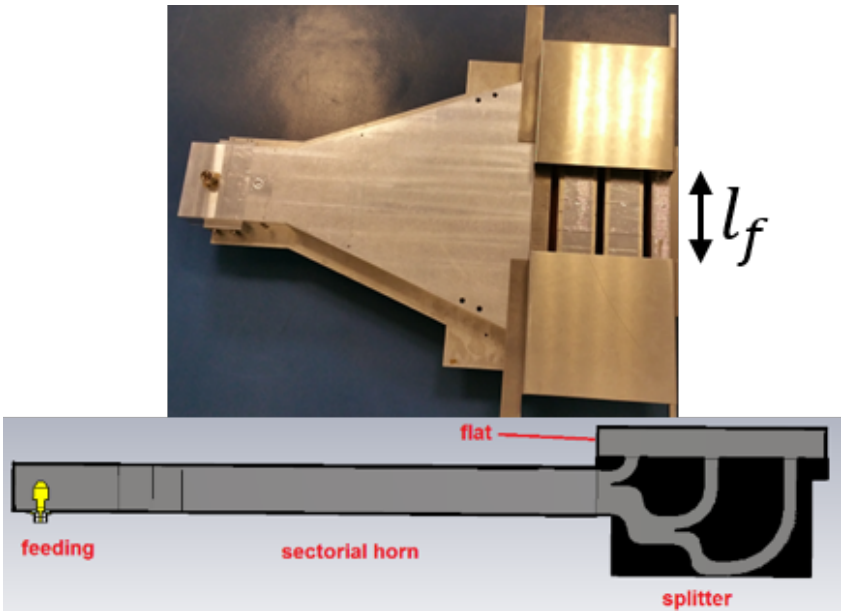

Figure 4.22: Global design of the antenna.

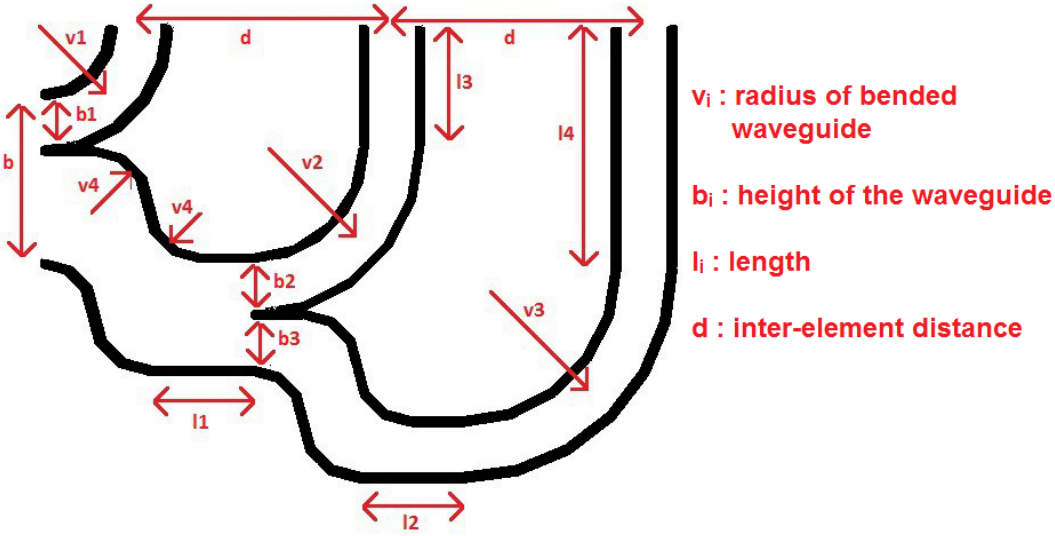

Figure 4.23: Design of the power splitter.

$$v_1 \times \pi/2 + \lambda_0 = v_4 \times \pi + l_1 + v_2 \times \pi/2 + l_3 \tag{4.3}$$

$$v_1 \times \pi/2 + 2\lambda_0 = 2v_4 \times \pi + l_1 + l_2 + v_3 \times \pi/2 + l_4 \tag{4.4}$$

In our case the aperture length a is very wide ($a = 400$ mm) so $\lambda_g \sim \lambda_0$.

Then, with the physical constraints (space between apertures d and height of apertures) we obtain:

$$v_1 + d = v_2 + l_1 + 2v_4 \tag{4.5}$$

$$v_1 + 2d = v_3 + l_2 + l_1 + 4v_4 \tag{4.6}$$

$$v_1 + b + 2v_4 - b_1/2 = l_3 + v_2 + b_3 + b_2/2 \tag{4.7}$$

$$v_1 + b + 4v_4 - b_1/2 = l_4 + v_3 + b_3/2 \tag{4.8}$$

The space between apertures d is fixed to $0.9\lambda_0$ to have a HPBW of 30° in E-plane. The b parameter is the width of the waveguide at the input of the horn ($b = 43.18$ mm). Resolution of this system gives:

$$l_1 = [2b + d(\pi - 2) - b_2 - b_1 - 2(b_3 + \lambda_0 - 4v_4)]/(\pi - 4) \tag{4.9}$$

$$l_2 = [d(\pi - 2) + b_2 + b_3 - 2(\lambda - 4v_4](\pi - 4) \tag{4.10}$$

$$l_3 = [2b(\pi-2) + 4d - b_1(\pi-2) - b_2(\pi-2) - 2b_3(\pi-2) - 4\lambda_0 + 8v_4(\pi-2)]/[2(\pi-4)] \quad (4.11)$$

$$l_4 = [2b(\pi-2) + 8d - b_1(\pi-2) - b_3(\pi-2) - 8\lambda_0 + 16v_4(\pi-2)]/[2(\pi-4)] \quad (4.12)$$

$$v_2 = [-2b - 2d + b_1 + b_2 + 2b_3 + 2\lambda_0 + v_1(\pi-4) - 2\pi v_4]/(\pi-4) \quad (4.13)$$

$$v_3 = [-2b - 4d + b_1 + b_3 + 4\lambda_0 + v_1(\pi-4) - 2\pi v_4]/(\pi-4) \quad (4.14)$$

b_1, b_2 and b_3 are fixed to $b/3$. We fixed arbitrarily $v_4 = b/3$ to have a positive solution for each parameters

4.2.2 Simulations and Measurement

In this first case is considered the mechanical reconfigurable antenna with metallic flaps.

4.2.2.1 Metallic flaps

The mobile metallic flaps are placed above the radiating apertures at a distance $h = \lambda_0/4$ to minimize the mismatching. We fixed $v_1 = \lambda_0/(2\pi)$ in order that the reflected wave by the flaps come back on the splitter and radiate in phase.

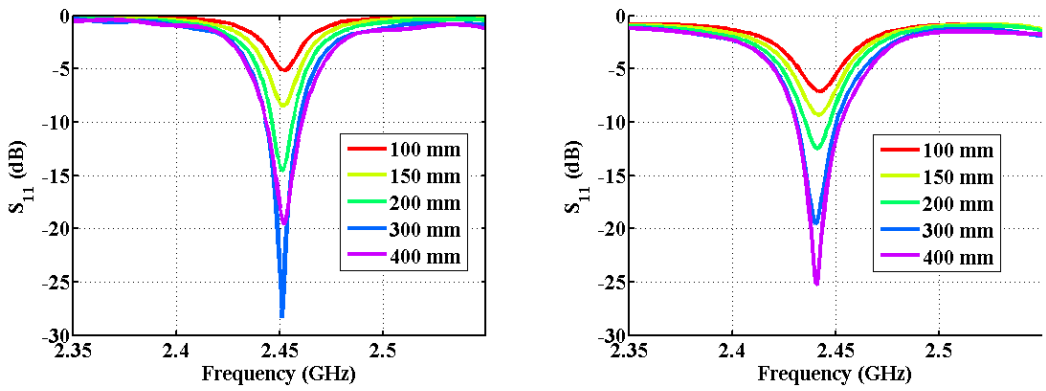

(a) (b)

Figure 4.24: S_{11} magnitude comparison with the metallic flaps. (a) Simulation. (b) Measurement.

The simulation was performed on CST Microwave Studio. Figure 4.24 presents the magnitude of reflection coefficient of the antenna for different values of the slots length

(l_f = 100 mm, l_f = 150 mm, l_f = 200 mm, l_f = 300 mm and l_f = 400 mm) between the two flaps l_f (see Fig. 4.22). There is a small frequency shift between simulation (Fig. 4.24(a)) and measurement (10 MHz see Fig. 4.24(b)). The antenna is matched ($S_{11} < -10$ dB) for l_f between 400 mm (no flaps over the apertures) and 200 mm. The magnitude of S_{11} for l_f = 100 mm is -5 dB in simulation and -7 dB in measurement.

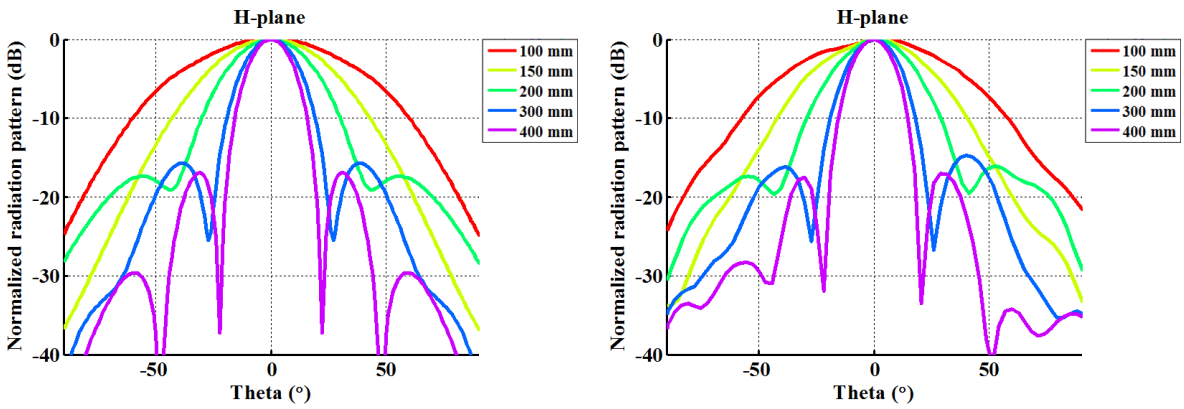

(a) (b)

Figure 4.25: Normalized H-plane radiation patterns with the metallic flaps. (a) Simulation. (b) Measurement.

The simulated radiation patterns are done at 2.45 GHz and the measured radiation patterns were performed in an anechoic chamber at 2.44 GHz.

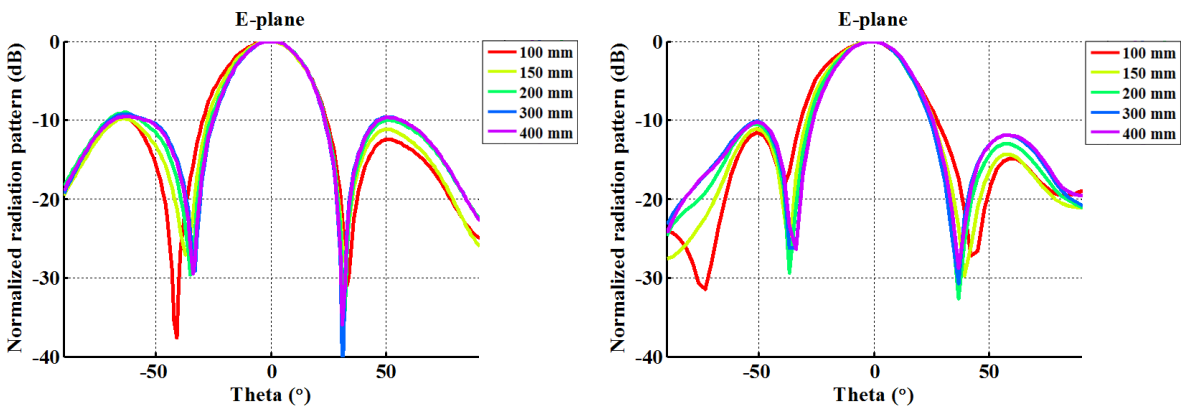

(a) (b)

Figure 4.26: Normalized E-plane radiation patterns with the metallic flaps. (a) Simulation. (b) Measurement.

The Figures 4.25 and 4.26 present respectively the H-and E-planes normalized radiation patterns in simulation and measurement for the different values of l_f. A good agreement can be observed between simulation and measurement. The radiation pattern in the E-plane doesn't change when the flaps move with a HPBW of 30° and side lobe level below to -10 dB. In the H-plane, the HPBW changes from 18° (flaps opened l_f = 400 mm) to 65.9° (flaps closed l_f = 100 mm) in simulation (see Fig. 4.26(a)) and from 17.8° (flaps opened l_f = 400 mm) to 63.1° (flaps closed l_f = 100 mm) in measurement (see Fig. 4.26(b)). The side lobe levels are below -15 dB.

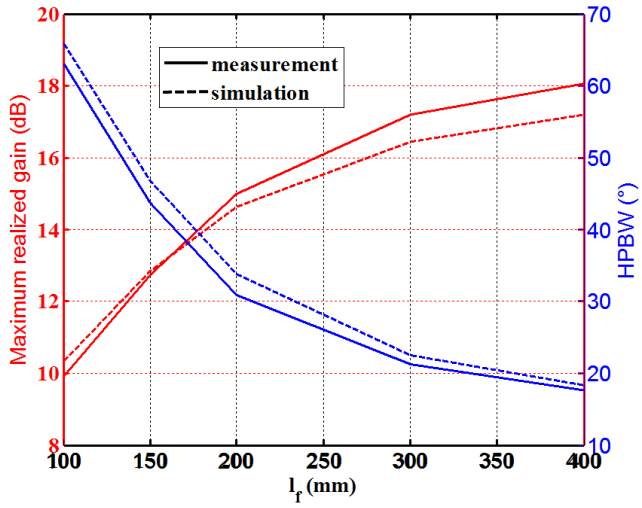

Figure 4.27: Gain and HPBW versus l_f with the metallic flaps.

The Figure 4.27 shows the HPBW and the maximum realized gain versus the distance l_f. The maximum realized gain varies between 10.3 to 17.2 dBi in simulation and 9.9 to 18.1 dBi in measurement because the HPBW varies from 66° to 18° in simulation and from 63.1° to 17° in measurement. Therefore, when the HPBW decreases, the gain increases because the antenna becomes more directive.

The table 4.6 summarizes the results in terms of HPBW and maximum realized gain in simulation and measurement for the different values of l_f when the metallic flaps are moved.

Even if this antenna gives good results, unfortunately the reconfigurability is mechanical, so it can be too slow for several applications. That's why an electrically reconfigurable antenna is designed with plasma lamps to replace metallic flaps.

Table 4.6: Results for all l_f values at 2.45 GHz in simulation and 2.44 GHz in measurement with the metallic flaps

Length (mm)	l_f = 100		l_f = 150		l_f = 200		l_f = 300		l_f = 400	
	Simu	Meas	Simu	Meas	Simu	Meas	Simu	Meas	Simu	Meas
HPBW (°)	65.9	63.1	46.8	43.7	33.8	31	22.5	21.3	18.4	17.8
Maximum realized gain (dBi)	10.33	9.9	12.9	12.7	14.6	15	16.4	17.2	17.19	18.1

4.2.2.2 Plasma flaps

Plasma wall was build using fluorescent lamps (4000K color temperature) which are arranged in parallel (see. Fig 4.28). The two first lamps are placed at ±50 mm from the center in order to have an aperture of l_f = 100 mm. The distance between two adjacent lamps is 6 mm due to the lamp socket bi-pin G13. The diameter and the length of the lamp are 26 mm and 590 mm respectively. The plasma wall is put above the radiating apertures at the same distance than the metallic flaps ($h = \lambda_0/4$).

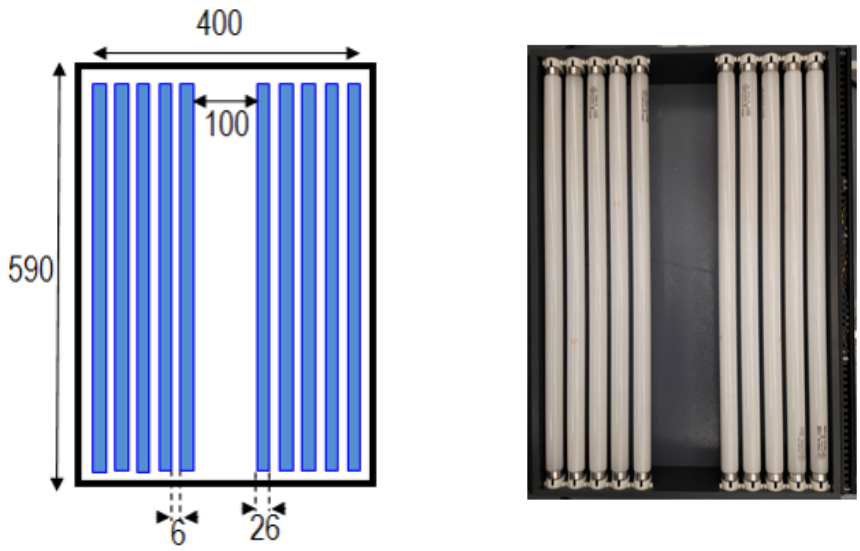

(a) (b)

Figure 4.28: Plasma wall. (a) Schematic of the plasma wall, (Unit in mm). (b) Manufactured plasma wall.

The lamps seen in the Figure 4.28 are numerated from the left to the right (L1 to L10). We evaluate the HPBW and maximum realized gain for 5 different l_f values (l_f = 100 mm, l_f = 164 mm, l_f = 228 mm, l_f = 292 mm and l_f = 400 mm). The studied configurations are shown in the table 4.7.

Table 4.7: Configuration for different values of l_f

Length (mm)	l_f = 100	l_f = 164	l_f = 228	l_f = 292	l_f = 400
Switching ON	all the lamps	all expect L5 and L6	L1, L2, L3, L8, L9 and L10	L1, L2, L9 and L10	-

The simulations were performed on CST Microwave Studio. Figure 4.29 shows the reflection coefficient of the antenna for the different values of l_f according to the lamps switched ON. There is a small frequency shift between simulation (Fig. 4.29(a)) and measurement (10 MHz see Fig. 4.29(b)). The antenna is matched ($S_{11} < -10$ dB) for all lengths (from 400 mm to 100 mm) in measurement and simulation. We can notice that with plasma flaps case, the antenna is matched even if l_f = 100 mm, while it was not the case for metallic flaps.

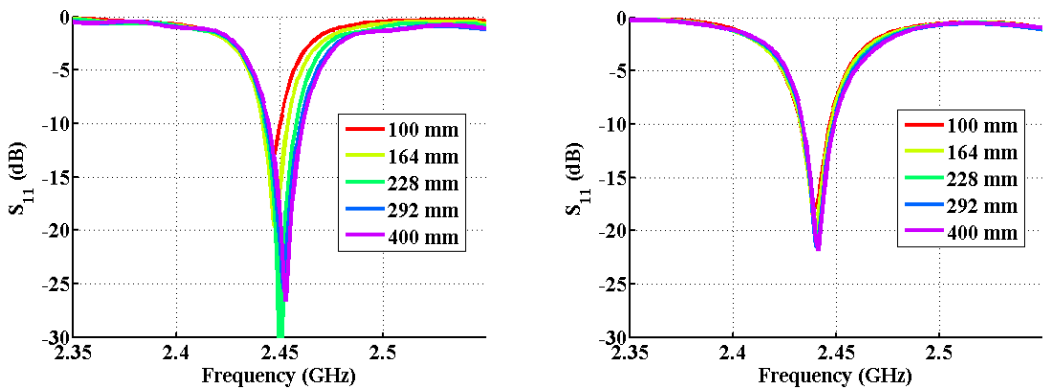

(a) (b)

Figure 4.29: S_{11} magnitude comparison with the plasma flaps. (a) Simulation. (b) Measurement.

The Figures 4.30 and 4.31 show respectively the H-plane and E-plane for the simulated and measured normalized radiation patterns and for different values of l_f. The simulated and measured results are in good agreement. In the E-plane, the radiation patterns are not changed whatever the value of the distance l_f with a HPBW almost of 30° and a side lobe level lower than -10 dB. In the H-plane, the HPBW varies from 62.6° (l_f = 100 mm) to 18° (l_f = 400 mm) in simulation (see Fig. 4.31(a)) and from 66.7° (l_f = 100 mm) to 17.3° (l_f = 400 mm) in measurement (see Fig. 4.31(b)).

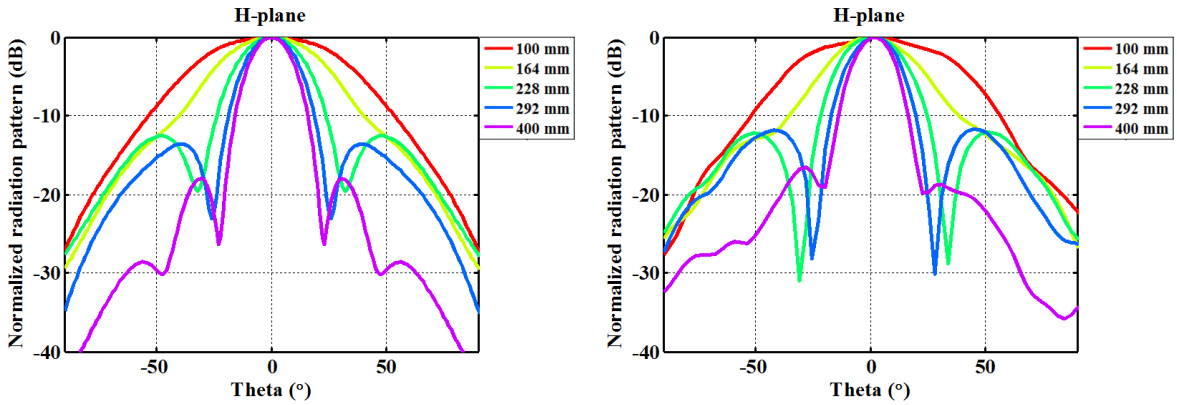

(a) (b)

Figure 4.30: Normalized H-plane radiation patterns with the plasma flaps. (a) Simulation. (b) Measurement.

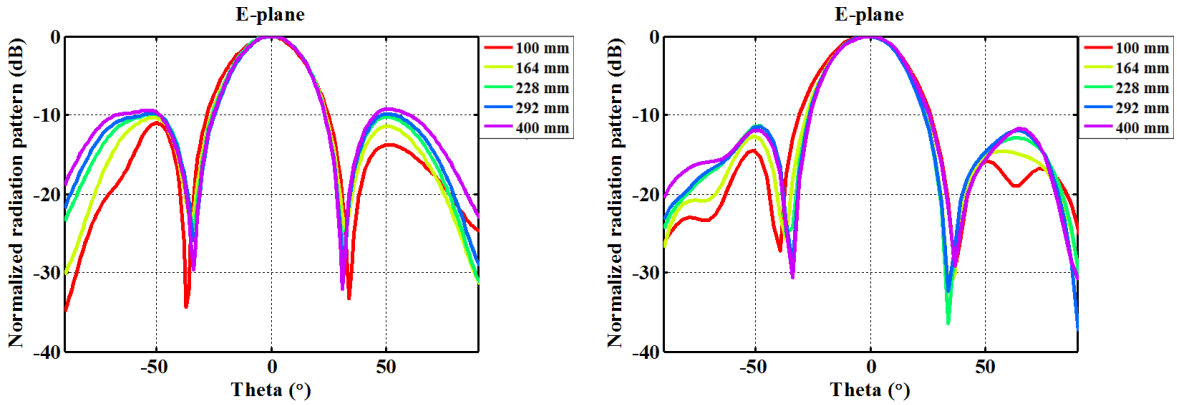

(a) (b)

Figure 4.31: Normalized E-plane radiation patterns with the plasma flaps. (a) Simulation. (b) Measurement.

The Figure 4.32 depicts the HPBW and the maximum realized gain versus the length l_f. The maximum realized gain varies between 11 to 17.1 dBi in simulation and 9.9 to 17.1 dBi in measurement.

The table 4.8 summarizes the HPBW and maximum realized gain results in simulation and measurement for the different values of l_f in the plasma flaps case.

The obtained results in the plasma flaps case are similar to the results with the metallic flaps. These results confirm that the use of plasma flaps allows to keep a good matching

for all values of the slot length and allows also to have an electrical control rather than mechanical one.

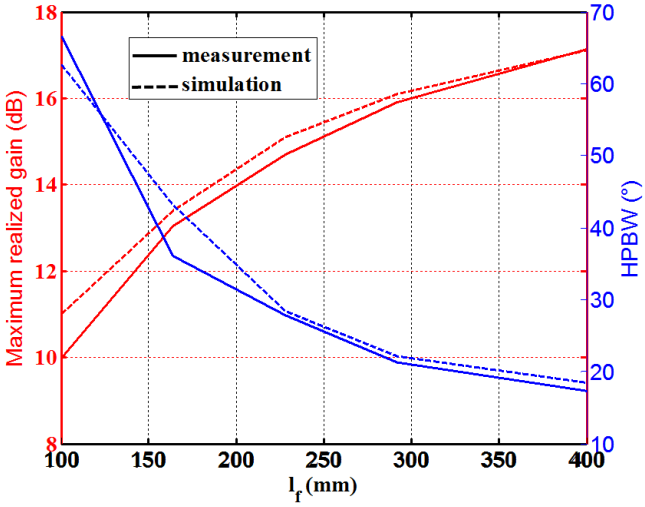

Figure 4.32: Gain and HPBW versus l_f with the plasma flaps.

Table 4.8: Results for all l_f values at 2.45 GHz in simulation and 2.44 GHz in measurement with the plasma flaps

Length (mm)	l_f = 100		l_f = 164		l_f = 228		l_f = 292		l_f = 400	
	Simu	Meas	Simu	Meas	Simu	Meas	Simu	Meas	Simu	Meas
HPBW (°)	62.6	66.7	43.2	36.1	28.4	27.9	22.1	21.3	18.4	17.3
Maximum realized gain (dBi)	11	10	13.4	13	15.1	14.7	16.1	15.9	17.1	17.1

4.3 Conclusion

In this chapter, plasma tubes have been used in order to reconfigure the beamwidth of radiation pattern in the H plane. Many configurations have been simulated and measured, showing the impact of the plasma tubes on the radiation patterns at 2.45 GHz and allowing to obtain beamwidth reconfigurability. Two structures have been studied in this chapter:

- A reconfigurable printed patches antenna array using plasma tubes to taper the different patches was presented. A parametric study has been done concerning the distance d between patches and lamps to find out the good value allowing to keep a good matching whatever the configuration. The radiation patterns of different configurations have been simulated at 2.45 GHz and measured at 2.48 GHz for $d = 6$ mm showing the impact of the plasma tubes and allowing to obtain beamwidth reconfigurability. This study also shows that, the noise is independent to the configurations but when the plasma is ON, it appears a very low modulation at ±100 KHz from the carrier frequency. An application has been also realized by using our antenna system as a receiving antenna for WIFI in order to access to internet.

- A high power pattern reconfigurable antenna has been designed with a horn antenna and a waveguide splitter coupled with a mechanical motion of metallic flaps and electrical reconfigurability with plasma flaps. The HPBW radiation pattern is fixed in the E-plane (30°) and changes in the H-plane from 17° (l_f = 400 mm) to 66° (l_f = 100 mm).

The main advantage of these antenna systems is to keep a good matching at the operating frequency for all configurations.

Bibliography

[1] O. Lafond, M. Caillet, B. Fuchs, S. Palud, M. Himdi, S. Rondineau, and L. Le Coq, "Millimeter wave reconfigurable antenna based on active printed array and inhomogeneous lens," *in Proceedings Microwave Conference, 2008. EuMC 2008. 38th European*, Oct. 2008, pp. 147-150.

[2] M. Caillet, O. Lafond, M. Himdi, "Reconfigurable Microstrip antennas in Millimeter Wave," *in Proc. 2006 IEEE MTT-S Int. Microwave Symposium Dig*, pp. 638-641, June 2006.

[3] D. S. Goshi, Y. Wang, and T. Itoh, "A compact digital beamforming SMILE array for mobile communications," *IEEE Transactions On Microwave Theory And Techniques*, Vol. 52, No. 12, December 2004.

[4] L. Le Garrec, "Etude et conception en bande millimetrique d'antennes reconfigurables basées sur la technologie des MEMS," *Thèse de doctorat - Université Rennes 1*, novembre 2003.

[5] CST, "Computer Simulation Technology," http://www.cst.com/

[6] M. T. Jusoh, M. Himdi, F. Colombel, and O. Lafond, "Performance and radiation patterns of a reconfigurable plasma corner-reflector antenna," *IEEE Antennas and Wireless Propagation Letters*, no 99, pp. 1137-1140, 2013.

[7] X. Li, Q. Liu, and J. Zhang, Design and application of high-power cavity-backed helical antenna with unit ceramic radome, Electronics Letters, vol. 51, no. 8, pp. 601-602, 2015.

[8] M.T Ali, T.A Rahman, M.R Kamarudin, and M Tan, "Reconfigurable linear array antenna with beam shaping at 5.8 GHz," *Microwave Conference*, 2008. APMC 2008. Asia-Pacific, pp. 16-20, 2008.

[9] A. D Olver and J. U I Syed, "Variable beamwidth reflector antenna by feed defocusing," *Microwaves, Antennas and Propagation, IEE Proceedings*, vol. 142, no. 5, 1995.

[10] F. Arndt, I. Ahrens, U. Papziner, U. Wiechmann, and R. Wilkeit, "Optimized E-Plane T-Junction Series Power Dividers," *IEEE Transactions on Microwave Theory and Techniques*, vol. 35, no. 11, pp. 10521059, Nov. 1987.

[11] A. Jouade, M. Himdi, A. Chauloux, and F. Colombel, "Pattern Reconfigurable Bended H sectoral Horn antenna for High Power applications," *IEEE Antennas and Wireless Propagation Letters*, vol. PP, no. 99, pp. 1-1, 2016.

Chapter 5

Plasma Antennas

The objective of this chapter is to discuss and study the use of plasma as radiating element. The main idea of this work is to design an antenna which can radiate (Plasma ON) or not (plasma OFF). The state of the art of plasma antennas has been discussed in the chapter 2 with different excitation techniques and different coupling techniques. This chapter is divided in two parts. The first part is dealing with the realization of monopole antenna using plasma fluorescent lamp with its performance. The performance of a dipole plasma antenna is presented in the second part.

5.1 Monopole Antenna

The plasma antenna introduced in this chapter is realized by using fluorescent lamp and is excited using AC supply. A cylindrical plasma tube is used as radiating element. A coupling sleeve is made in order to couple an RF signal from the Electromagnetic source to the plasma tube. The modeling and realization of the plasma antenna are described and the performance of the monopole antenna is presented.

5.1.1 Modeling and Realization

In this section, we describe the plasma antenna based on a fluorescent tube and its RF coupling part. The idea is to design a monopole plasma antenna. The illustration of the antenna system is shown in Figure 5.1 for a dipole configuration that is the final objective of this study. The antenna is composed of a fluorescent lamp fed by a coaxial probe through a particular coupling system leading to the radiation of the plasma tube. The height of the commercial fluorescent lamp is 590 mm and the tube diameter is 26 mm. For the final design, a reflector of 1 $m \times 1$ m (see Fig. 5.1) is placed below the antenna at a distance d from the antenna system in order to increase the gain and to reduce the back radiations.

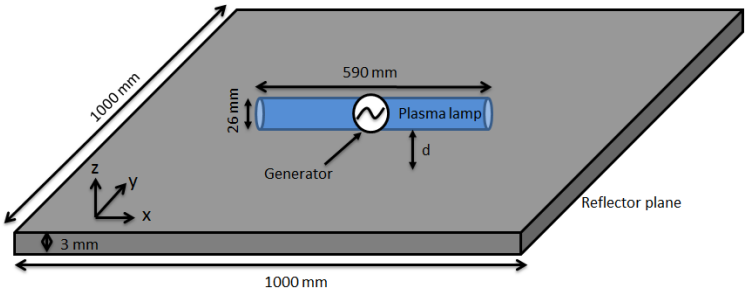

Figure 5.1: System model.

For simulations performed with CST Microwave Studio, the tube containing the gas is made from lossy pyrex glass with $\epsilon_r = 4.82$, $\tan\delta = 0.005$ and thickness of 0.5 mm. Furthermore, we used the same Drude model as in chapter 4, with the parameters ($\nu = 900$ MHz and $\omega_p = 44\ 10^9$ rad/s). The distance d is fixed at $\lambda/4$ at 600 MHz.

Due to the glass, there is not a physical contact between the inner coaxial line and the plasma. Therefore a coupling system is necessary to fix this problem. Furthermore, the E-field must be parallel to plasma tube (horizontal electromagnetic E-field). The coupling area between SMA connector and the lamp is composed by a metallic ring surrounding the plasma tube and an outer metallic cylinder (see Figs. 5.2(a) and 5.2(b)). The width of the ring is 10 mm and this ring is shielded by the outer cylinder whose diameter and width are 70 mm and 40 mm respectively. The inner coaxial line is connected to the ring while its ground is linked to the outer cylinder.

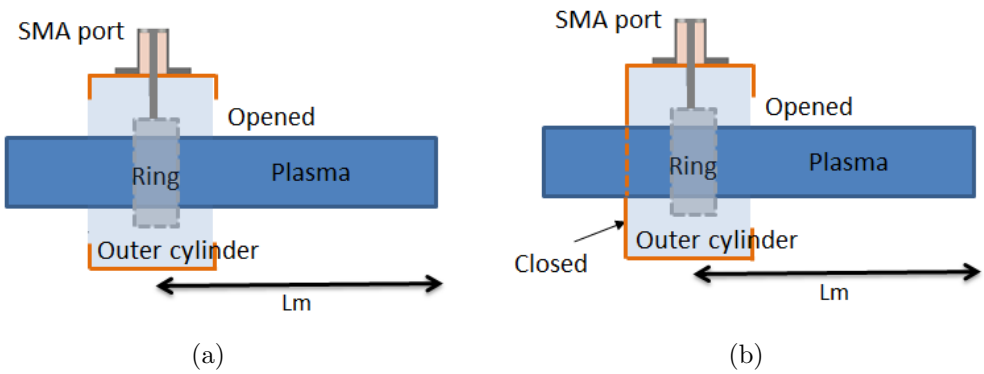

Figure 5.2: Coupling system. (a) Symetric cavity. (b) Dissymetric cavity.

In the first time two flaps with an aperture of 45 mm is placed in both sides (see fig. 5.2(a)). In this coupling system, the field distribution has vertical and horizontal components and due to the symmetry this field distribution cancels mutually (see Fig.

5.3(a)). Consequently the system doesn't excite the plasma. In order to have a field distribution along the tube, the coupling system must be dissymmetric (see Fig. 5.3(b)) by opening one side and closing another side. Therefore, a horizontal strong electric field can be coupled to the plasma and allowing the tube to radiate (see Fig. 5.2(b)).

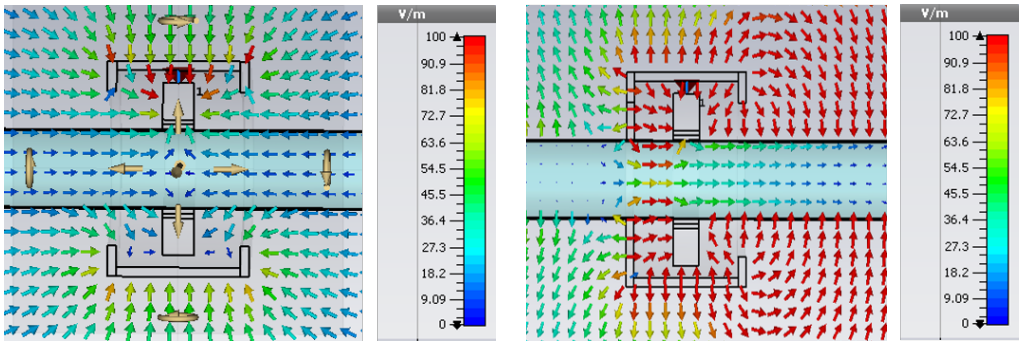

(a) (b)

Figure 5.3: E-field distribution. (a) Symetric cavity. (b) Dissymetric cavity.

The power to energize the 18-W commercial fluorescent lamps is supplied by an electronic ballast with specification of 220-240 V, 50-60 Hz. The realized ring and outer cylinder are presented respectively in Figures 5.4(a) and 5.4(b). The monopole antenna prototype without reflector is shown in Figure 5.5.

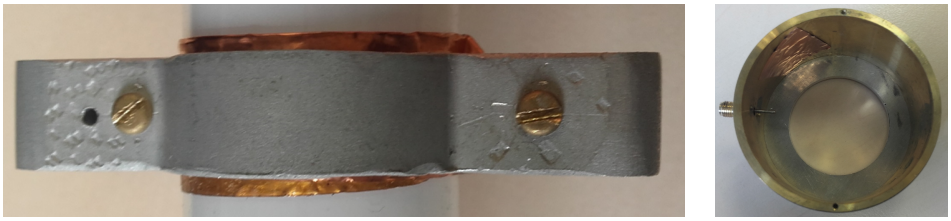

(a) (b)

Figure 5.4: Prototypes. (a) Ring. (b) Outer cylinter.

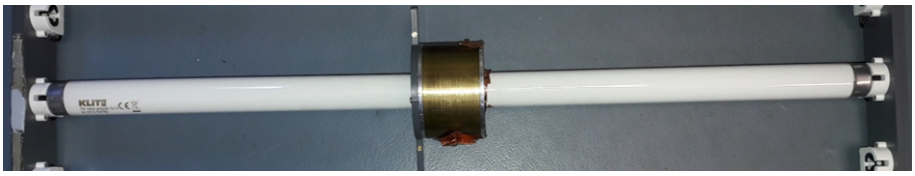

Figure 5.5: Realized plasma monopole antenna.

5.1.2 Results and discussion

The Figure 5.6 presents the current distribution along the tube for different frequencies. This current distribution allows to know the length of the lamp in term of guided wavelength and how the antenna will radiate. Between two minimums, the distance is evaluated and this distance correspond to $\lambda_g/2$ (λ_g is guided wevelength). This system is similar to the conductor coated by a dielectric [1],[2]. We are in this case because the plasma is coated by the glass (see Fig. 5.7). It justifies, the effective permittivity obtained by applying the following formula:

$$\epsilon_{eff} = (\frac{\lambda_0}{\lambda_g})^2 \tag{5.1}$$

The Figure 5.6 shows that the effective permittivity is similar and equals almost to 2 for all frequencies. This Figure 5.6 shows also at the frequencies (500 MHz and 550 MHz) that there is more radiation towards the opened side than to the closed side but when the frequency increases (600 MHz and 700 MHz), the coupling system present leakage, therefore the radiation is almost similar in two directions.

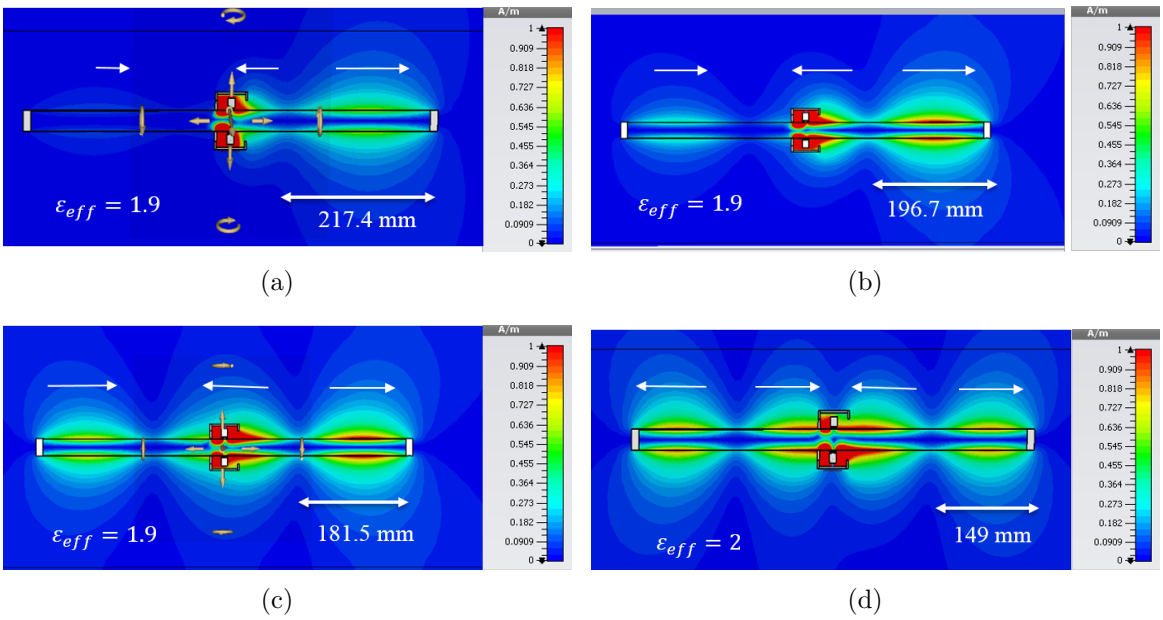

Figure 5.6: Current distribution for different frequencies. (a) 500 MHz. (b) 550 MHz. (c) 600 MHz. (d) 700 MHz.

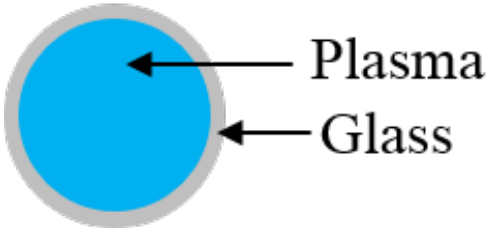

Figure 5.7: Plasma coated by a glass

The simulated and measured magnitude of the S_{11} parameters are shown in Figure 5.15. The simulated and measured results are quite in good agreement. This antenna is not very well matched but the S_{11} is lower than -6 dB around 600 MHz. Nevertheless, even if the antenna is not perfectly matched, the mismatching level does not prevent the measurement of radiation patterns and gain.

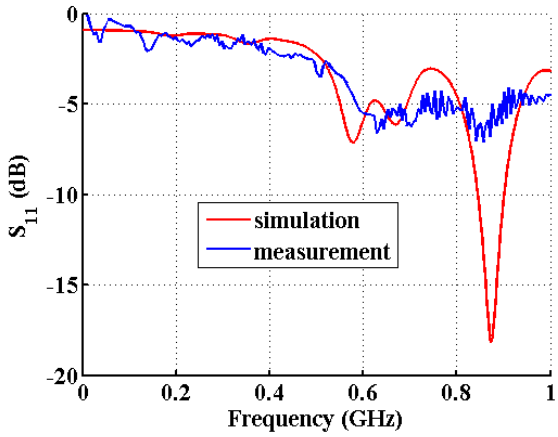

Figure 5.8: Simulated and measured S_{11} magnitude of the monopole without refector plane.

Radiation patterns have been measured in order to validate the simulation results and to demonstrate the reconfigurable capability (plasma ON or OFF) of such an antenna system. Measurements have been performed in a SATIMO anechoic chamber (near fields setup) with a peak gain accuracy equals to ±0.8 dBi. The radiation patterns of the antenna without and with reflector are studied.

5.1.2.1 Antenna without reflector

The radiation patterns of the monopole antenna without reflector are presented in this section. The Figure 5.9 shows the radiation patterns for simulation at 550 MHz and measurement at 490 MHz in the E-and H-planes respectively. The simulated and measured

radiations are quite similar. It is easier to see that in the E-plane, the antenna radiates more in direction of the opened side. In all cases, we observe a shift on frequency between measurement and simulation due to the inadequate knowledge of the exact plasma parameters.

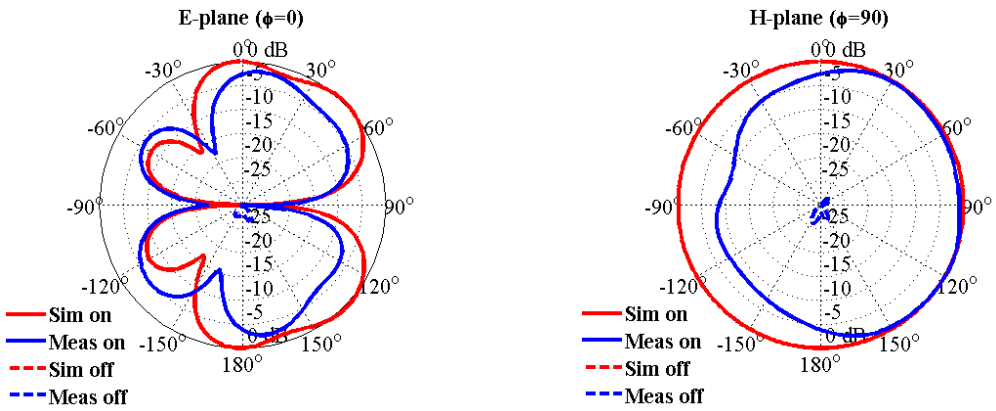

(a) (b)

Figure 5.9: Normalized radiation patterns for the simulation at 550 MHz and measurement at 490 MHz. (a) E-plane, E_θ component. (b) H-plane, E_ϕ component.

The radiation patterns for simulation at 600 MHz and measurement at 540 MHz in the E-and H-planes respectively are presented in Figure 5.10.

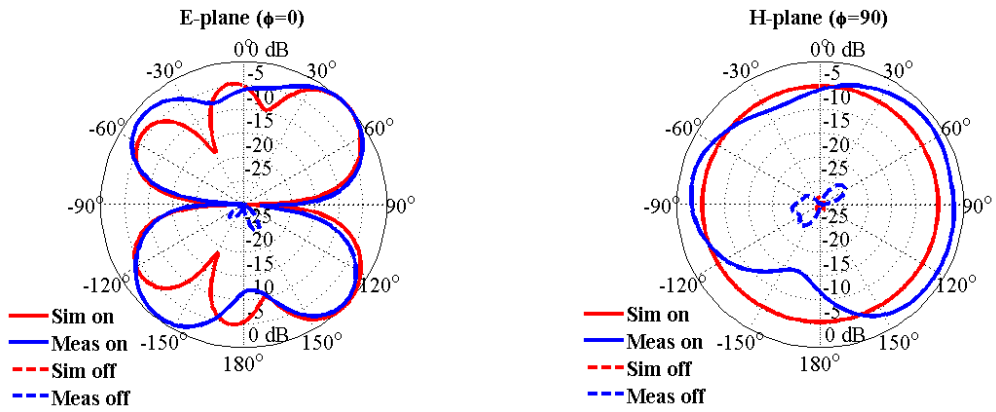

(a) (b)

Figure 5.10: Normalized radiation patterns for the simulation at 600 MHz and measurement at 540 MHz. (a) E-plane, E_θ component. (b) H-plane, E_ϕ component.

The Figures 5.9(b) and 5.10(b) show that radiation patterns in H plane are not omni-directionnal because the antenna is put on a pylon made from polyvinyl-chloride (PVC).

For the plasma OFF case and for all frequencies in simulation and measurement, the gain of antenna is strongly decreased (under -25 dBi). The results show that when the plasma is OFF, the antenna does not radiate or can become furtive in a reception antenna case.

The simulated and measured maximum realized gain for our antenna system without reflector are shown in table 5.1. We can notice that the gain in simulation and measurement are quite similar even if real plasma media induces loss because it can not be considered like a perfect metal.

From the gain, the efficiency of the antenna is evaluated and shown in table 5.2. The radiated efficiency for the simulated frequencies is equal 35.4% (550 MHz) and 47.1% (600 MHz) and for the measured frequencies 26.9% (490 MHz) and 43.3% (540 MHz). The total efficiency which takes account the mismatching of the antenna is shown in the table 5.2.

Table 5.1: Maximum realized gain in simulation and measurement for the monopole without reflector.

	Simulated frequencies		**Measured frequencies**	
Frequency (MHz)	550	600	490	540
Gain plasma ON case (dBi)	-3.1	0.1	-4.3	-2.1
Gain plasma OFF case (dBi)	-34	-32	-29.7	-23.5

Table 5.2: Simulated and measured efficiency for the monopole without refector

	Simulated frequencies		**Measured frequencies**	
Frequency (MHz)	550	600	490	540
Radiated efficiency (%)	35.4	47.1	26.9	43.3
Total efficiency (%)	24.2	35	11.9	13

5.1.2.2 Antenna with reflector

This section presents the radiation patterns of the antenna with reflector.

The Figure 5.11 represents the simulated (at 550 MHz) and measured (at 490 MHz) radiation patterns in E and H-planes. The simulation and measurement are in good agreement.

The Figure 5.12 shows the same results but for others frequencies.

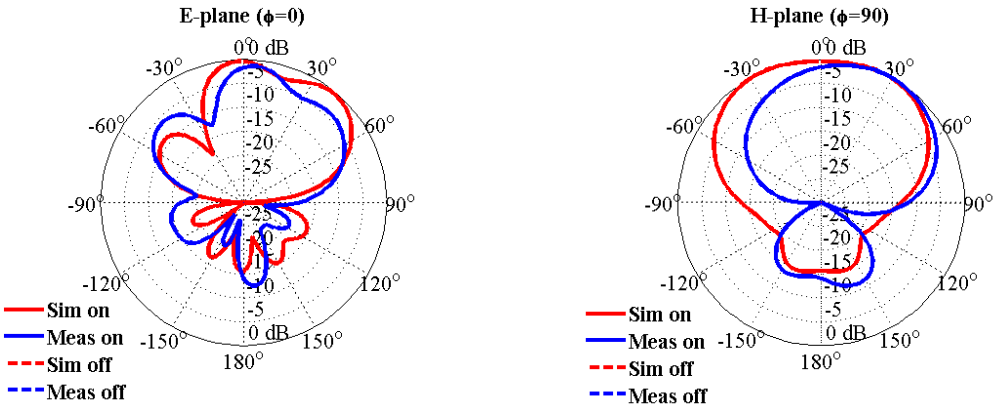

(a) (b)

Figure 5.11: Normalized radiation patterns for the simulation at 550 MHz and measurement at 490 MHz. (a) E-plane, E_θ component. (b) H-plane, E_ϕ component.

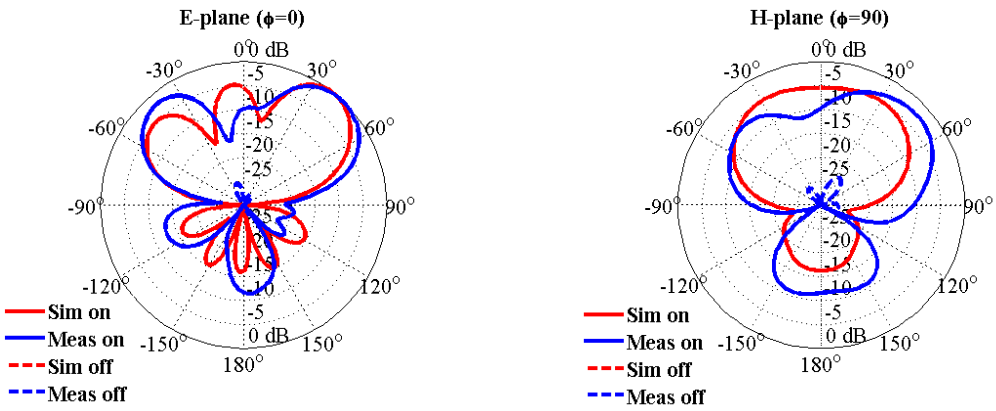

(a) (b)

Figure 5.12: Normalized radiation patterns for the simulation at 600 MHz and measurement at 540 MHz. (a) E-plane, E_θ component. (b) H-plane, E_ϕ component.

The simulated and measured maximum realized gain for the antenna system with reflector are presented in table 5.3. The maximum realized gain is better in this case thanks to the reflector plane added behind the plasma antenna and allowing to reduce back side radiation.

Table 5.3: Maxismum realized gain in simulation and measurement for the monopole with reflector.

	Simulated frequencies		**Measured frequencies**	
Frequency (MHz)	550	600	490	540
Gain plasma ON case (dBi)	2.5	5	-0.3	1
Gain plasma OFF case (dBi)	-28.8	-27	-28	-22.1

The coupling system presented is not symmetric and this dissymmetry may cause problems. Therefore the next idea is to design a dipole in order to have a symmetrical coupling.

5.2 Dipole Antenna

5.2.1 Modeling and Realization

Now, to design a dipole plasma antenna, we use two adjacent coupling systems at the lamp center and we divide the input signal through a (-3 dB/180°) hybrid to balance the feeder. The current distribution becomes symmetric along the x axis (for example at 600 MHz as seen in Figure 5.14). The simulated and manufactured prototype are shown in Figure 5.13.

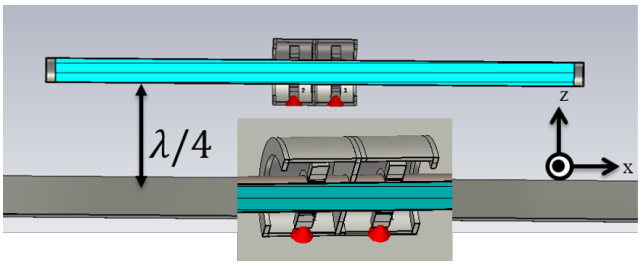

(a)

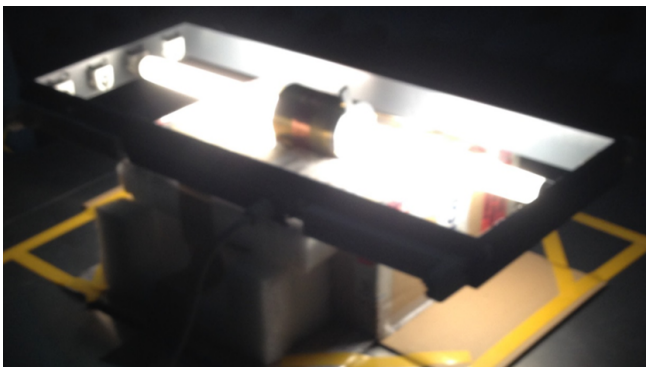

(b)

Figure 5.13: Plasma Antennas. (a) Simulated. (b) Manufactured.

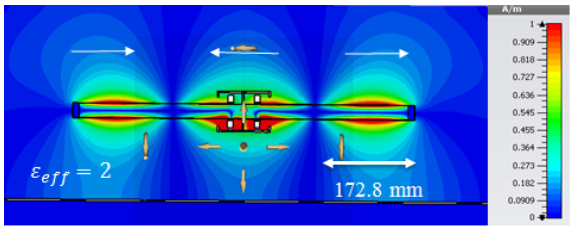

Figure 5.14: Current distribution at 600 MHz.

5.2.2 Results and discussion

The simulated and measured magnitude of the S_{11}/S_{22} parameters are shown in Figure 5.15 before to put the (-3 dB/180°) hybrid. The reflection coefficients are similar for the two inputs both in simulation and measurement. However, the antenna is not very well matched experimentally. This defect can be due to the plasma which is not well modelized with CST. Moreover, the manufacturing of the feeding system and the thickness of glass can also explain this mismatching. Nevertheless, even if the antenna is not perfectly matched, the mismatching level does not prevent the measurement of radiation patterns and gain.

The simulated and measured radiation patterns of the dipole antenna with reflector are presented at four different frequencies. The ports 1 and 2 are fed through a (-3 dB/180°) hybrid coupler. The shape of the radiation pattern changes with frequency due to the different length of lamp compared to the wavelength. Moreover as you can see with the next results, it exists a frequency shift between simulation and measurement probably due to the non exact values of plasma parameters during modelisation.

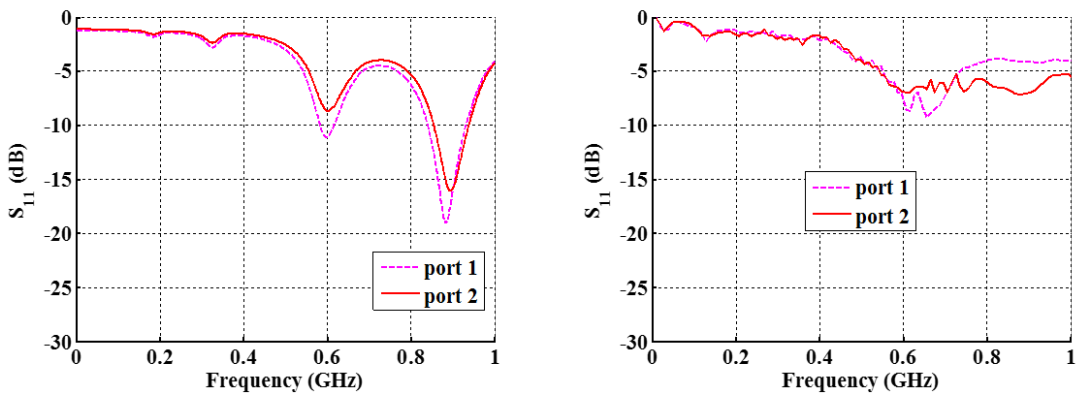

Figure 5.15: S_{11} magnitude comparison. (a) Simulation. (b) Measurement.

The Figure 5.16 shows the simulated (at 470 MHz) and measured (at 410 MHz) radi-

ations patterns in E-plane (Fig. 5.16(a)) and H-plane (Fig. 5.16(b)). For both simulation and measurement, each radiation pattern is normalized to the maximum value of its electric-field in plasma ON case. We can notice that, the radiation patterns in simulation and measurement are quite similar. The radiation patterns in E-plane are in the broadside direction and are relatively narrow due to reflector effect (array effect due to the dipole image). In the H-plane, the radiation patterns are wider.

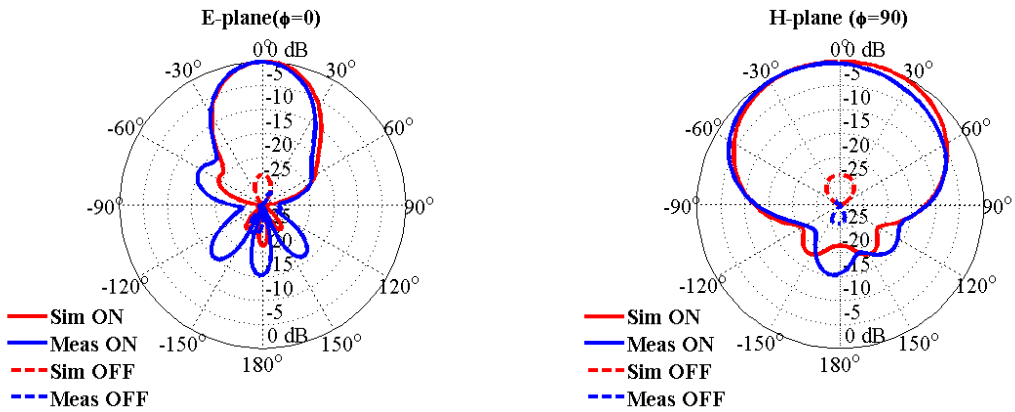

(a) (b)

Figure 5.16: Normalized radiation patterns for the simulation at 470 MHz and measurement at 410 MHz. (a) E-plane, E_θ component. (b) H-plane, E_ϕ component.

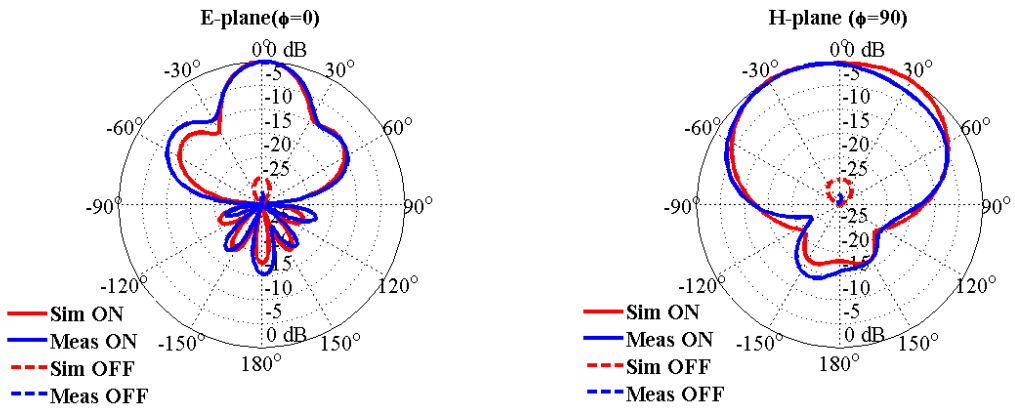

(a) (b)

Figure 5.17: Normalized radiation patterns for the simulation at 530 MHz and measurement at 450 MHz. (a) E-plane, E_θ component. (b) H-plane, E_ϕ component.

The Figure 5.17 presents the radiation patterns for simulation at 530 MHz and mea-

surement at 450 MHz in the E and H-planes respectively. The simulated and measured radiations are quite similar. We can notice that, in the E-plane (5.17(a)) the radiation becomes less directional regarding the radiation patterns in E-plane for the previous frequency (Fig. 5.16(a)).

The radiation patterns for simulation at 600 MHz and measurement at 520 MHz in the E-and H-planes respectively are shown in Figure 5.18. In the E-plane (5.18(a)) we remark that three lobes appear due to the length of the plasma tube compared to the wavelength at this frequency.

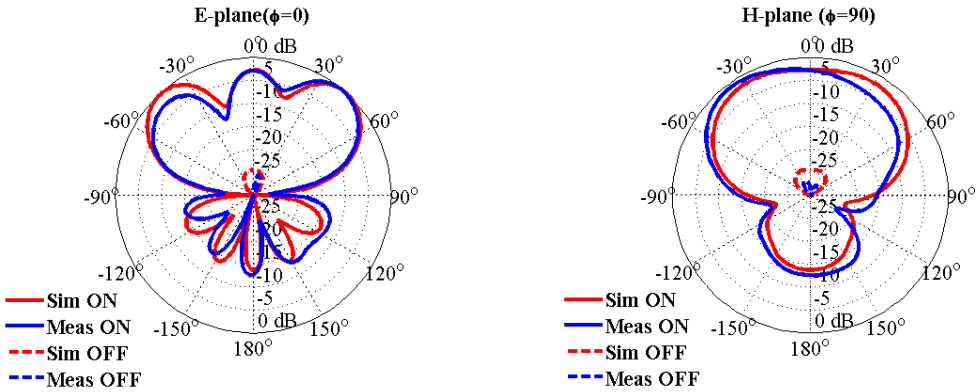

(a) (b)

Figure 5.18: Normalized radiation patterns for the simulation at 600 MHz and measurement at 520 MHz. (a) E-plane, E_θ component. (b) H-plane, E_ϕ component.

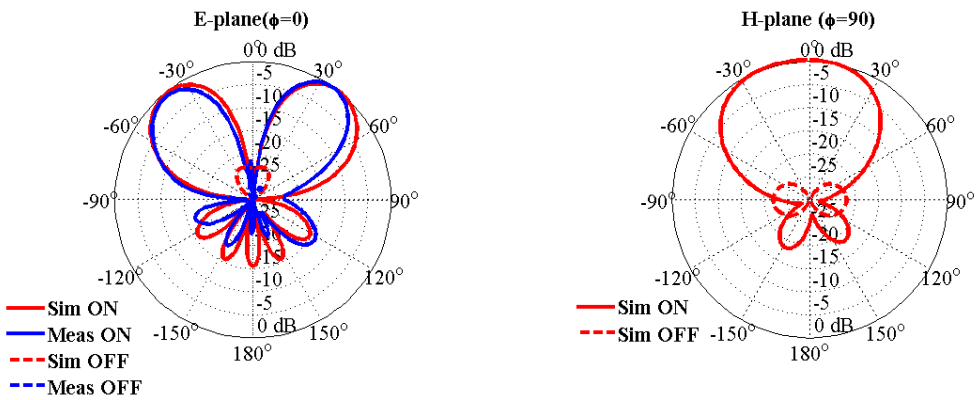

(a) (b)

Figure 5.19: Normalized radiation patterns. (a) E-plane E_θ component, for the simulation at 675 MHz and measurement at 600 MHz. (b) H-plane, E_ϕ component, for the simulation at 675 MHz .

The Figure 5.19 depicts the radiation patterns for simulation at 675 MHz and measurement at 600 MHz in the E plane. We can notice that, the radiation patterns present two lobes and a null in $\theta = 0°$ direction. The H-plane is presented in simulation but not in measurement due to the difficulty to plot the H-plane in the plane $\theta = 40°$ where the radiation pattern in E-plane has its maximum value.

In the plasma OFF case and for all frequencies in simulation and measurement, the normalized radiations patterns are below than -25 dB. The results show that when the plasma is OFF, the antenna does not radiate or can become furtive in a reception antenna case.

The tables 5.4 and 5.5 show respectively the simulated and measured maximum realized gain for our antenna system.

Table 5.4: Maximum realized gain in simulation for different frequencies

Frequency (MHz)	470	530	600	675
Maximum gain of plasma ON (dBi)	-1.1	2.3	3.7	3.5
Maximum gain of plasma OFF (dBi)	-24.9	-22.5	-20.5	-18.6

Table 5.5: Maximum realized gain in measurement for different frequencies

Frequency (MHz)	410	450	520	600
Maximum gain of plasma ON(dBi)	-3.1	-0.4	1.3	4
Maximum gain of plasma OFF(dBi)	-26.5	-28.6	-24.	-20.6

As we said before, there is a frequency shift between simulation and measurement. It could be reduced if the real plasma frequency of the fluorescent lamp was determined.

5.3 Conclusion

A plasma monopole and dipole antennas was presented and completely characterized in terms of radiation patterns and gain. A feeding system was designed to couple electromagnetic signal from the input coaxial line to the plasma tube to be radiated. The simulated and measured results are quite in good agreement except the frequency shift of the antenna behavior. This defect could be improved by a better acknowledgment of the plasma frequency of the plasma media. From our acknowledgment, these antenna systems are one of the first investigated monopole and dipole plasma antennas with measurement of radiation patterns and positive gain.

Bibliography

[1] H. Lebbar, M. Himdi, and J. P. Daniel, "Transmission line analysis of printed monopole," *Electronics Letters*, vol. 28, no. 14, pp. 13261327, Jul. 1992.

[2] V. Akan and E. Yazgan, "Analysis of the relation between printed strip monopole and dielectric coated thin cylindrical monopole," *in 2010 10th Mediterranean Microwave Symposium*, 2010, pp. 7780.

Chapter 6

General conclusion and future works

6.1 General conclusion

The use of plasma in communication systems is very interesting since plasma can be appear and disappear in microseconds. At the beginning of this thesis a state of the art on plasma has been discussed. Theory of interaction of electromagnetic waves with plasma is introduced. The main parameter that governs the interaction is the ratio of electromagnetic wave frequency ω to plasma angular frequency ω_p, which is in turn related to electron number density of plasma. The methods of characterization of plasma found in the literature have been presented. The state of the art on plasma used as reflector antennas and radiating elements has been done.

A plasma Faraday cage using a spiral fluorescent lamp has been presented. Two types of antennas (patch and monopole) operating at 2.45 GHz were placed inside the plasma Faraday cage allowing to see the impact of the polarization. The antenna systems have been simulated, fabricated and measured. The performance of the antenna systems (patch + lamp) and (monopole + lamp) has been validated. It was interesting to note that the radiation of the patch (first case) can be strongly reduced when the plasma is ON. This means that the lamp acts as a Faraday shielding effect especially on the angular sector $\theta = \pm 20°$. Furthermore, the obtained results show that this spiral lamp allows to reconfigure the radiation pattern of the patch (first case only) but not for the monopole. The measured radiation patterns are in a good agreement with simulation ones.

Reconfigurable antennas using plasma tubes and so to obtain a reconfigurable beamwidth of radiation pattern in H plane have been studied. Two types of reconfigurable plasma antennas have been simulated, fabricated and measured. The first one is a reconfigurable printed patches antenna array using plasma tubes to taper the different patches and the second one is a slot antennas array where plasma flaps are used to close the aperture of the slots. The performance of the printed patches array with the wall of plasma tubes has been validated and provide a reconfigurable beamwidth. The measured radiation patterns

are in good agreement with simulation ones. The performance of the slot antenna array has been also validated and it was proven that the performance of plasma flaps is similar to metallic flaps ones.

By using plasma fluorescent lamp, two antennas (monopole and dipole) were simulated, fabricated and measured at different frequencies. Based on the measurement results, it can be concluded that, the fluorescent lamp with an AC excitation can be used to radiate radio signals. The measured radiation patterns are in a good agreement with simulation ones but a frequency shift of the antenna behavior is observed.

6.2 Future works

Based on the works done on plasma antennas, the following points are some other prospective studies that can be carried out in future:

- Find different lengths of the plasma fluorescent tube in order to realize a plasma Yagi antenna. This Yagi can be realized by using reflector and directors. The reflector plasma tube is slightly longer than the driven plasma dipole, whereas the directors (plasma tube) are a little shorter.

- Develop a collaboration with the plasma manufacturer laboratory in order to have a good knowledge of the plasma parameters and to have different shapes of the plasma fluorescent lamp. This collaboration will permit to improve the performance of ours antennas and to have accurate results since we now the plasma parameters.

- See the possibility to have mini plasma fluorescent lamps allowing to work in high frequencies.

Publications

Peer-reviewed international journals

O. A. Barro, M. Himdi, and O. Lafond, "Reconfigurable Patch Antenna Radiations Using Plasma Faraday Shield Effect", *IEEE Antennas and Wireless Propagation Letters*, vol. 15, pp. 726-729, 2016.

O. A. Barro, M. Himdi, and O. Lafond, "Reconfigurable Radiating Antenna Array Using Plasma Tubes", *IEEE Antennas and Wireless Propagation Letters*, vol. 15, pp. 1321-1324, 2016.

Peer-reviewed international conferences

O. A. Barro, O. Lafond, and H. Himdi, "Reconfigurable antennas radiations using plasma Faraday cage", in *2015 International Conference on Electromagnetics in Advanced Applications (ICEAA)*, 2015, pp. 545-548.

O. A. Barro, M. Himdi, and O. Lafond, "Performance of switchable patches array using plasma commercial fluorescent lamps", in *2016 10th European Conference on Antennas and Propagation (EuCAP)*, 2016, pp. 1-4.

O. A. Barro, M. Himdi, and O. Lafond, "Performances of Monopole Plasma Antenna", in *2017 10th European Conference on Antennas and Propagation (EuCAP)*, 2017, pp. 1-4. [Accepted]

List of Figures

List of Tables

Abstract

Plasma is the 4th state of matter with complex permittivity that can be exploited to give advantages in communication systems. Its negative permittivity allows to have similar characteristics as metal material in terms of electrical conductivity. Since many years, plasma antennas have been studied due to their ability to be conductor or transparent for electromagnetic waves. The main advantage of using plasma antennas instead of metallic ones is that they allow electrical control rather than mechanical one. Therefore, this thesis aimed to use plasma as an alternative to metal in the design of reconfigurable antennas. The first part of this thesis is dedicated to the state of the art on plasma in communication systems. The second part presents the use of plasma spiral lamp as Faraday Shield effect in order to protect antennas. Two types of antennas (patch and monopole) operating at 2.45 GHz are placed inside this plasma spiral lamp. The third part discusses about reconfigurable antennas using plasma tubes in order to reconfigure the half power beam width of the radiation pattern in H plane. Two types of antenna array have been studied: The first one is a printed patches antenna array and the second one is a slotted antennas array allowing high power utilization. The fourth part deals with plasma as radiating element. Two plasma antennas using commercially available fluorescent lamp have been studied. All the antenna systems presented in this thesis have been simulated, manufactured and measured.

Keywords: Plasma antenna, reconfigurable antenna, reconfigurable plasma antenna, Reconfigurable plasma Faraday shield effect.

Résumé

Le plasma est le quatrième état de la matière avec une permittivité complexe qui peut être exploitée pour donner des avantages aux systèmes de communications. Entre autres, une permittivité négative lui permet d'avoir des caractéristiques similaires aux matériaux métalliques en termes de conductivité électrique. Depuis de nombreuses années, les antennes plasma ont été étudiées en raison de leur capacité à être conductrices ou transparentes vis-à-vis des ondes électromagnétiques. Le principal avantage de l'utilisation d'antennes à base de plasma au lieu d'éléments métalliques est qu'elles permettent un contrôle électrique plutôt que mécanique. Par conséquent, cette thèse vise à utiliser le plasma comme une alternative au métal dans la construction des antennes reconfigurables. La première partie de cette thèse est consacrée à l'état de l'art sur l'utilisation du milieu plasma dans les systèmes de communications. Une lampe fluorescente spirale utilisée comme une cage de Faraday afin de protéger des antennes est présentée dans la deuxième partie. Deux types d'antennes (patch et monopole) fonctionnant à 2,45 GHz sont placés à l'intérieur de cette lampe spirale. La troisième partie se focalise sur les réseaux d'antennes utilisant des tubes plasma pour reconfigurer l'ouverture du digramme de rayonnement dans le plan H. Deux types de réseaux d'antennes sont étudiés : le premier est un réseau de patchs imprimés et le second est un réseau d'antennes à fentes permettant de supporter des hautes puissances. La quatrième partie traite l'utilisation du plasma comme élément rayonnant. Deux antennes plasma (monopole et dipôle) utilisant une lampe fluorescente disponible dans le commerce ont été étudiées. Tous les systèmes antennaires présents dans cette thèse ont été simulés, fabriqués et mesurés.

Mots clés: Antenne à plasma, antenne reconfigurable, antenne à plasma reconfigurable, effet de blindage d'une cage de Faraday à plasma reconfigurable.